Missouri S&T Library and Learning Resources

Scholars' Mine

Masters Theses

Student Theses and Dissertations

2010

Methodology and applications of electrostatic discharge current reconstruction by near-field scanning technique

Wei Huang

Follow this and additional works at: https://scholarsmine.mst.edu/masters_theses

Part of the Electrical and Computer Engineering Commons

Department:

Recommended Citation

Huang, Wei, "Methodology and applications of electrostatic discharge current reconstruction by near-field scanning technique" (2010). *Masters Theses*. 5421.
https://scholarsmine.mst.edu/masters_theses/5421

This thesis is brought to you by Scholars' Mine, a service of the Missouri S&T Library and Learning Resources. This work is protected by U. S. Copyright Law. Unauthorized use including reproduction for redistribution requires the permission of the copyright holder. For more information, please contact scholarsmine@mst.edu.

METHODOLOGY AND APPLICATIONS OF ELECTROSTATIC DISCHARGE CURRENT RECONSTRUCTION BY NEAR-FIELD SCANNING TECHNIQUE

by

WEI HUANG

A THESIS

Presented to the Faculty of the Graduate School of the

MISSOURI UNIVERSITY OF SCIENCE AND TECHNOLOGY

In Partial Fulfillment of the Requirements for the Degree

MASTER OF SCIENCE IN ELECTRICAL ENGINEERING

2010

Approved by

David J. Pommerenke, Advisor
James L. Drewniak
Jun Fan

© 2010
Wei Huang
All Rights Reserved

ABSTRACT

Electrostatic discharge (ESD) can cause interference in or damage to circuits or systems in many ways e.g., by E- field or H- field coupling or via conduction paths. Although one can roughly estimate the voltage and current at the injection location during an ESD event, the real offending parameter is mostly the ESD current spreading throughout the system. Those currents can be simulated if great simplifications of the system are acceptable. However, even in moderately complex systems, the ability to simulate is limited by a lack of models and computational resources. Independent of the complexity, but obviously not free of its own limitations, is a measurement technique that captures the current as a function of time and location through the system.

This article describes an ESD current measurement technique that permits reconstruction the injected current spreading as a movie from the magnetic near-field scanning results. It describes the validation of the technique using a simplified case study. The study examined the simulation and measurement of a simplified PCB ESD structure; the design, characterization, modeling, and optimization of current scanning probes; the implementation and analysis of time domain and frequency domain scanning methods; the scanning raw data frequency and directional response compensation algorithms; the current spreading visualization methods and implementation; the modeling of simplified PCB current injection structure and verification of ESD current reconstruction results; two directions of system-level analysis with current reconstruction scanning method.

ACKNOWLEDGEMENTS

I would like to express my deepest gratitude to my advisor, Dr. David Pommerenke, for patiently guiding me throughout my graduate life in general and throughout my research in particular. His guidance and support continue to stimulate me to bring out my best.

I would also like to thank Dr. James L. Drewniak and Dr. Jun Fan for their support throughout my research. Both served on my committee and proved insightful comments.

I am grateful also to Giorgi Muchaidze, Jayoo Koo, Peng Shao, Xiao Jiang, Dazhao Liu, and many other students in the EMC laboratory for their supports of my projects, and most importantly, for their friendship.

Last, but not the least, I owe special thanks to my father who has supported me through my engineering education, and to my wonderful mother and my young sister who have always believed in me.

TABLE OF CONTENTS

ABSTRACT....iii

ACKNOWLEDGEMENTS....iv

TABLE OF CONTENTS.... v

LIST OF ILLUSTRATIONS.... viii

LIST OF TABLES.... xv

SECTION

1. INTRODUCTION.... 1

2. SIMPLIFIED PCB ESD STRUCTURE.... 2

3. PROBES FOR CURRENT RECONSTRUCTION.... 5

3.1. FIELD COUPLING DURING ESD....5

3.2. SURFACE CURRENT PROBE....7

3.2.1. Structure.... 7

3.2.2. Characterization.... 9

3.2.2.1 Directional Rejection.... 9

3.2.2.2 Coupling Factor.... 12

3.2.2.3 Cable Loss.... 14

3.3. TRACE CURRENT PROBE....16

3.3.1. Concept of Differential H_z Probe.... 16

3.3.2. Structure and Design.... 17

3.3.3. Characterization.... 26

3.3.3.1 Self-Inductance.... 26

3.3.3.2 Directional Rejection.... 29

3.3.3.3 Sideway Spatial Resolution.... 30

3.3.3.4 Common Mode Rejection.... 35

3.3.3.5 Coupling Factor.... 44

3.3.3.6 Cable Loss.... 48

3.3.4. Simulation Analysis.... 48

3.3.4.1 Probe Modeling Analysis.... 49

3.3.4.2 Current Coupling Analysis.... 53

4. CURRENT RECONSTRUCTION SCANNING METHODS 76
4.1. TIME DOMAIN SCANNING METHOD...76
4.1.1. Block Diagram and Scanning Setup 76
4.1.2. Scanning Raw Data Analysis... 78
4.2. FREQUENCY DOMAIN SCANNING METHOD 82
4.2.1. Block Diagram and Scanning Setup 82
4.2.2. Scanning Raw Data Analysis... 85
4.3. SCANNING DATA PROCESS 87
4.3.1. Probe Frequency Response Compensation. 87
4.3.1.1 Deconvolution Methodology 87
4.3.1.2 Surface Current Probe Compensation....................................... 89
4.3.1.3 Trace Current Probe Compensation.. 94
4.3.2. Probe Directional Response Compensation.. 97
4.4. CURRENT SPREADING VISUALIZATION..101
4.4.1. Current Magnitude Visualization... 101
4.4.1.1 Linear Scale Image 101
4.4.1.2 Log Scale Image. 103
4.4.2. Current Vector Visualization 104
4.4.3. Linear Interpolation of Image 105
4.4.4. Current Reconstruction Viewer (GUI)…………………………….106
5. SCANNING RESULTS SIMULATION VERIFICATION 107
5.1. CURRENT RECONSTRUCTION STRUCTURE MODELING 107
5.2. RECONSTRUCTED SURFACE CURRENT VERIFICATION....................113
5.3. RECONSTRUCTED TRACE CURRENT VERIFICATION.........................118
6. SYSTEM-LEVEL CURRENT RECONSTRUCTION SCANNING.................... 128
6.1. LOCAL RESONANCE AND RESPONSE ANALYSIS 128
6.1.1. Background and Objective.. 128
6.1.2. Experimental Setup 128
6.1.3. Scanning Results Analysis 130
6.2. SYSTEM-LEVEL ESD INTERFERENCE ANALYSIS 135
6.2.1. Background and Objective.. 135

6.2.2. Experimental Setup 136
6.2.3. Scanning Result Analysis. 138
7. CONCLUSION AND FUTURE WORKS 140
7.1. CONCLUSION 140
7.2. FUTURE WORKS 140
7.2.1. Predict of Local Response for Arbitrary Excitations 140
7.2.2. Analysis of a Probe's Influence on Local Field 141
BIBLIOGRAPHY 142
VITA 143

LIST OF ILLUSTRATIONS

Page

Figure 2-1. Layout of the PCB for ESD current spread scanning 2

Figure 2-2. The simplified PCB ESD injection setup.. 3

Figure 2-3. Injected current spreading on ground plane 4

Figure 2-4. Current return of the test structure (side view) 4

Figure 3-1. Injected surface current spreading 5

Figure 3-2. Current spreading and coupling around probe - side view 5

Figure 3-3. Most concerned coupling around a probe 6

Figure 3-4. Shielded vertical-loop probe 7

Figure 3-5. Out layer of a shielded PCB vertical-loop probe 8

Figure 3-6. Inner layer of a shielded PCB vertical-loop probe... 8

Figure 3-7. Finished coaxial probe and PCB probe with ferrites 9

Figure 3-8. Shielded loop probe in maximum and minimum coupling orientations 10

Figure 3-9. Shielded probe shows acceptable directional rejection characteristic 10

Figure 3-10. Unshielded probe in max and min H-field coupling orientations 11

Figure 3-11. Unshielded loops probe shows nearly no directional rejection.................... 11

Figure 3-12. Experimental setup for measuring coupling frequency response 12

Figure 3-13. H-field coupling frequency response of a loop probe in TEM cell.............. 13

Figure 3-14. Experimental setup for probe’s S11 measurement...................................... 14

Figure 3-15. Deembed of cable loss 15

Figure 3-16. Measured loss of the probe cable 15

Figure 3-17. Conventional H-field probe and its H-field coupling 16

Figure 3-18. Differential turns loops structure 17

Figure 3-19. Differential turn loop captures H_z components of trace current 17

Figure 3-20. The 4 Layers pcb shielding for a differential turn probe 18

Figure 3-21. Top layer (CMC connection layer) 19

Figure 3-22. Middle layer 1 (top shielding layer)... 19

Figure 3-23. Middle layer 2 (dual loops layer) 20

Figure 3-24. Bottom layer (bottom shielding layer) 20

Figure 3-25. Supporting PCB with CMC for differential H_z probe 21
Figure 3-26. Ferrites on the coaxial connection 22
Figure 3-27. Hybrid method for common mode rejection 22
Figure 3-28. Using ferrite as H-field shielding 23
Figure 3-29. PCB of differential H_z probe 23
Figure 3-30. Detail structure of the second version differential H_z probe 24
Figure 3-31. Datasheet of the common mode chock for differential H_z probe 25
Figure 3-32. Assembled differential H_z probe 25
Figure 3-33. The Self-Inductance of the common mode chock on circuit model 26
Figure 3-34. Experimental setup of probe inductance measurement by TDR 27
Figure 3-35. TDR measurement of common mode chock 27
Figure 3-36. TDR inductance measurement of CMC + 3mm loops 28
Figure 3-37. TDR inductance measurement of CMC + 0.1mm loops 28
Figure 3-38. D0 response and D90 rejection measurement setup 29
Figure 3-39. D0 response and D90 rejection measurement result 30
Figure 3-40. Sideway spatial resolution measurement setup 31
Figure 3-41. Sideways movement 31
Figure 3-42. Spatial resolution of 3mm wide loop probe at touching distance 32
Figure 3-43. Both loops couple trace current 33
Figure 3-44. Trace current coupling cancels out 33
Figure 3-45. One loop coupling dominates 34
Figure 3-46. Magnitude and phase measurement while moving probe sideways 34
Figure 3-47. Sideway spatial resolution decreases with probe's height increases 35
Figure 3-48. Evaluation process of plane surface current coupling 36
Figure 3-49. Trace current coupling for differential H_z probe 37
Figure 3-50. Trace current coupling for shielded vertical-loop probe 37
Figure 3-51. Area for surface current coupling rejection test 38
Figure 3-52. Locations and orientations of the probes during analysis 38
Figure 3-53. The S21 results of ground current coupling into the two probes 39
Figure 3-54. S11 of the simplified ESD injection structure 40
Figure 3-55. Surface current coupling circuit model 41

Figure 3-56. Calculated surface current coupling rejection 42
Figure 3-57. Positions where E-Field or edge current h-field coupling dominate............ 43
Figure 3-58. Probe S21 response at several E-field dominated locations......................... 44
Figure 3-59. Experiment setup of trace current coupling with network analyzer 45
Figure 3-60. Coupling experiments of a differential Hz probe on different traces........... 45
Figure 3-61. The coupling results of a differential H_z probe on different traces 46
Figure 3-62. Circuit model of trace current coupling 46
Figure 3-63. Frequency response of current coupling on simplified probe model 47
Figure 3-64. S11 result of a differential H_z probe.. 48
Figure 3-65. The differential H_z probe's CST and HFSS models 49
Figure 3-66. Pure PCB probe for model comparison 49
Figure 3-67. S11 comparison for simulation and measurement results............................ 50
Figure 3-68. Probe's trace current coupling in simulation and measurement 50
Figure 3-69. Comparison of simulation and measurement coupling response................. 51
Figure 3-70. Pure PCB loop structure probe Vs complete differential H_z probe.............. 51
Figure 3-71. Comparison of complete probe and pure PCB probe.................................. 52
Figure 3-72. Common mode chock datasheet.. 53
Figure 3-73. The height from probe to the trace (Dz).. 53
Figure 3-74. Magnetic flux of the trace current 54
Figure 3-75. Probe's coupling frequency response with different Dz 54
Figure 3-76. Probe's effective coupling drops with Dz increase 55
Figure 3-77. Curve fit lines for 100MHz frequency coupling 55
Figure 3-78. Definition of Dx: sideways offset 56
Figure 3-79. To scale drawing of probe and trace parameters... 57
Figure 3-80. S21 as a function of frequency at different sideways offsets (Dx) 58
Figure 3-81. S21 magnitude vs sideways offset Dx for several frequencies 58
Figure 3-82. S21 magnitude vs. Dx variance @ 100MHz 59
Figure 3-83. Probe loop width + center shielding width 60
Figure 3-84. To scale drawing when Dx = 0, maximum coupling occurs........................ 60
Figure 3-85. To scale drawing when Dx = 1.9 mm, minimum coupling occurs 61
Figure 3-86. To scale drawing when Dx = 3 mm, 180 degree out of phase coupling 61

Figure 3-87. To scale drawing of simulation parameters 62
Figure 3-88. Probe's sideway spatial resolution for different trace width........................ 63
Figure 3-89. Magnetic fluxes crossing the loops concentrated on the trace edges........... 63
Figure 3-90. Dx varies from 0 to 1 mm when trace width = 2.8mm 64
Figure 3-91. Magnetic coupling of 0.1 and 0.5 mm wide trace....................................... 64
Figure 3-92. Dx = 1/2*(Probe_W+Probe_CW)) when Trace_W> Probe_W 65
Figure 3-93. Dx = 1/2*(Trace_W + Probe_CW)) when Trace_W > Probe_W............... 65
Figure 3-94. Probe_CW = Trace_W = 0.5 mm 66
Figure 3-95. Probe_CW = 0.5 mm, Trace_W = 0.1 mm 66
Figure 3-96. Probe_CW = 0.5 mm, Trace_W = 2.8 mm 67
Figure 3-97. Probe spatial resolution for different trace when Dz = 0.1 mm, ... 67
Figure 3-98. Probe spatial resolution for different trace when Dz = 0.5 mm 68
Figure 3-99. Top and side view of the differential H_z probe and trace............................. 69
Figure 3-100. Probe's coupling frequency responses during rotation 70
Figure 3-101. S21 magnitude vs probe rotation degree at several frequency points........ 70
Figure 3-102. To scale drawing of differential H_z probe and trace 71
Figure 3-103. Probe's coupling frequency responses during rotation 72
Figure 3-104. Probe's normalized directional response in several frequencies................ 72
Figure 3-105. Probe's E-field coupling of unshielded vias increase during rotation 73
Figure 3-106. The via's loop from this differential H_z probe 73
Figure 3-107. SPICE model of the differential H_z probe and coupling mechanism......... 74
Figure 3-108. Comparison between SPICE, full wave models and measurement 75
Figure 4-1. The block diagram of time domain scanning method................................... 77
Figure 4-2. TLP and oscilloscope scanning setup 78
Figure 4-3. Movie frames of time domain scanning raw data (X-orientation)................ 79
Figure 4-4. Movie frames with coupled trace current hardly visible............................... 80
Figure 4-5. Movie frames of time domain scanning raw data (Y-oriented) 81
Figure 4-6. The Frequency domain scanning method 82
Figure 4-7. Network analyzer scanning setup.. 83
Figure 4-8. TLP and NWA time domain waveforms 84
Figure 4-9. Movie frames of frequency domain scanning raw (X-oriented).................... 85

Figure 4-10. Movie frames of frequency domain scanning raw data (Y-oriented) 86
Figure 4-11. Probe frequency response compensation flow chart 88
Figure 4-12. Experimental setup of measuring H-Field strength in the TEM cell 89
Figure 4-13. Measured induced loop voltage on probe 90
Figure 4-14. Circuit model of field coupling 90
Figure 4-15. Comparison of S21 between measured and simulated coupling factors...... 91
Figure 4-16. The created compensation functions during deconvolution........................ 92
Figure 4-17. Comparison of recovered field strength and measured field strength.......... 93
Figure 4-18. Experimental setup for measuring voltage of the TEM cell 93
Figure 4-19. Trace current probe calibration method 94
Figure 4-20. Probe frequency coupling response of a differential H_z probe 94
Figure 4-21. Probe loss of a differential H_z probe 95
Figure 4-22. The created compensation functions during deconvolution........................ 95
Figure 4-23. Measured differential Hz probe voltage signal 96
Figure 4-24. Comparison of deconvoluted current and measured current....................... 96
Figure 4-25. Probe with deficient directional frequency response 97
Figure 4-26. Probe's normalized directional response in several frequencies................. 98
Figure 4-27. Probe with better directional frequency response 98
Figure 4-28. Probe's normalized directional response in several frequencies................. 99
Figure 4-29. Commonly measured orthogonal data set 100
Figure 4-30. Probe's Vx/Vy monotone decreasing curve... 100
Figure 4-31. Relations of Vx, Vy and V on the normalized directional response 101
Figure 4-32. 2D image of compensated Jy component... 102
Figure 4-33. Comparison of linear fixed and floating scale 103
Figure 4-34. 2D images of scanning data with different log scale color map factor 103
Figure 4-35. Vector visualization of current reconstruction scanning data 104
Figure 4-36. Linear interpolation effect of scanning data... 105
Figure 4-37. Current reconstruction viewer (GUI) 106
Figure 5-1. Top view of the PCB current injection model 107
Figure 5-2. Suspected influence factors for excitation ports 108
Figure 5-3. Boundary of the PCB ESD structure model 109

Figure 5-4. Free space around the excitation port 109
Figure 5-5. Frequency domain verification of excitation port on the structure 109
Figure 5-6. Frequency domain verification of port 2 coupling on the structure 110
Figure 5-7. Time domain verification of port 2 coupling on the structure 110
Figure 5-8. Simulated surface current on PCB ESD structure – top view 111
Figure 5-9. Simulated surface current on PCB ESD structure – side view 111
Figure 5-10. Simulated H-field on top side of PCB ESD structure 112
Figure 5-11. Simulated H-field on bottom side of PCB ESD structure 112
Figure 5-12. Simulated current density J_x distribution on top of the ground plane 113
Figure 5-13. Simulated field H_y distribution on top of the ground plane 113
Figure 5-14. Probes at different heights over the ground plane 114
Figure 5-15. Comparison of H_x component over ground plane with different heights .. 114
Figure 5-16. Jx from CST simulation 115
Figure 5-17. Jx from current reconstruction near-field scanning 115
Figure 5-18. Jy from CST simulation 116
Figure 5-19. Jy from current reconstruction near-field scanning 116
Figure 5-20. H-Field probe location in CST simulation 117
Figure 5-21. Comparison of reconstructed scanning result and simulation result 117
Figure 5-22. Position where sideway offset coupling response is measured 118
Figure 5-23. The local magnetic field coupling at trace cross section 118
Figure 5-24. Comparison of different probes in sideways offset response 119
Figure 5-25. Comparison of different probes in scanning area 120
Figure 5-26. Hx components over the PCB after ground plane injection 120
Figure 5-27. Hy components over the PCB after ground plane injection 121
Figure 5-28. Simulation analysis of the field components over PCB 121
Figure 5-29. Hz components dominated near board edges 122
Figure 5-30. Hz probe locations under differential Hz probe in simulation 123
Figure 5-31. Comparison of local Hz with or without differential Hz probe 123
Figure 5-32. The local H_z of cases with or without differential H_z probe 124
Figure 5-33. Comparison of port current with or without differential H_z probe 125
Figure 5-34. Local H_z component changes after putting a differential H_z probe 125

Figure 5-35. Comparison of simulated and reconstructed trace current in spreading 126
Figure 5-36. Comparison of simulated and reconstructed trace current 127
Figure 6-1. Excitation signal and modified frequency domain ESD gun 129
Figure 6-2 Injection location and ground strap connection at the Macbook 129
Figure 6-3. Shielded H_z field probe for near-field scanning 130
Figure 6-4. Measurement result showing injection is not started 130
Figure 6-5. Measurement result shows injection current reaches USB port.................. 131
Figure 6-6. Measurement result shows current and H_z field spreading at 0.3ns............. 131
Figure 6-7. Measurement result shows current and H_z field spreading 132
Figure 6-8. Measurement result shows current and H_z field spreading 132
Figure 6-9. Locate local response in current reconstruction viewer 133
Figure 6-10. Zoomed in to find resonance object and frequency 134
Figure 6-11. Correlated current reconstruction and resonance scanning results 135
Figure 6-12. Injection location of printer server 136
Figure 6-13. Printer server prepared for double side scanning 136
Figure 6-14. Network analyzer step function excitation 137
Figure 6-15. Board local sensitivity scanning result 137
Figure 6-16. System function layout for failure analysis 138
Figure 6-17. Max current density occurred during injection - top side 139
Figure 6-18. Max current density occurred during injection - bottom side 139
Figure 7-1. Predict of local response from excitation and scanning results 140

LIST OF TABLES

Page

Table 5.1. Measurement results of suspected influence factors for simulation 108

1. INTRODUCTION

Electrostatic discharge (ESD) can damage or disrupt a system. Researchers have approached the study of system-level ESD from different directions, such as ESD generator modelling [1], in-circuit measurements [2], air discharge analysis [3], numerical simulation of currents and fields, and protection circuit analysis.

One effective method of analyzing ESD robustness is to use a scanning system to localize ESD-sensitive areas or traces [4, 5, 6]. In conjunction with the circuit information the root cause of a system-level problem often can be fully understood.

As in near-field scanning, however, the connection between local results (e.g., a sensitive area or strong fields in near-field electromagnetic interference, or EMI scanning) and system-level performance is not obvious. To understand ESD one needs to understand which current densities, field strengths and derivatives are to be expected at a given location if an ESD is injected into a test point.

The sensitive areas found by near-field susceptibility scanning might not be those that receive a lot of current or field strength during an ESD. Thus, the current spreading during an ESD event needs to be known to connect local sensitivity data with system-level failures.

This thesis describes the methodology of an ESD current measurement technique that allows reconstructing the injected current spreading as a movie from the magnetic near-field scanning results. The development covers test structure design and current spreading / field coupling analysis; current scanning probe design, characterization, modeling, and optimization; implementation and analysis of time domain and frequency domain scanning methods; scanning raw data frequency and directional response compensation algorithm; current spreading visualization method and implementation; modeling of current injection structure and verification of current reconstruction results; applications and analysis of system-level current reconstruction scanning.

2. SIMPLIFIED PCB ESD STRUCTURE

To formulate a proof of concept for current reconstruction by near-field scanning methodology, the structure of the device under test (DUT) and the experiments based on it must be simple and meaningful. Figure 2-1 shows the printed circuit board (PCB) structure used here for concept proof measurement.

Figure 2-1. Layout of the PCB for ESD current spread scanning

The structure is a simple two layer PCB with three traces on the top layer and a solid ground plane on the bottom layer. Signal probing for all the traces can be performed via SMA male to male connectors on the back side of the PCB. The outer conductors of these connectors are connected to a very large aluminum ground. Current is injected via a coaxial connection on the edge of the ground layer to permit easy numerical modeling. Figure 2-2 shows the setup.

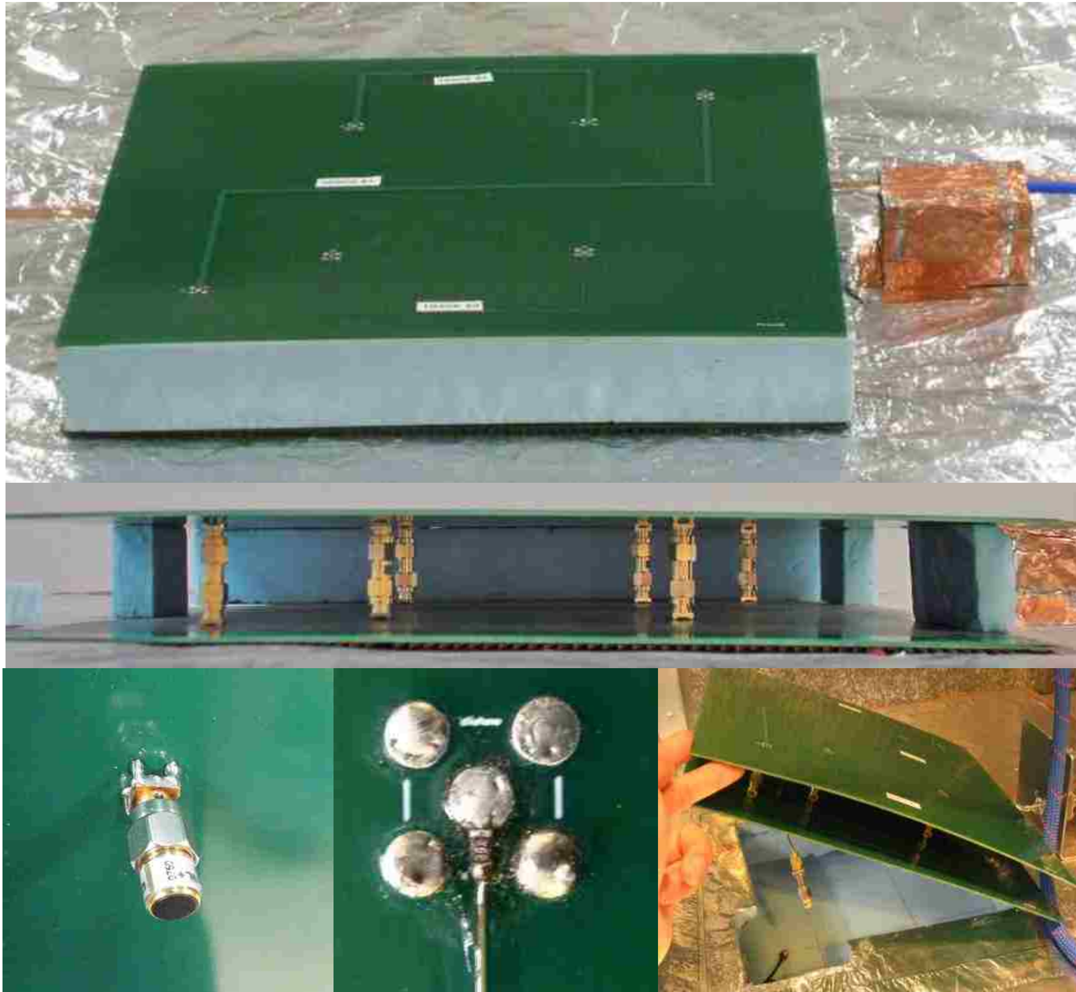

Figure 2-2. The simplified PCB ESD injection setup

In this ESD current injection setup, the injected current spreads from the coax center conductor through both sides of the ground plane. It returns via the outer conductors of the six SMA connectors down to the aluminum ground, then back to the injection cable through the injection structure. The spread and return of the current are shown in Figure 2-3 (top view) and Figure 2-4 (side view).

In this test setup, two types of current are generated during an ESD event: First, the current flows on the solid plane, which is directly injected. Second, the current runs on the traces, which are coupled from the injected current. The aim of the ESD current reconstruction scanning is to reconstruct the current density of the injected ground plane

surface current and the current magnitude of the coupled trace current using possible near-field scanning methods.

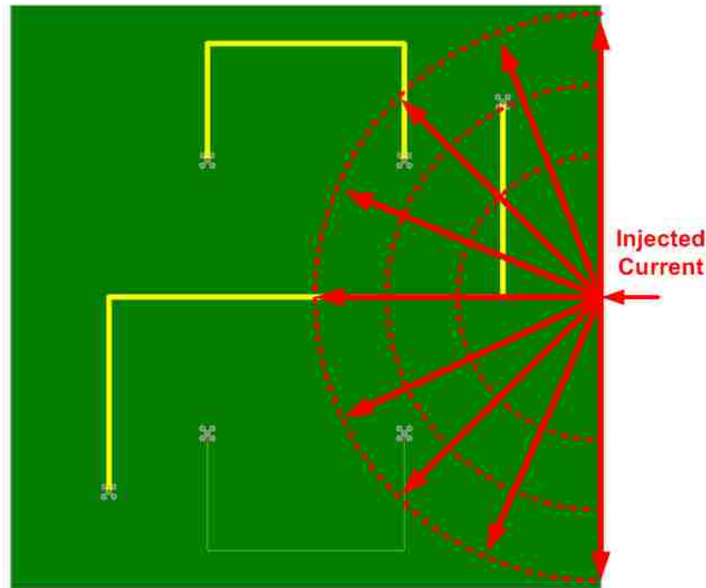

Figure 2-3. Injected current spreading on ground plane

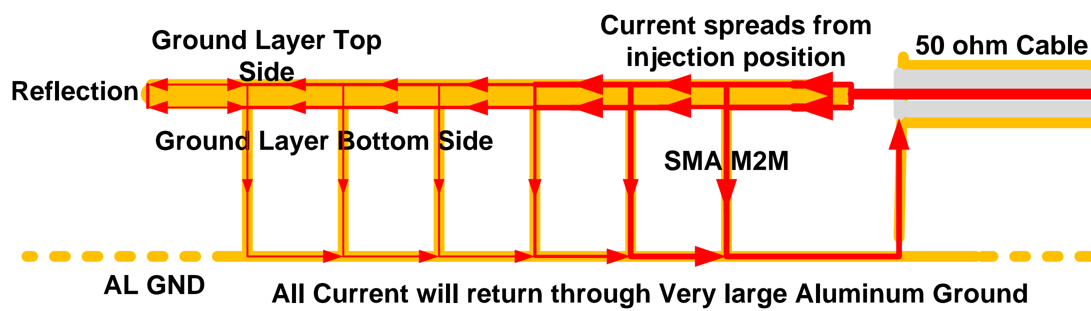

Figure 2-4. Current return of the test structure (side view)

3. PROBES FOR CURRENT RECONSTRUCTION

3.1. FIELD COUPLING DURING ESD

Before choosing a probe for ESD current reconstruction, the E-field and H-field coupling between the probe and the test structure during ESD event must be clearly understood. Figure 3-1 shows the injected current spreading on the top side of the PCB. Figure 3-2 and Figure 3-3 show the important field coupling paths around the probes.

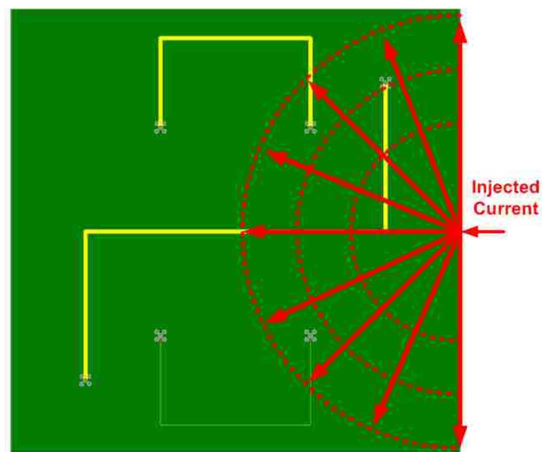

Figure 3-1. Injected surface current spreading

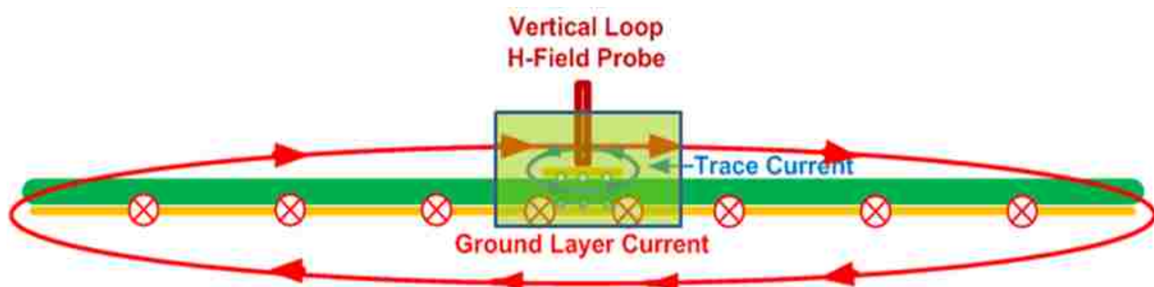

Figure 3-2. Current spreading and coupling around probe - side view

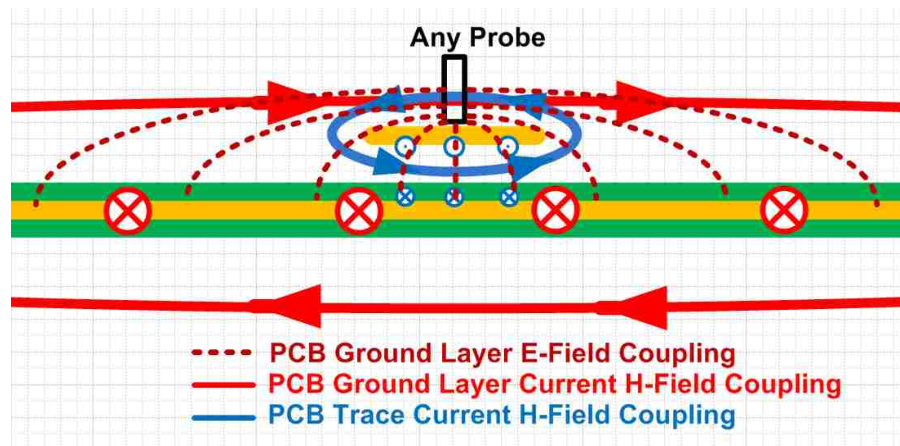

Figure 3-3. Most concerned coupling around a probe

The E-field coupling between the ground plane and any probe can be very strong, but it is not related to either type of current; therefore, the scanning current probe must suppress the E-field. If it does not, the E-field coupling might easily override the H-field coupling from the current.

The H-field coupling between the plane current and the probe directly reflects the current density on the ground layer, and the H-field coupling between the trace and the probe directly reflects the coupled trace current. Using a surface current probe measuring H_x and H_y can obtain the approximate plane surface current density. However, the magnetic fields from the traces currents are often much weaker than the magnetic fields from the ground layer surface current. Therefore, it is difficult to measure the trace currents by the same H-field probe for ground plane surface current.

Luckily, the local H_z components from the two types of current are not the same. The coupled trace current generates H_z components around it, especially around the trace edges. Whereas the injected surface current on the ground layer generates very weak H_z components on the center of the PCB. The trace current, therefore, can be measured by probing the H_z components on the PCB.

3.2. SURFACE CURRENT PROBE

The probe used to measure the surface current can be a shielded vertical-loop probe measuring H_x and H_y components. Since the H_x and H_y components generated from the coupled trace current are overwhelmed by the H_x and H_y components from the ground plane surface current. For following measurements in this thesis, coaxial shielded vertical-loop probes and multilayer PCB shielded vertical-loop probes are used to measure and reconstruct the ground plane surface current.

3.2.1. Structure.

The coaxial vertical-loop probe is shielded by its outer conductor as indicated by Figure 3-4.

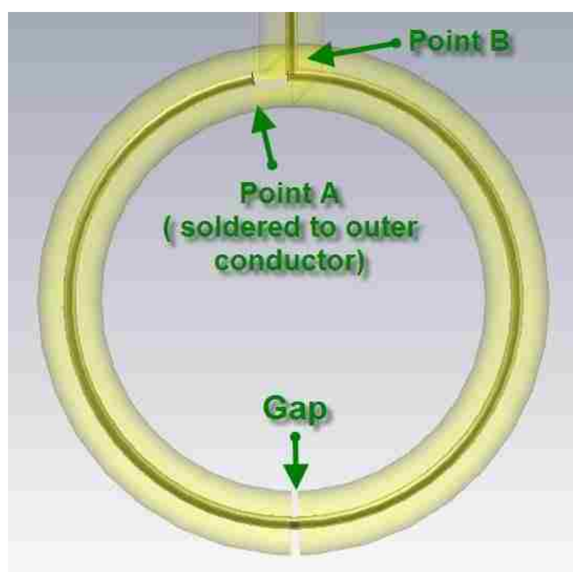

Figure 3-4. Shielded vertical-loop probe

From the structure, the loop of the probe is formed by its inner conductor. When H-field goes through the loop, it creates a voltage on the inner conductor loop (between point A and point B). The E-field is largely shielded by the outer conductor, except only

the exposed section of the inner conductor at the small gap in the outer conductor. This gap is intended only to remove the H-field shielding of the coax.

The shielding of the multilayer-PCB shielded vertical-loop probes is formed by outer layers, vias and slot plating, as shown in Figure 3-5. The corresponding "shielded loop" is a trace loop on an inner layer as shown in Figure 3-6.

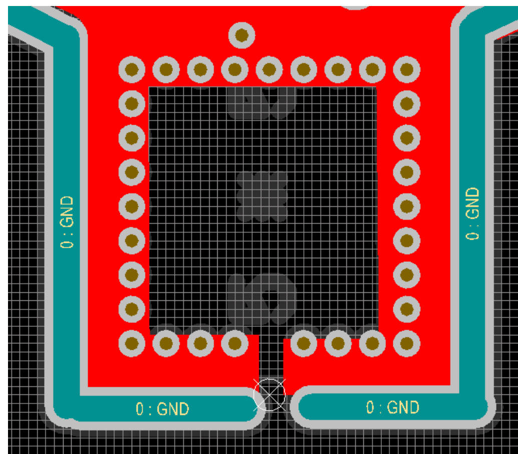

Figure 3-5. Out layer of a shielded PCB vertical-loop probe

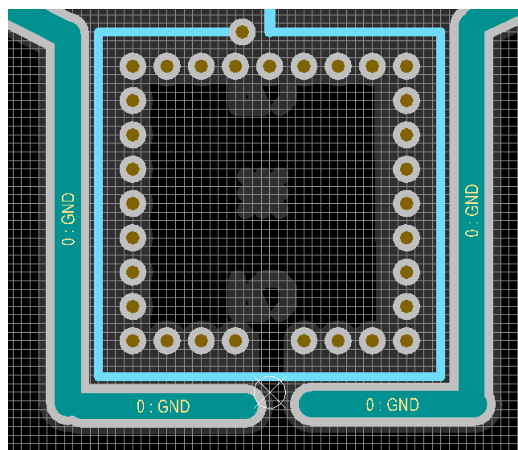

Figure 3-6. Inner layer of a shielded PCB vertical-loop probe

To further reduce E-field coupling and other common mode signal, ferrites can be added on the coaxial cable, as shown in Figure 3-7:

Figure 3-7. Finished coaxial probe and PCB probe with ferrites

3.2.2. Characterization. To successfully recover surface current density or field strength from probe's induced loop voltage signal, the understanding of a loop probe's characteristics is of great significance. A probe's transfer coefficient, loss and directional response need to be evaluated to estimate how well the surface current density or field strength can be recovered.

3.2.2.1 Directional Rejection. An important characteristic of a surface current probe is the directional rejection performance. An ideal surface current probe should response to the surface current flowing in the maximum coupling direction, and not response to the flowing current in the orthogonal direction. A directional rejection test is needed to check if the surface current probe rejects well to the surface current flowing on the orthogonal direction to its maximum coupling direction and if there is any other unwanted couplings.

A loop probe's directional rejection characteristics can be checked at locations where injected surface current flowing direction or local H-field direction are well known, such as a position near the current injection location or inside a TEM cell.

Figure 3-9 shows the measurement of a shielded single loop probe’s responses near the current injection location with its maximum and minimum coupling orientations. The loop size is about 40 mm^2. Figure 3-11 is the result comparison of such measurement. This probe shows acceptable directional rejection performance.

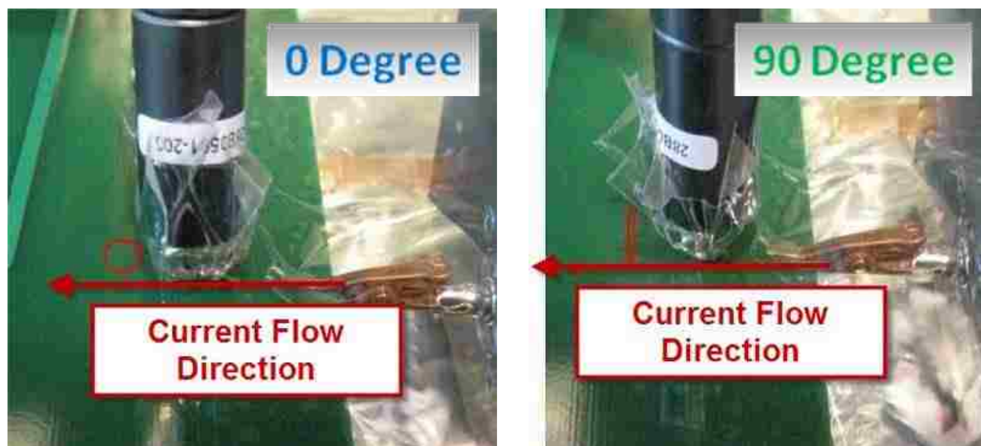

Figure 3-8. Shielded loop probe in maximum and minimum coupling orientations

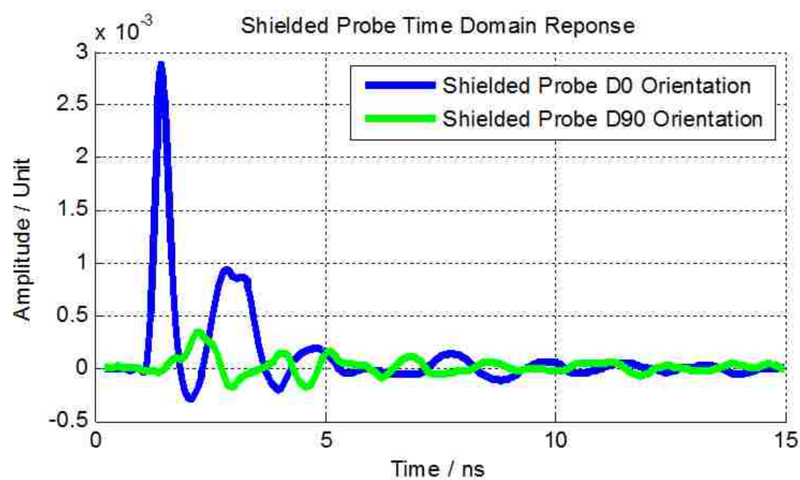

Figure 3-9. Shielded probe shows acceptable directional rejection characteristic

The same measurement is tested on an unshielded multiple loops probe. The measurement setup is shown in Figure 3-10 and the directional rejection performance is shown in Figure 3-11. This probe doesn't show an acceptable directional rejection performance.

Figure 3-10. Unshielded probe in max and min H-field coupling orientations

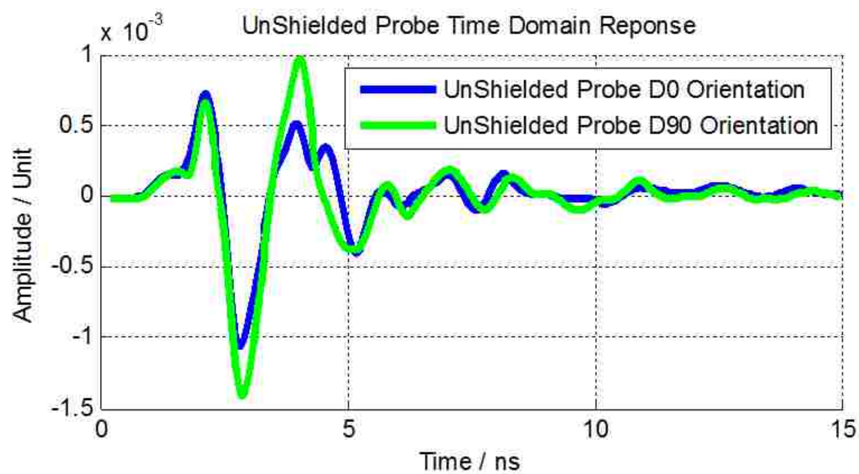

Figure 3-11. Unshielded loops probe shows nearly no directional rejection

At the maximum coupling orientation, a surface current probe detects both plane surface current coupling and the E-field coupling. At the orthogonal orientation, it should detect only the E-field coupling. Therefore from the waveform comparisons shown in Figure 3-11, the E-Field coupling can be much stronger than the plane surface current coupling during ESD current injection and can even dominate most peaks for unshielded loop probe. In brief, a shielded loop probe has acceptable directional rejection performance while an unshielded loop probe won't work for such scenario.

3.2.2.2 Coupling Factor. To use a probe to capture a transient magnetic field and recover it numerically, one must know the probe's magnetic coupling frequency response, or transfer coefficient, and then make sure that the probe has enough linear coupling bandwidth to cover the main spectrum of the transient magnetic field. A compensation function of the coupling frequency response can then be calculated to recover the main part of the transient magnetic field from induced loop voltage. A TEM cell experiment is conducted to measure the H-field coupling frequency response of a loop probe as shown in Figure 3-12:

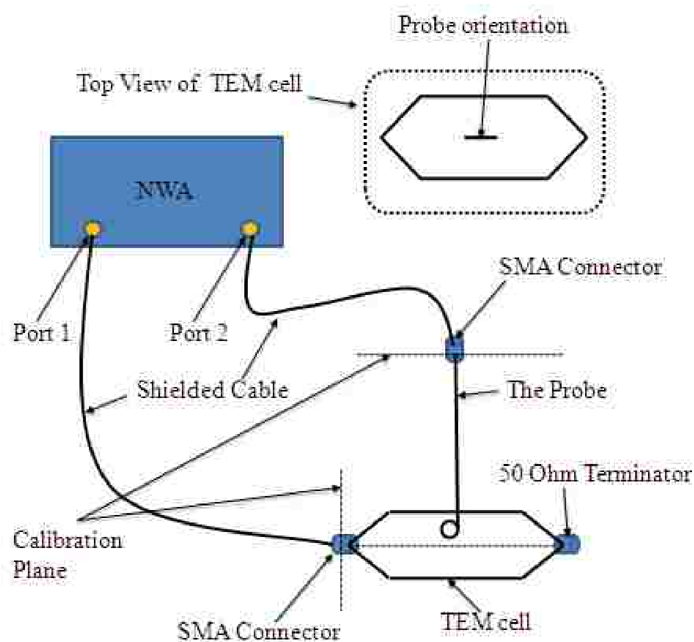

Figure 3-12. Experimental setup for measuring coupling frequency response

Inside a TEM cell, the E and H field can be calculated directly from excitation. The E-field strength equals excitation voltage / the distance between the TEM cell chassis and septum, and the H-field strength can be calculated by E-field strength / 377 Ohm.

A shielded loop probe is placed inside a TEM cell and orientated to the maximum coupling direction. This measurement will take the S21 data and use it to calculate the probe coupling frequency response. The H-field recover function of this probe will be mainly based on the linear region of this measurement, and then model the coupling frequency response and extended the response in frequency up to the resonance frequency. Figure 3-13 is the S21 measurement result of such experimental setup:

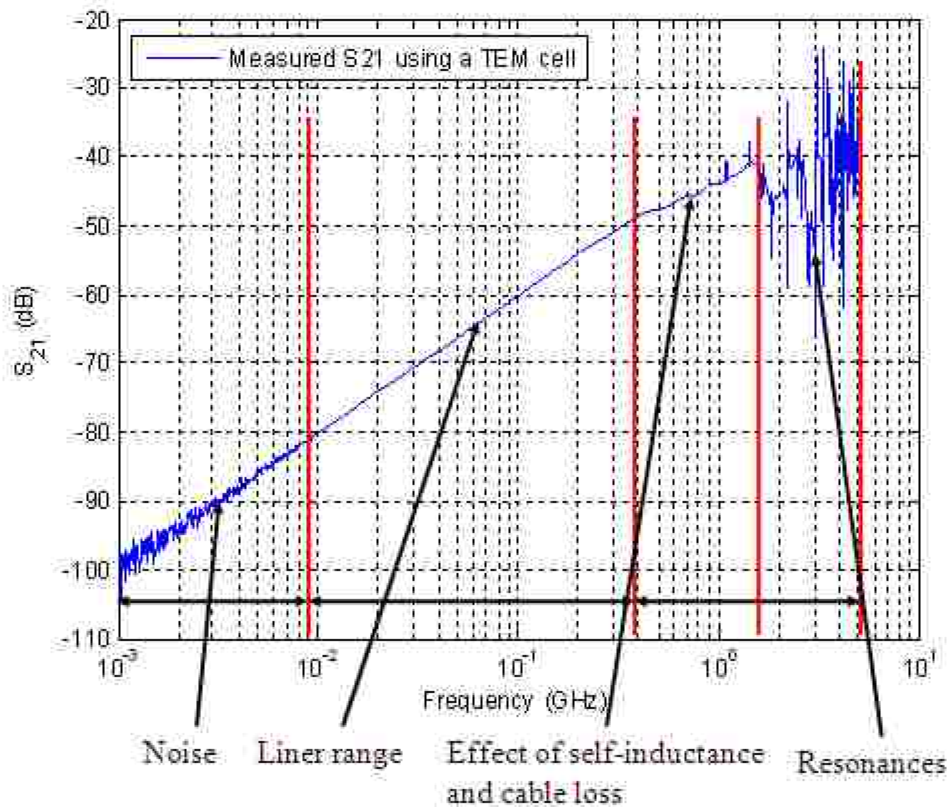

Figure 3-13. H-field coupling frequency response of a loop probe in TEM cell

The TEM cell does not perform over 1 GHz due to its none-TEM resonances. But the S21 result indicates not only the linear inductive coupling range and flat response range that are needed for coupling response modeling, but also the frequency ranges where noise or resonance occur. The H-field coupling response will be flattened out at high frequency due to the self and mutual inductance of a loop probe.

3.2.2.3 Cable Loss. The cable loss needs to be known for calculating the frequency compensation factor of the probe's H-field coupling frequency response. The reason is that the probe's calibration measurement contains the loss factor while the model of the loop inductive coupling response does not. To better model the probe's coupling response from calibration data and extend for wider frequency range, the probe's cable loss factor needs to be extracted.

The two type experiments can be conducted to measure the probe's loss factor. The first measurement is measuring the S11 data. The probe is hold in the air with no surrounding objects. The calibration is done on the plane of the SMA connector so that the S11 contains two times the cable loss plus the reflection at the loop. This is shown in Figure 3-14. The reflection of the loop will not be a nice short at high frequency so this will cause some error. At our case, the loop impedance at the interested frequency range (1 MHz to 2 GHz) is much smaller than 50 Ohm so this method works (The higher frequency components will be low passed in data process).

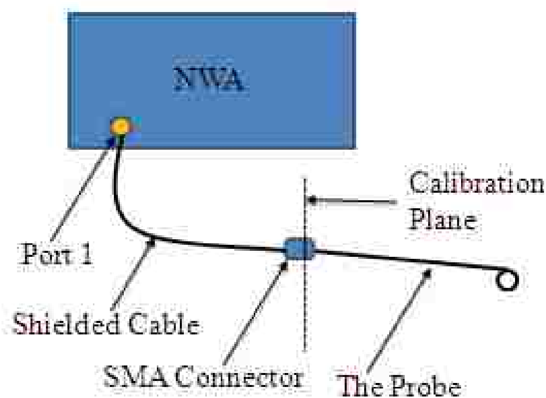

Figure 3-14. Experimental setup for probe's S11 measurement

A more common and precise way to measure the cable loss is deembed. The S parameters of two same type cables with different length are measured as shown in Figure 3-15. Then the cable loss and connector loss can be extracted precisely.

The results of two types probe cable loss measurement are shown in Figure 3-16. The deembed method shows better precision and the S11 method shows some ripple but overall the data is okay for current reconstruction measurement.

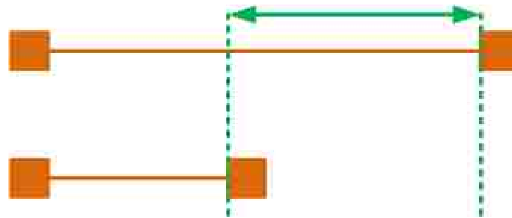

Figure 3-15. Deembed of cable loss

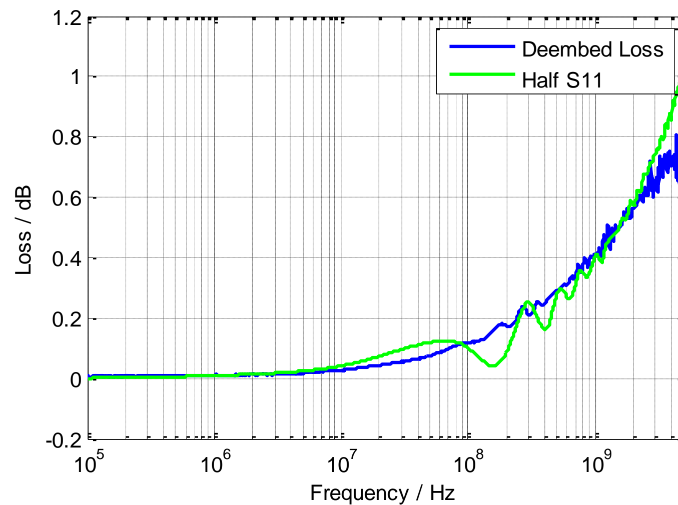

Figure 3-16. Measured loss of the probe cable

3.3. TRACE CURRENT PROBE

Conventionally, the H-field probe is based on one loop or multi-turn loops to capture H-field flux going through the probes; shielding can be made against E-field coupling from any other paths, but such probes will always get H-field coupling from both the surface current on planes and current on the traces:

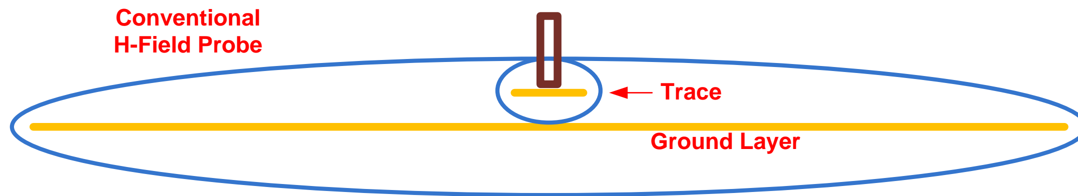

Figure 3-17. Conventional H-field probe and its H-field coupling

In this geometry and coupling paths, if current flowing on ground plane is much larger than current on the trace, the H-Field probe will only reflect current flowing on ground layer. (The result is based on a shielded loop probe; otherwise the E-field coupling which in the measurement was even larger than the H-field coupling from the ground layer will dominate). For such application, a differential Hz probe was designed to measure the coupled trace current during ESD injection.

3.3.1. Concept of Differential H_z Probe. The breakthrough point for measuring trace current in such scenario is to measure the difference of the H_z components around the trace. A differential turn loop pairs as Figure 3-18 would have such response to the trace current. A probe based on that structure would have much stronger response to trace current, but much less response to ground plane surface current due to the difference of flux curve shapes:

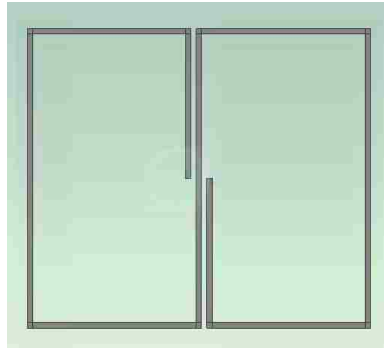

Figure 3-18. Differential turns loops structure

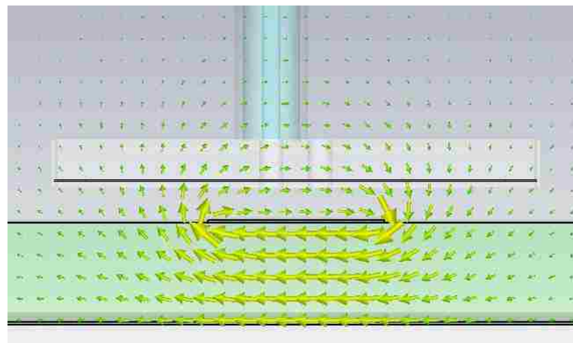

Figure 3-19. Differential turn loop captures H_z components of trace current

This dual loops structure was originated by Mr. Lim from Samsung and was build, tested, reviewed and improved by MST EMC Group.

3.3.2. Structure and Design. The first generation (pure loops) of the probe was not E-field shielded and failed to works as expected. However, several improvements ideas were implemented to make it works finally; the first improvement is the multilayer PCB shielding in Figure 3-20:

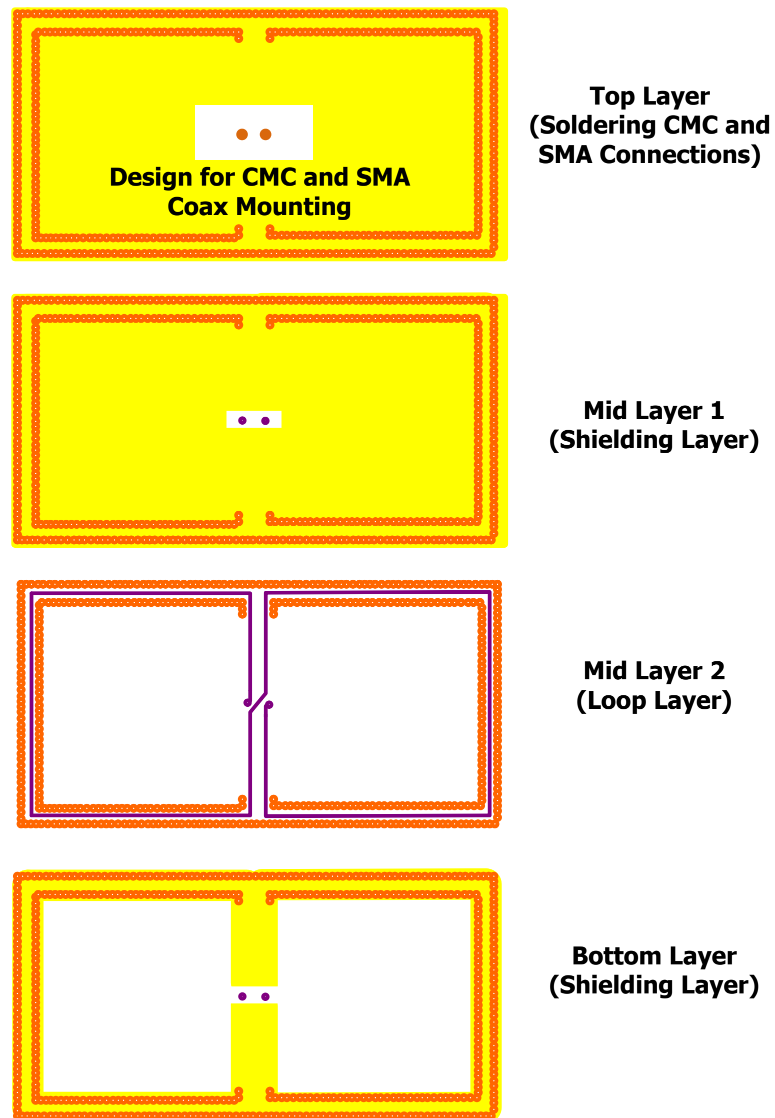

Figure 3-20. The 4 Layers pcb shielding for a differential turn probe

The top layer is shown in Figure 3-21. It is designed to mount common mode choke (CMC) and a supporting PCB. 2 pads in the center are designed for the coupling loop's connection to common mode chock. Other area is poured with copper for the soldering of supporting PCB and additional shielding.

Figure 3-21. Top layer (CMC connection layer)

Figure 3-22 shows the middle layer 1 - top shielding layer. This layer together with the bottom layer will shield the area near the 2 loops against E-field coupling and force magnetic flux going through the 2 loops. However, there is a gap in the center to allow ends of the loops go up to top layer for connection to CMC.

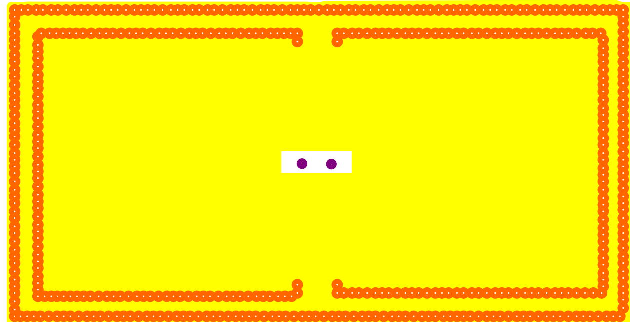

Figure 3-22. Middle layer 1 (top shielding layer)

Figure 3-23 shows the middle layer 3 - dual loops layer. Many plated vias or slots are designed around the loops for edge E-field shielding and connection between the top and bottom shielding.

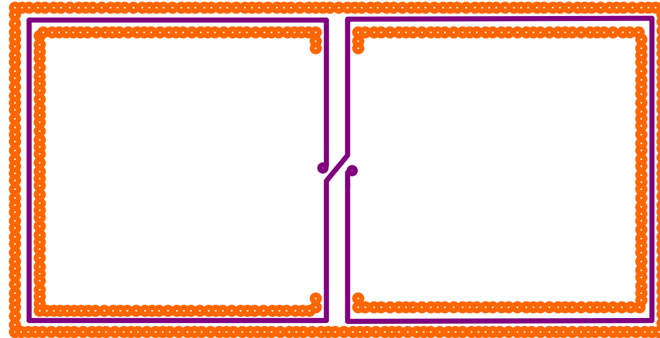

Figure 3-23. Middle layer 2 (dual loops layer)

Figure 3-24 shows the bottom shielding layer. It is similar to the top shielding layer expect the loop areas are opened for magnetic coupling and the center gap is designed against eddy current on the shielding.

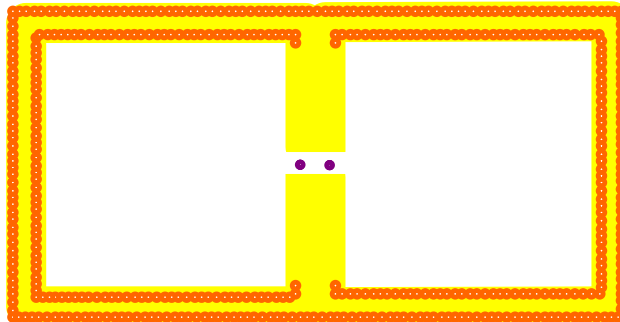

Figure 3-24. Bottom layer (bottom shielding layer)

Rejection for the common mode current on the dual loops probe is mainly achieved by putting a common mode choke. To reduce the turns (inductance) of the current path, the common mode check is directly soldering between the loop structure PCB and

semirigid SMA coaxial cable with a supporting PCB to support all of them as Figure 3-25 shows:

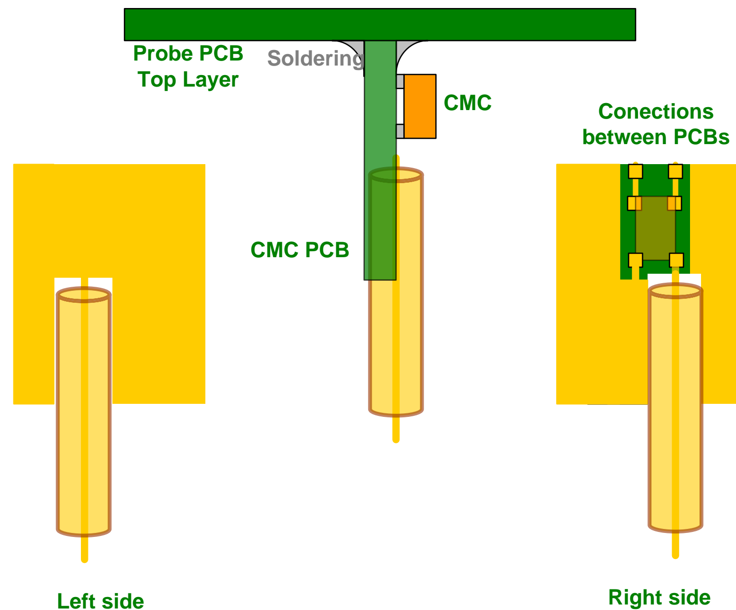

Figure 3-25. Supporting PCB with CMC for differential H_z probe

Additional common mode rejection is achieved by putting ferrites on the coaxial connection before connection of the shielding from copper tapes as Figure 3-26 shows. Those ferrites work similar to the common mode chock to suppress the common mode current on the dual loop structure. There will be a lot of common mode current on the shielding too but after the connection of the shielding to the coax cable, many more ferrites can be added.

There were 2 additional ideas for the common mode rejection but were not implemented due to the difficulty of mechanical works or cost. One idea is the hybrid method as Figure 3-27 shows. But only symmetric E-field coupling can be suppressed by this method. Another idea is using ferrites to guide the magnetic coupling of the plane surface current bypass the two loops of the probe as Figure 3-28 shows.

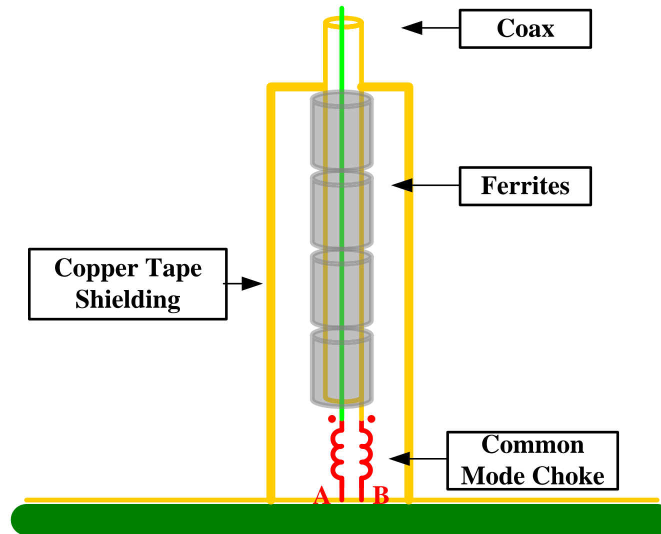

Figure 3-26. Ferrites on the coaxial connection

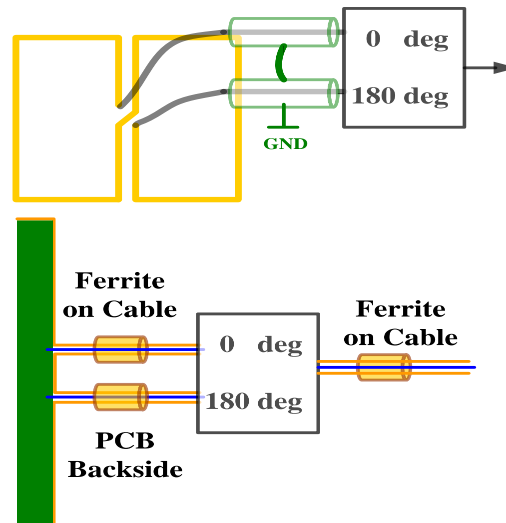

Figure 3-27. Hybrid method for common mode rejection

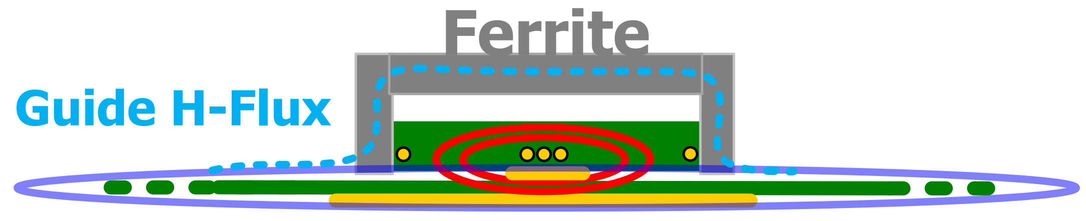

Figure 3-28. Using ferrite as H-field shielding

The different sizes and styles of the probe were designed and build as Figure 3-29 shows.

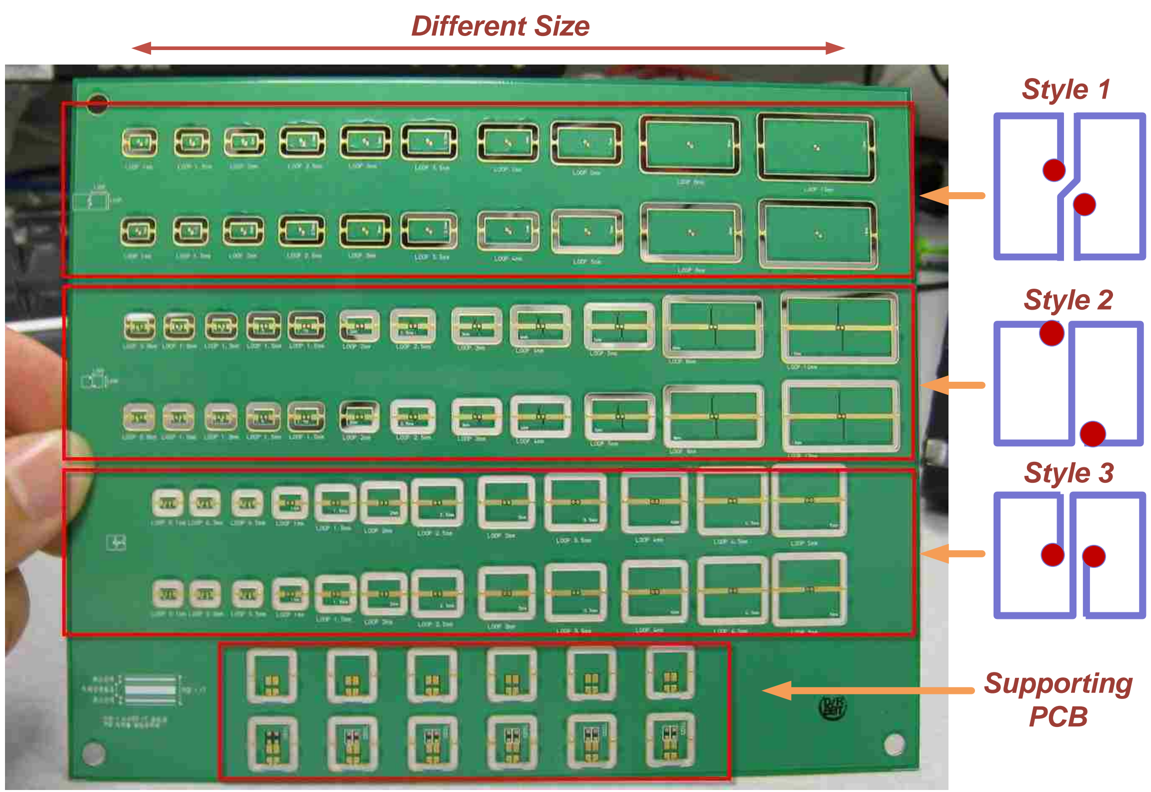

Figure 3-29. PCB of differential H_z probe

The detailed structure of the second version differential H_z probe is shown in Figure 3-30.

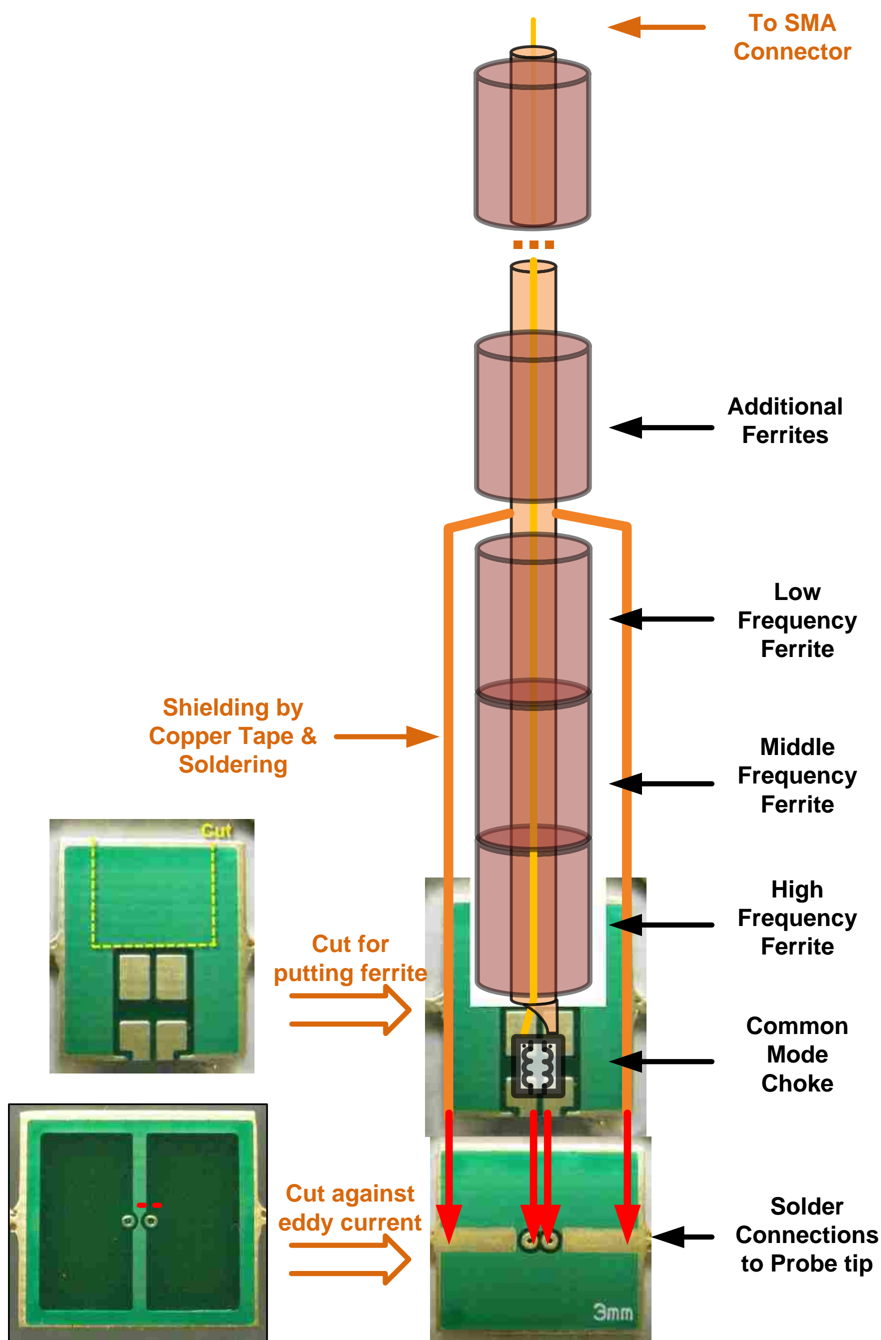

Figure 3-30. Detail structure of the second version differential H_z probe

Figure 3-31 shows the datasheet of the common mode chock selected for this probe (TCM1210H-500-2P). It features 8.5GHz cut-off frequency and self resonance higher than 3GHz. Figure 3-32 is a picture of an assembled differential H_z probe.

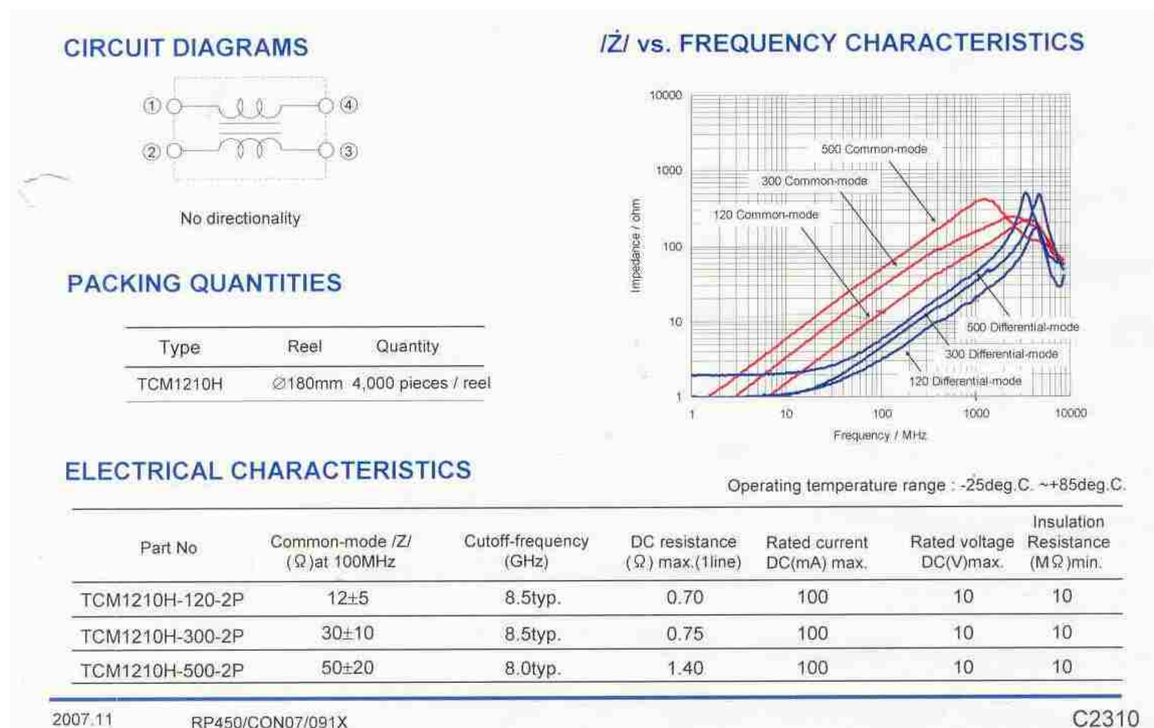

CIRCUIT DIAGRAMS

No directionality

/Ż/ vs. FREQUENCY CHARACTERISTICS

PACKING QUANTITIES

Type	Reel	Quantity
TCM1210H	∅180mm	4,000 pieces / reel

ELECTRICAL CHARACTERISTICS

Operating temperature range : -25deg.C. ~+85deg.C.

Part No	Common-mode /Z/ (Ω)at 100MHz	Cutoff-frequency (GHz)	DC resistance (Ω) max.(1line)	Rated current DC(mA) max.	Rated voltage DC(V)max.	Insulation Resistance (MΩ)min.
TCM1210H-120-2P	12±5	8.5typ.	0.70	100	10	10
TCM1210H-300-2P	30±10	8.5typ.	0.75	100	10	10
TCM1210H-500-2P	50±20	8.0typ.	1.40	100	10	10

2007.11 RP450/CON07/091X C2310

Figure 3-31. Datasheet of the common mode chock for differential H_z probe

Figure 3-32. Assembled differential H_z probe

3.3.3. Characterization. To successfully recover coupled trace current from the differential H_z probe's induced loop voltage. The understandings of this probe's characteristics, such as its RF current return paths, field coupling and rejection performance, sideway spatial resolution, coupling frequency response and coupling directional response are very important for current reconstruction purpose.

3.3.3.1 Self-Inductance. The self-inductance of the differential Hz probe is important to known for estimating its frequency coupling behavior, such as the inductance of the main coupling loops and non-coupling sections on the current return path. The common mode chock is one of the most important self-inductance factors because at high frequency, the impedance of the chock will increase and be comparable to the 50 ohm load and dramatically depress the frequency response and even cause resonance. The simplified circuit model is shown in Figure 3-33:

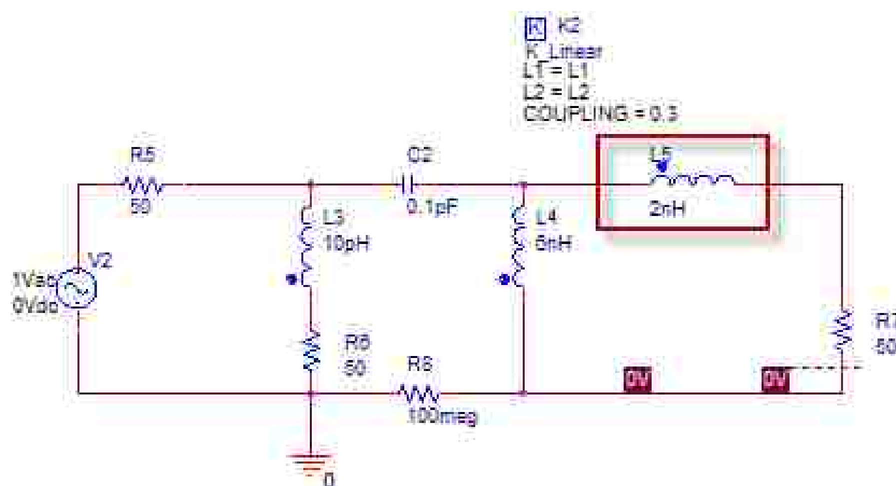

Figure 3-33. The Self-Inductance of the common mode chock on circuit model

The self-inductance of the probe can be measured by either a network analyzer, or TDR (time-domain reflector). The TDR measurement for sections of probe's current path is shown below. Figure 3-34 shows the experimental setup of TDR measurement.

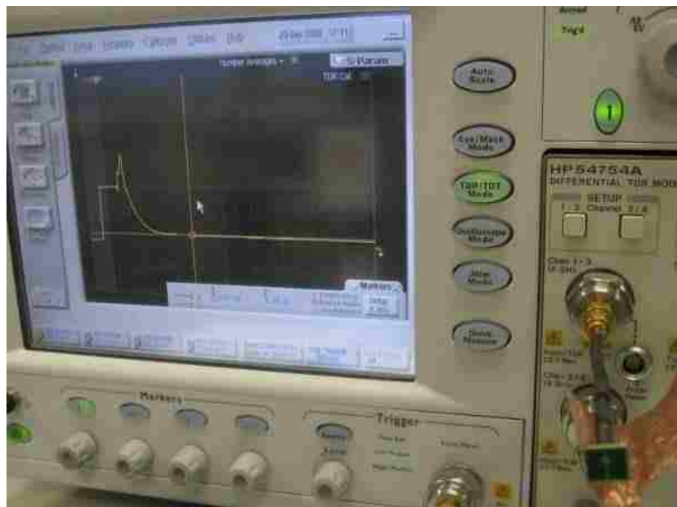

Figure 3-34. Experimental setup of probe inductance measurement by TDR

To measure only the inductance of the loop, the two vias of the loops was shorted so that the measurement reflects the current path of the probe excluding the loops (mainly common mode chock self-inductance), as Figure 3-35 shows:

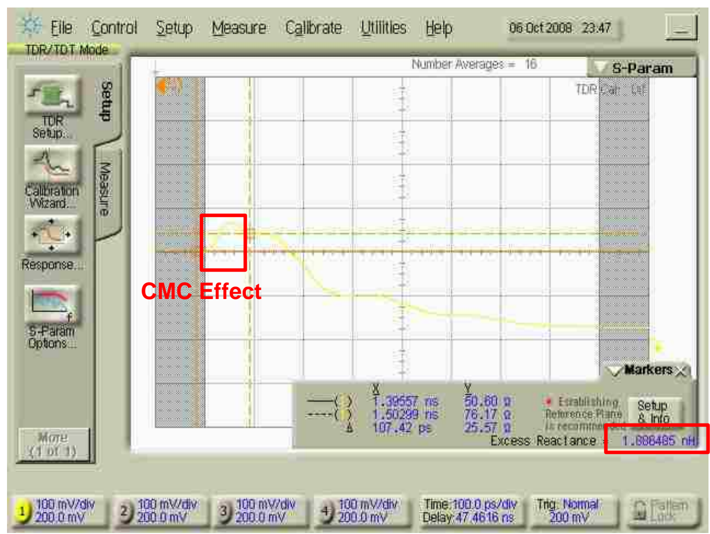

Figure 3-35. TDR measurement of common mode chock

Without shorting the vias of the loops, the current path of a 3mm wide loop probe is measured as Figure 3-36 shows. Then the current path of a 0.1 mm wide loop probe is measured as Figure 3-37 shows:

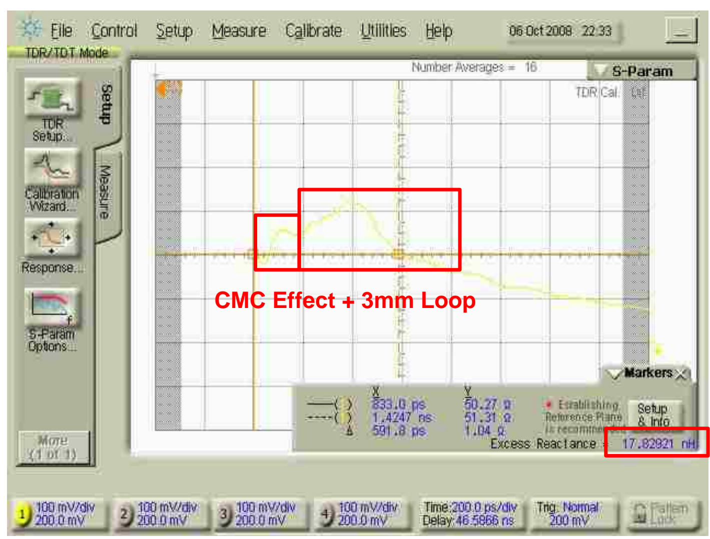

About 17.8 nH for CMC + 3mm Loop

Figure 3-36. TDR inductance measurement of CMC + 3mm loops

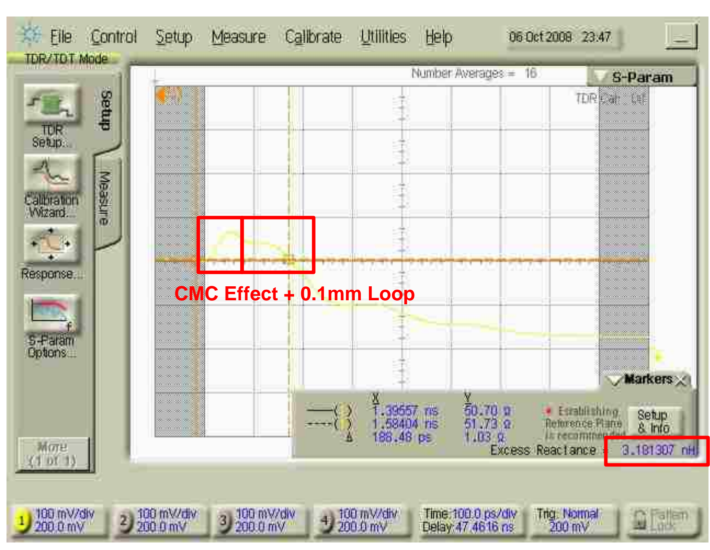

about 3.2 nH for CMC + 0.1mm Loop

Figure 3-37. TDR inductance measurement of CMC + 0.1mm loops

From the measurement, the self-inductance of the probe excluding the loops is around 2nH, at 1GHz its impedance will be around 13 ohm and will start to depress the frequency response. In addition, the common mode chock's differential current path has sharp resonance near 3-4GHz as previous data sheet shows, so the working frequency range of this probe is estimated to be up to 2 GHz.

3.3.3.2 Directional Rejection. Same as the surface current probe, the directional rejection is fairly important to correctly recover the current flowing directions from scanning. Figure 3-38 is the directional rejection measurement of the differential Hz probe. The D0 is the maximum coupling probe orientation and the D90 represents rotating the probe 90 degree, which is the expected minimum coupling response.

Figure 3-38. D0 response and D90 rejection measurement setup

The result of the directional rejection is shown in Figure 3-39. From the result above, the 90 rejection is around 30 dB, pretty good for the 3 mm wide loop differential Hz probe. After 200MHz, the effects of the dielectric loss, probe self and mutual inductance are starting depress the frequency response, and the resonance occurs at 3GHz, which is properly caused by common mode chock. However, the probe still has inductance coupling during D90 orientation (20 dB per decade increase frequency

response), this is due to the probe vias' loop, and detailed analysis is at simulation analysis part.

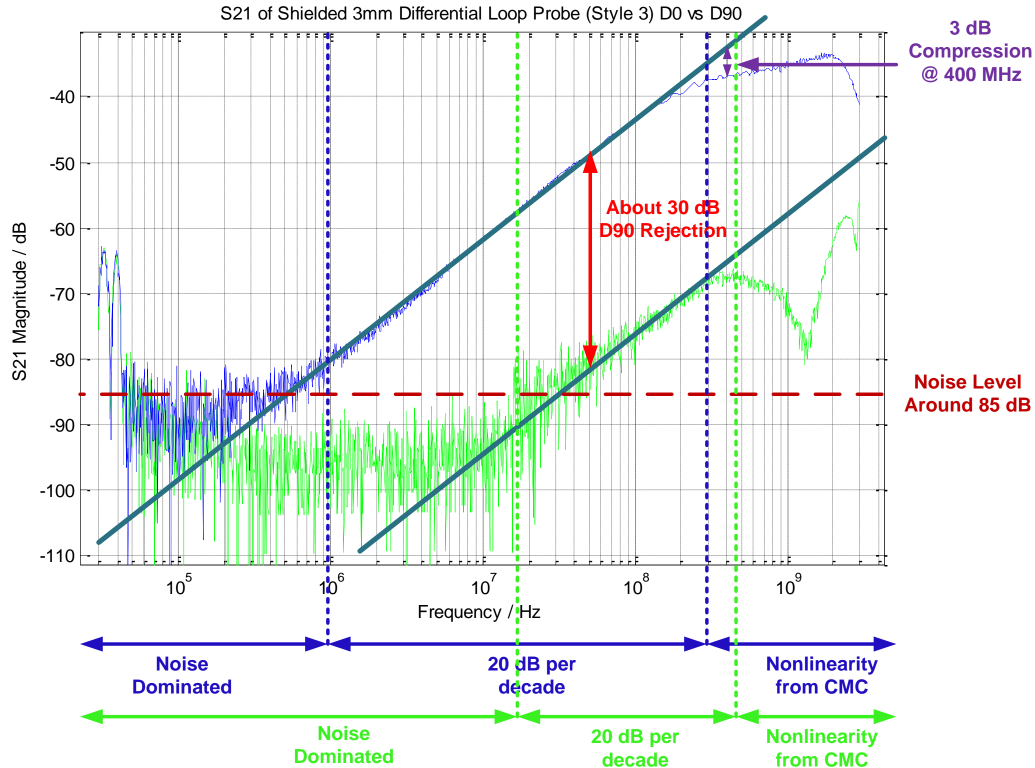

Figure 3-39. D0 response and D90 rejection measurement result

3.3.3.3 Sideway Spatial Resolution. Spatial resolution is how well the probe can resolve the field strength in space. For the case of differential Hz trace current probe, the sideway spatial resolution for trace current coupling is important to resolve the trace current during scanning.

The experimental setup of using probe station for sideway spatial resolution measurement is shown in Figure 3-40**.** The probe was adjusted to maximum coupling orientation as good as possible (the station can rotate slowly), then the S21 frequency response is recorded for every small steps the probe moved sideways, as Figure 3-41 shows.

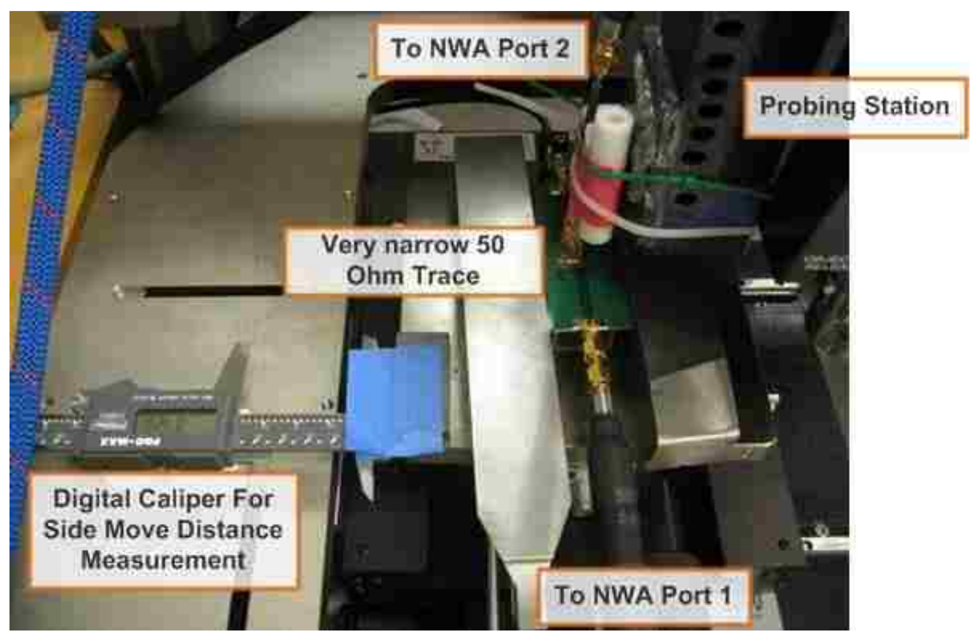

Figure 3-40. Sideway spatial resolution measurement setup

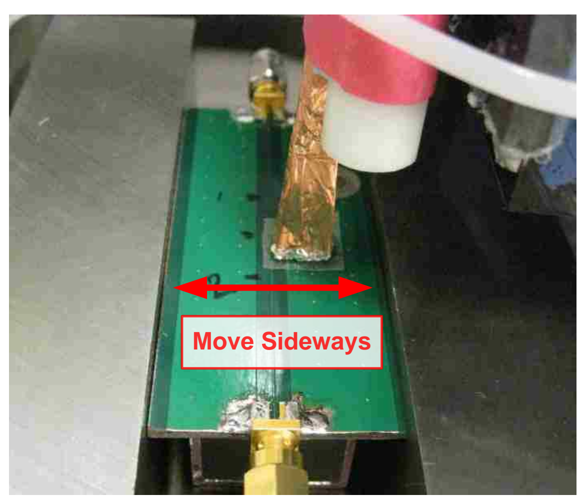

Figure 3-41. Sideways movement

The sideways offset distance is measured by a digital caliper which has resolution up to 0.01mm. The trace width for this measurement needs to be as small as possible as the trace width determines the resolution of this measurement. The trace used for this

sideway spatial resolution is around 0.1 mm wide. The recorded data were plotted at a single frequency in the probe's linear region against its sideway offset distances as Figure 3-42 shows:

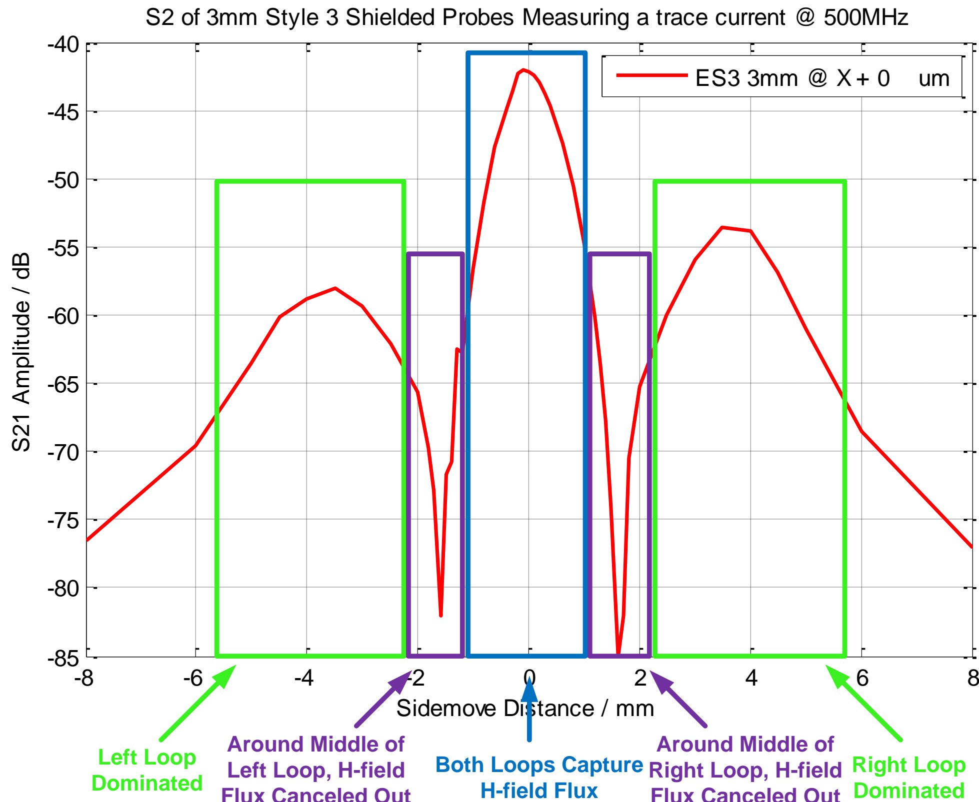

Figure 3-42. Spatial resolution of 3mm wide loop probe at touching distance

The result above shows the 3 dB drops spatial resolution is about 0.6 mm, which is very good for a 3 mm wide loop probe. There are 2 unusual effects for the spatial resolution result. First, the coupling drops to noise level shapely when trace is under one loop of the probe. Second, there are 2 side peaks around 12 dB lower in magnitude than the center peak of the center peak. Considering the probe structure, the positions of the loops and the S21 spatial resolution results, such coupling mechanism is in those 3 cases.

3.3.3.3.1 Both Loops Couple Trace Current. When the trace center is right under the middle of the probe, the magnetic flux of the trace current will cross both probe loops so the probe get the maximum coupling as the Figure 3-43 shows:

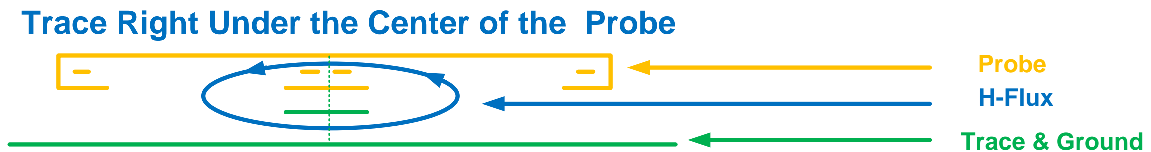

Figure 3-43. Both loops couple trace current

3.3.3.3.2 Trace Current Coupling Cancels Out. When the trace center is under one loop of the probe, magnetic flux from the trace current gets a chance to cancel out the coupling when the magnetic flux goes in and out of the one loop are equal as Figure 3-44 shows:

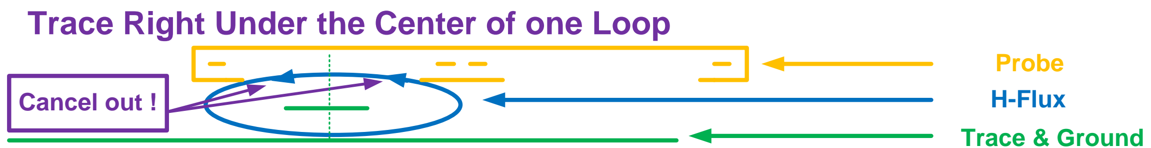

Figure 3-44. Trace current coupling cancels out

3.3.3.3.3 One Loop Coupling Dominates. When the probe moves farther than the trace current cancels out distance, the magnetic flux goes in the opposite direction of case 1 for one loop and the trace current coupling shows up again as Figure 3-45 shows:

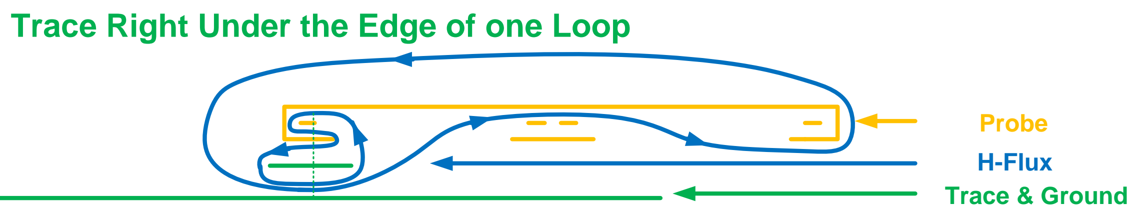

Figure 3-45. One loop coupling dominates

Figure 3-46 shows a measurement to testify the explanation by measuring S21 magnitude and phase in the linear coupling region at the same time with network analyzer zero band setup while move the probe across a trace. It shows the phase change of 180 degree right after the coupling cancelation locations (two dips highlighted in green lines).

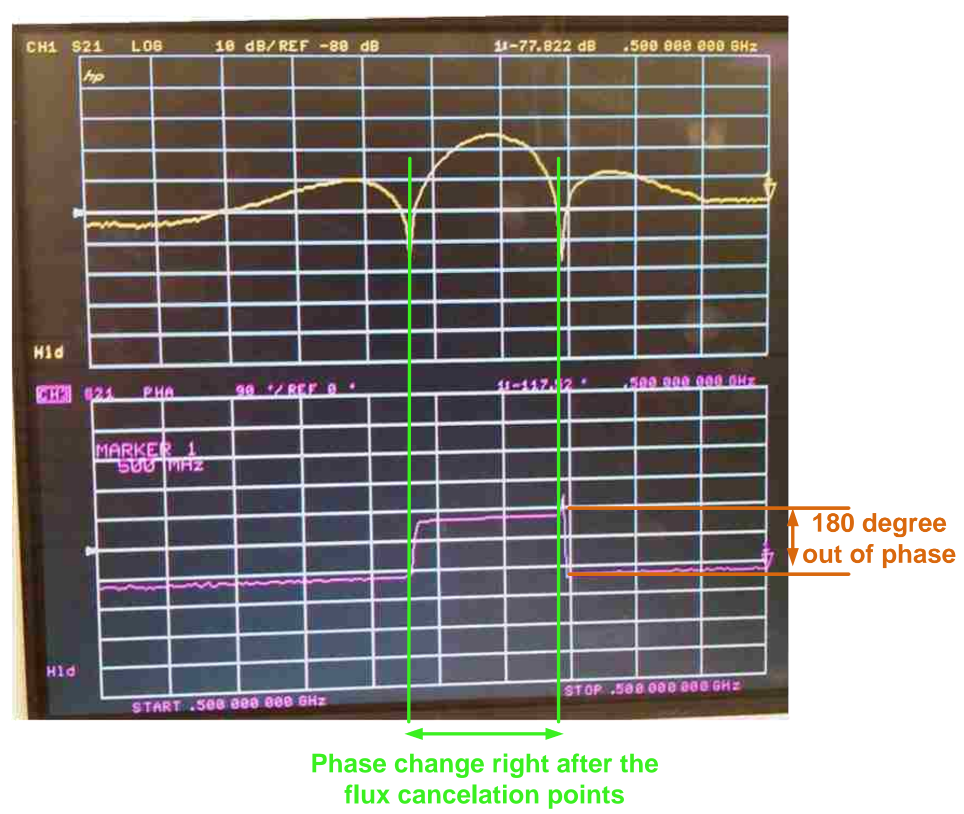

Figure 3-46. Magnitude and phase measurement while moving probe sideways

The probe's sideway spacial resolution for trace current measurement changes with the height from probe to trace due to the distribution of the magnetic flux from trace current. Figure 3-47 shows a comparison of a differential H_z probe's sidway spacial resolution at different hieight.

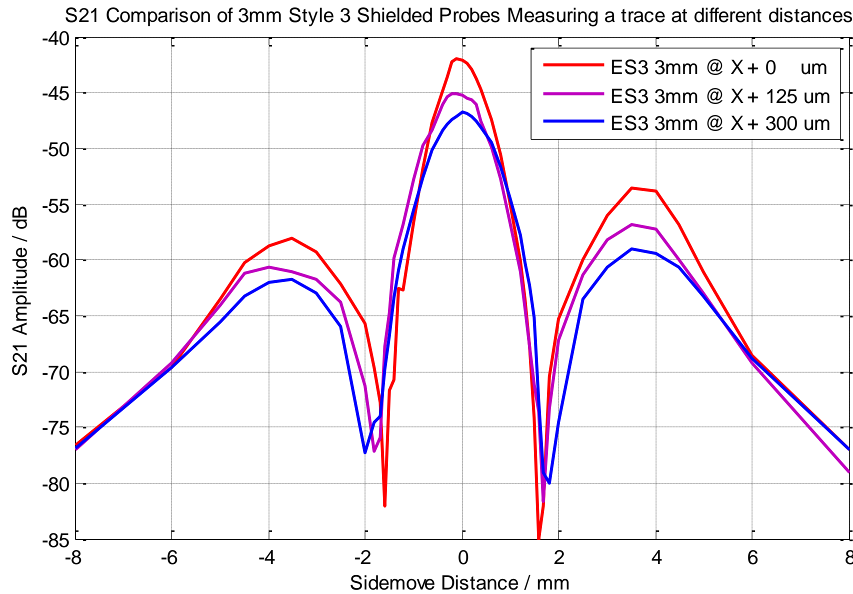

Figure 3-47. Sideway spatial resolution decreases with probe's height increases

From this measurement results, the current coupling decreases a lot and the sideway spatical resolution decreased somewhat for just 300 um distance. This indecates that puting the probe closer to trace is pretty effective for the incease of both probe's trace current coupling sensitivity and sideway spacital resolution.

3.3.3.4 Common Mode Rejection. To make sure the measurement of the differential H_z probe couples to the current of trace right under it with enough rejection to other coupling sources, such as injected plane surface current under the trace, reflected or flapped current around the board edges and strong E-field coupling from the plane, (In here, these couplings are considered as common mode coupling because they are

undesired couplings relative to the trace current coupling) the probe's common mode rejection needs to be well evaluated for measurement validation.

3.3.3.4.1 Plane Surface Current Coupling Rejection. Since the differential H_z probe is designed to reject surface current coupling and response to trace current coupling, the rejection needs to be evaluate. In the following analysis, a method to evaluate the rejection is performed by comparing the coupling of shielded vertical-loop probe and shielded differential Hz probe to injected surface current.

The rejection performance will change depends on several parameters, such as the location above the plane with injected surface current, and loop size and via size of the differential Hz probe, and the trace coupling factor for Deconvolution. Therefore, the surface current coupling rejection ability of a differential H_z probe during scanning the initial ESD injection setup is evaluated by comparison of it's coupling to the coupling of a shielded loop probe (no surface current coupling rejection) with their trace current coupling compensation. The comparison process is shown in Figure 3-48:

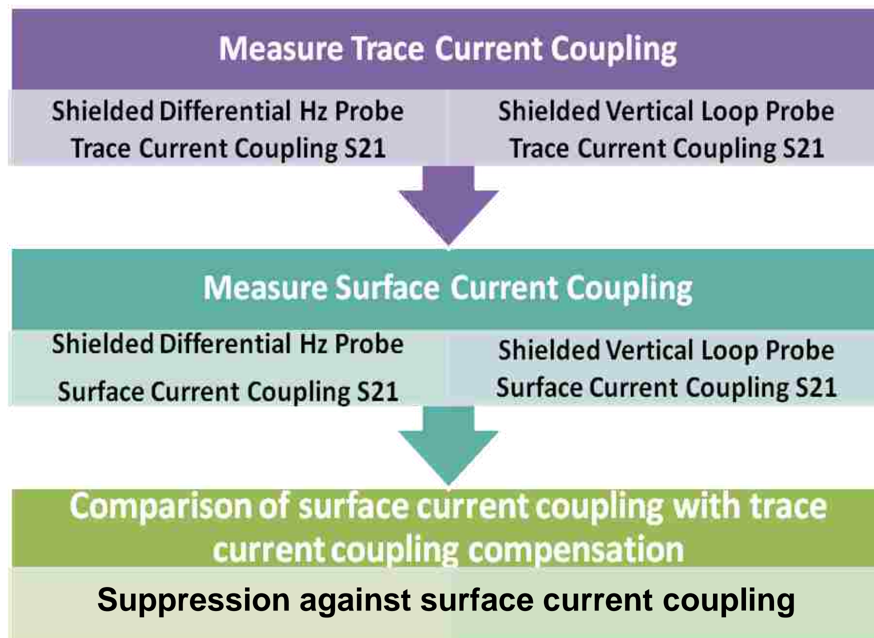

Figure 3-48. Evaluation process of plane surface current coupling

The trace current coupling is the probe's factor to trace. The detailed measurement and results are discribed in 3.3.3.5. The results are below:

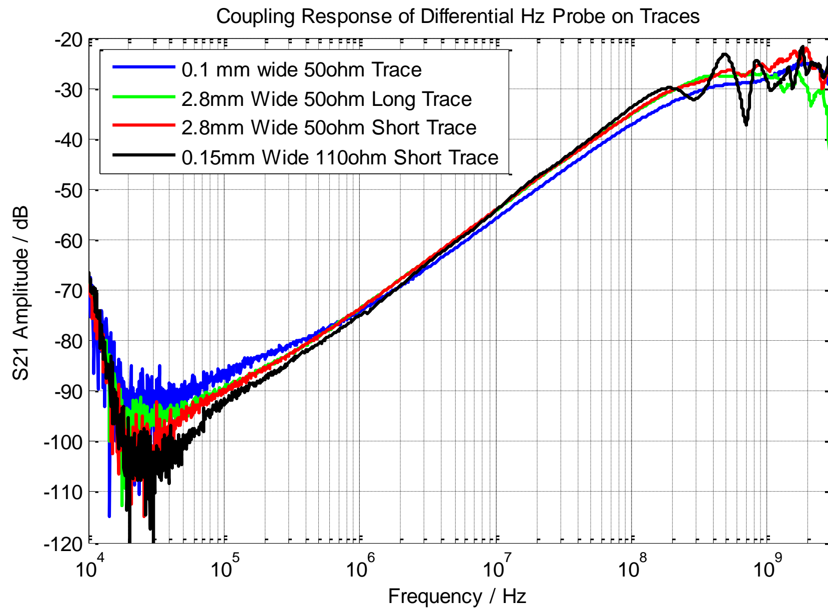

Figure 3-49. Trace current coupling for differential H_z probe

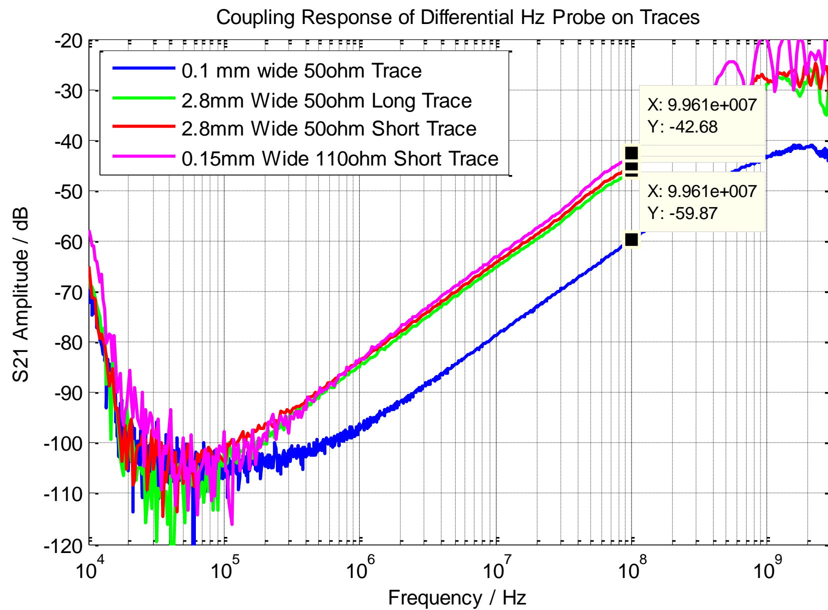

Figure 3-50. Trace current coupling for shielded vertical-loop probe

The area for surface current coupling test is shown in Figure 3-51:

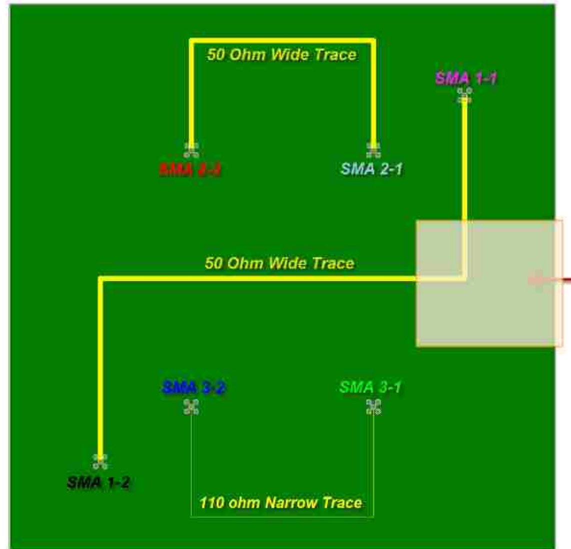

Figure 3-51. Area for surface current coupling rejection test

Location and orientation of the probes during surface current coupling rejection analysis is shown in Figure 3-52:

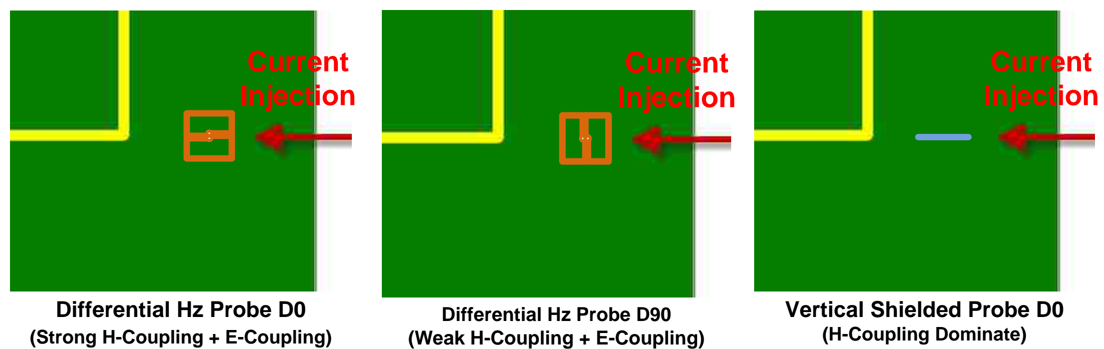

Figure 3-52. Locations and orientations of the probes during analysis

From the left picture (differential Hz probe D0 orientation), injected current right under the probe is flowing left, so the current coupling is maximized by such orientation. Such coupling from the ground layer will be minimized if probe is putted perpendicular to the injected current flow direction (differential Hz probe D90 orientation) as the middle picture. The differential Hz probe's coupling is in D90 orientation needs to be check for the probe's dynamic range of its trace current coupling over suppressed H- and E-Coupling and reflected current coupling. The right picture shows the shielded vertical-loop probe is put in the maximum coupling orientation. The S21 results from the injection port to the probe are plot in Figure 3-53:

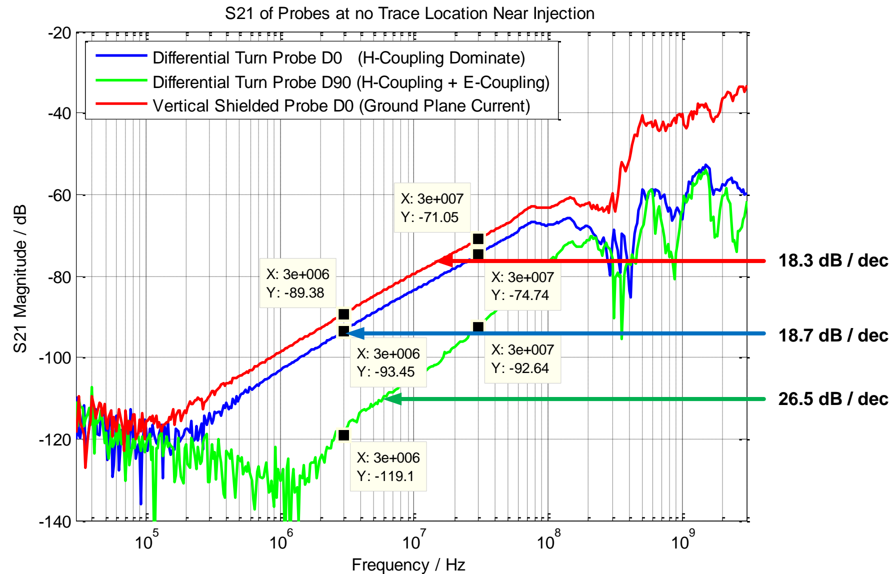

Figure 3-53. The S21 results of ground current coupling into the two probes

Both the S21 results of shielded loop probe and differential Hz probe in D0 orientation show around 20dB/dec increases, indicating they are dominated by H-field coupling. The S21 of differential Hz probe in D90 orientation shows about 26.5 dB/dec increases, indicating it is dominated by both E- and H coupling. The S21 couplings are related to current by probe factor in frequency domain as below:

$$m_{probe} = \frac{10^{\frac{S_{21}probe(dB)}{20}} \times Z_0}{2\pi f}$$

$$I = \frac{V_2}{j2\pi f \times m_{probe}}$$

$$S_{21}SurfaceCurrent = \frac{V_2}{V_1} = \frac{V_2}{\frac{1}{2}V_{source}} = \frac{V_2}{\frac{1}{2}I \times 50}$$

Note: m_{probe} is the equivalent mutual inductance between trace and probe, $S_{21}probe(dB)$ is the S21 from one port of a match trace to the probe measuring the trace current, Z_0 is the characteristic impedance of the trace, I is the trace current, V_2 is the probe induced loop voltage, $S_{21}SurfaceCurrent$ is the surface current coupling of the probe measured in Figure 3-53. The third equation works when the injection of the structure can be treat as a short. Figure 3-54 is the S11 of the injection port. Structure resonance occurs over 300MHz and the comparison won't work over 300 MHz.

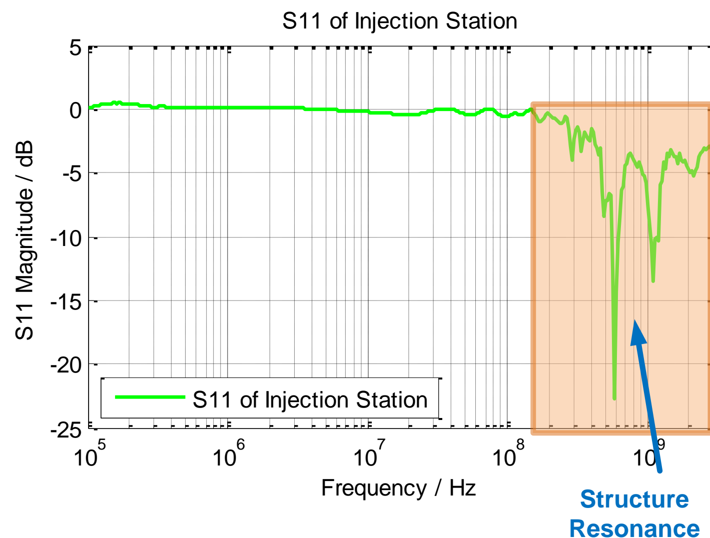

Figure 3-54. S11 of the simplified ESD injection structure

The simplified surface current coupling circuit model is shown in Figure 3-55. The current path of the PCB ESD structure is very complex. For here it is simplified into two paths - top and bottom surface and generally works as a passive network.

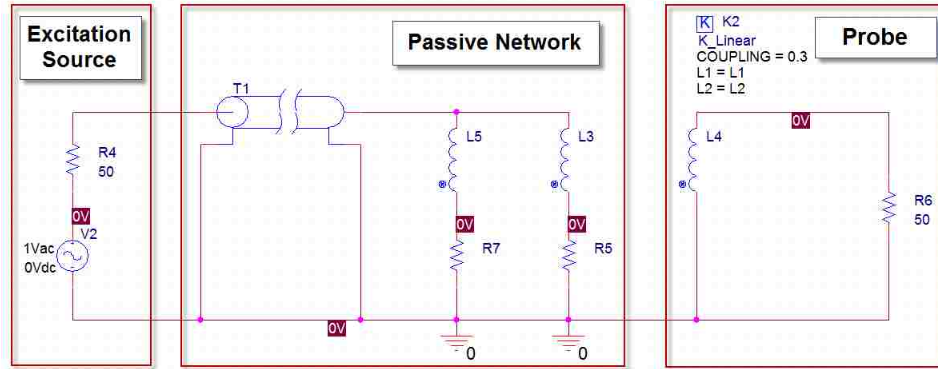

Figure 3-55. Surface current coupling circuit model

The ratio of the coupling on the shielded loop probe and differential H_z probe is not related to the details of the network as it is passive. Equation of the ratio is followed:

$$\frac{I_{Ver_equ}}{I_{Dif_equ}} = \frac{\dfrac{V_{port2_Ver_Coupling}}{2\pi f \cdot m_{Ver}}}{\dfrac{V_{port2_Dif_Coupling}}{2\pi f \cdot m_{Dif}}} = \frac{\dfrac{\frac{V_{port2_Ver_Coupling}}{V_{port1}}}{2\pi f \cdot m_{Ver}}}{\dfrac{\frac{V_{port2_Dif_Coupling}}{V_{port1}}}{2\pi f \cdot m_{Dif}}} = \frac{\dfrac{S_{21_Ver_Coupling}}{2\pi f \cdot m_{Ver}}}{\dfrac{S_{21_Dif_Coupling}}{2\pi f \cdot m_{Dif}}} = \frac{\dfrac{S_{21_Ver_Coupling}}{S_{21_Ver_probefactor} \times R}}{\dfrac{S_{21_Dif_Coupling}}{S_{21_Dif_probefactor} \times R}}$$

$$= \frac{S_{21_Ver_Coupling} \times S_{21_Dif_probefactor}}{S_{21_Dif_Coupling} \times S_{21_Ver_probefactor}}$$

Processed surface current coupling suppression ratio from the equation above over the measurement frequency range is shown in Figure 3-56:

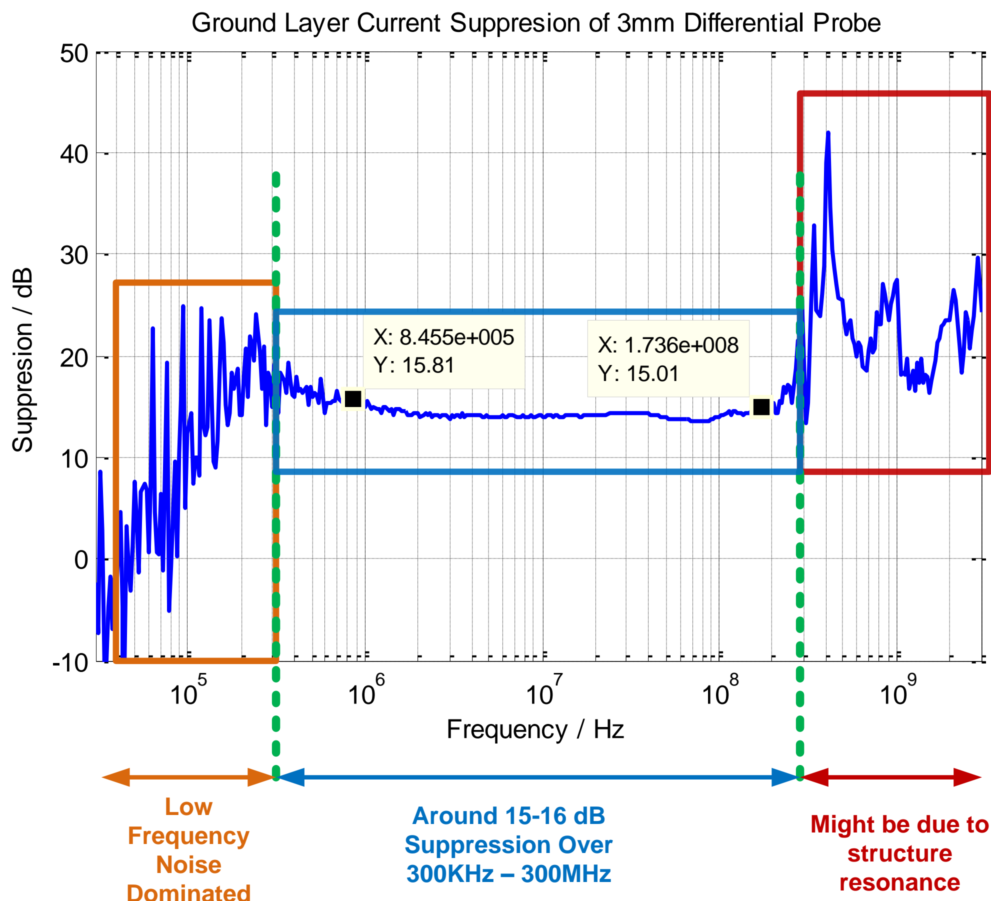

Figure 3-56. Calculated surface current coupling rejection

The comparison result shows this differential H_z trace current probe has roughly 15 dB rejections for the injection surface current. Such rejection is not a perfect rejection of plane surface current coupling, but it allows some of the coupled trace current to be visible after scanning. More detailed analysis of such rejection will be discussed at simulation verification process in section 5.3.

3.3.3.4.2 Plane E-Field & Edge Current Coupling Rejection. Couplings of the differential Hz probe at several positions where plane E-Field or edge current H-field coupling dominates are measured to verify the probe's dynamic range under the cross talk of those rejections. Positions of probe are shown in Figure 3-57:

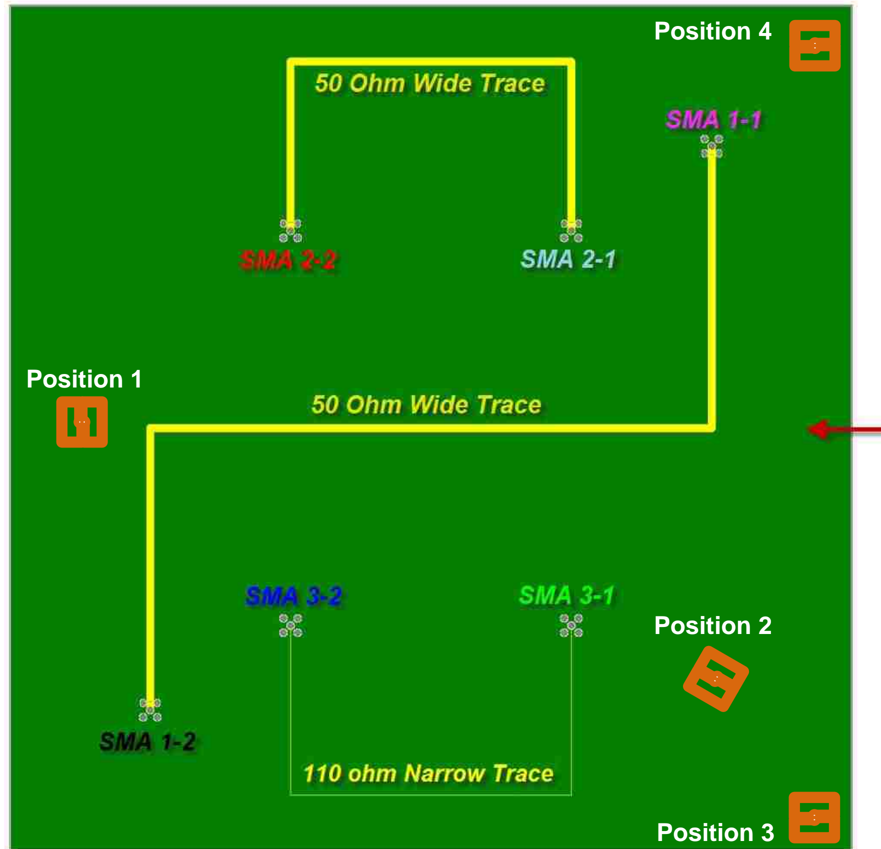

Figure 3-57. Positions where E-Field or edge current h-field coupling dominate

Probe at position 1 have minimized coupling from the direct injected current but some coupling from reflected surface current, edge current and trace current. Such current coupling is relatively weak and therefore the probe coupling is dominated by E-field. Probe at position 2 have the similar coupling effect.

Probe coupling at position 3 and 4 are mostly likely dominated by E-field, however their positions are near the edges of the structure, where the edge currents on the ground plane generates some Hz components. Those Hz components are not well suppressed by differential Hz probe and therefore some common mode H-field coupling will dominate in certain frequency range. Figure 3-58 is coupling response of the probe at locations mentioned above:

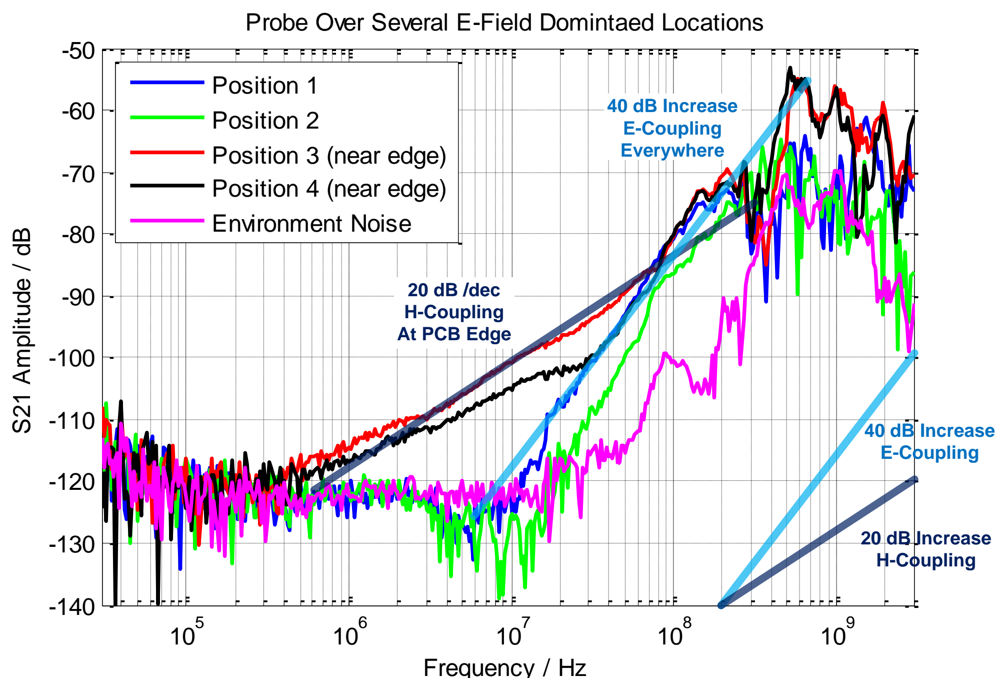

Figure 3-58. Probe S21 response at several E-field dominated locations

From Figure 3-58, most area with E-field coupling dominated after 100MHz, although there are some H-field couplings from the plane edge current, such coupling is not strong and left enough dynamic range for trace current coupling in that frequency range.

3.3.3.5 Coupling Factor. For using a probe to capture a transient current on trace and recover it numerically, the probe's magnetic coupling frequency response needs to be known to make sure that it has enough linear range bandwidth to cover the main spectrum of the transient current. Then a frequency compensation function of the coupling frequency response can be created to recover the main part of the transient current from the induced loop voltage signal. The following trace current experiment (Figure 3-59) is conducted to measure the H-field coupling frequency response of a probe:

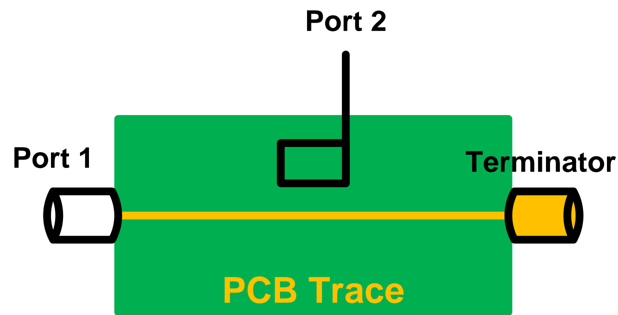

Figure 3-59. Experiment setup of trace current coupling with network analyzer

The trace current coupling frequency response experiment of a probe is conducted on several traces, including a well matched very narrow 50 ohm trace and 3 traces on the initial current reconstruction structure, as Figure 3-60 shows:

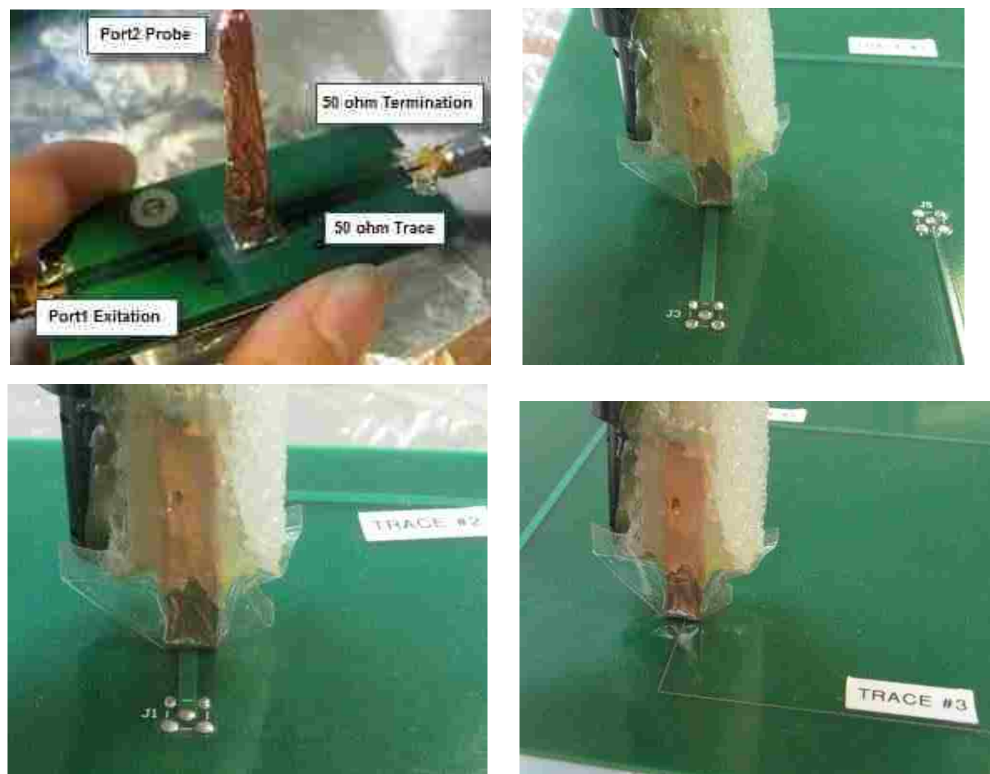

Figure 3-60. Coupling experiments of a differential Hz probe on different traces

The results of the differential Hz probe's coupling frequency responses on the 4 traces are shown in Figure 3-61. The simplified circuit model of trace current coupling on this probe is shown in Figure 3-62 (complex circuit model will be analyzed at the end of probe simulation analysis):

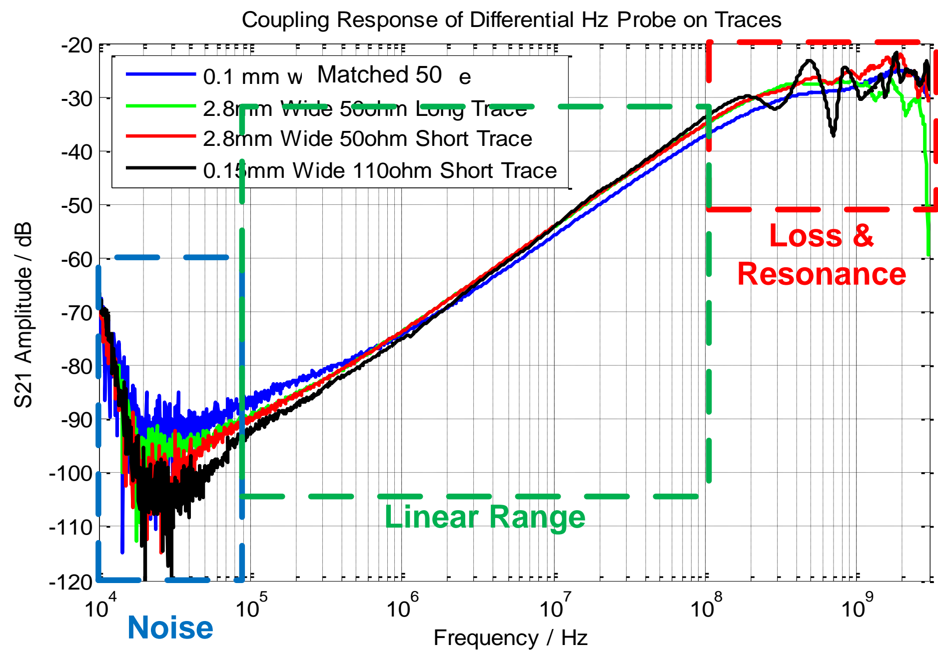

Figure 3-61. The coupling results of a differential H_z probe on different traces

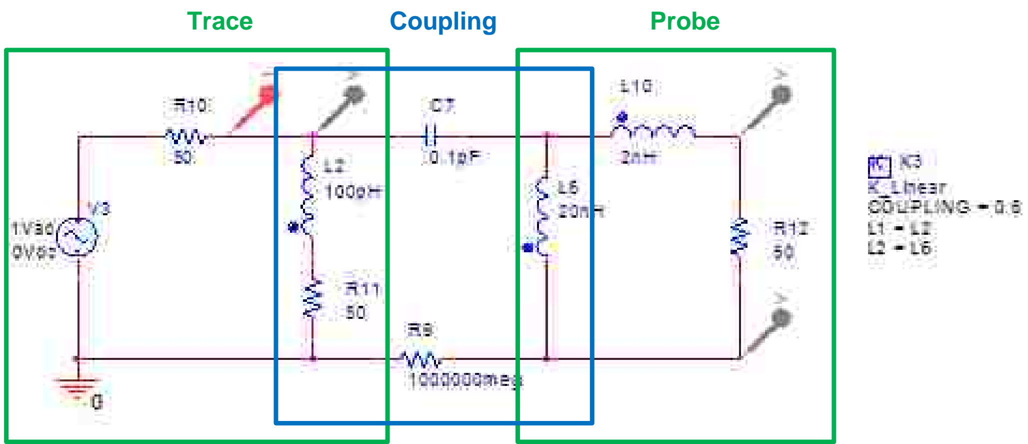

Figure 3-62. Circuit model of trace current coupling

The current on the trace and frequency response of coupling between excitation current and the probe in previous circuit model are simulated in spice and shown in Figure 3-63:

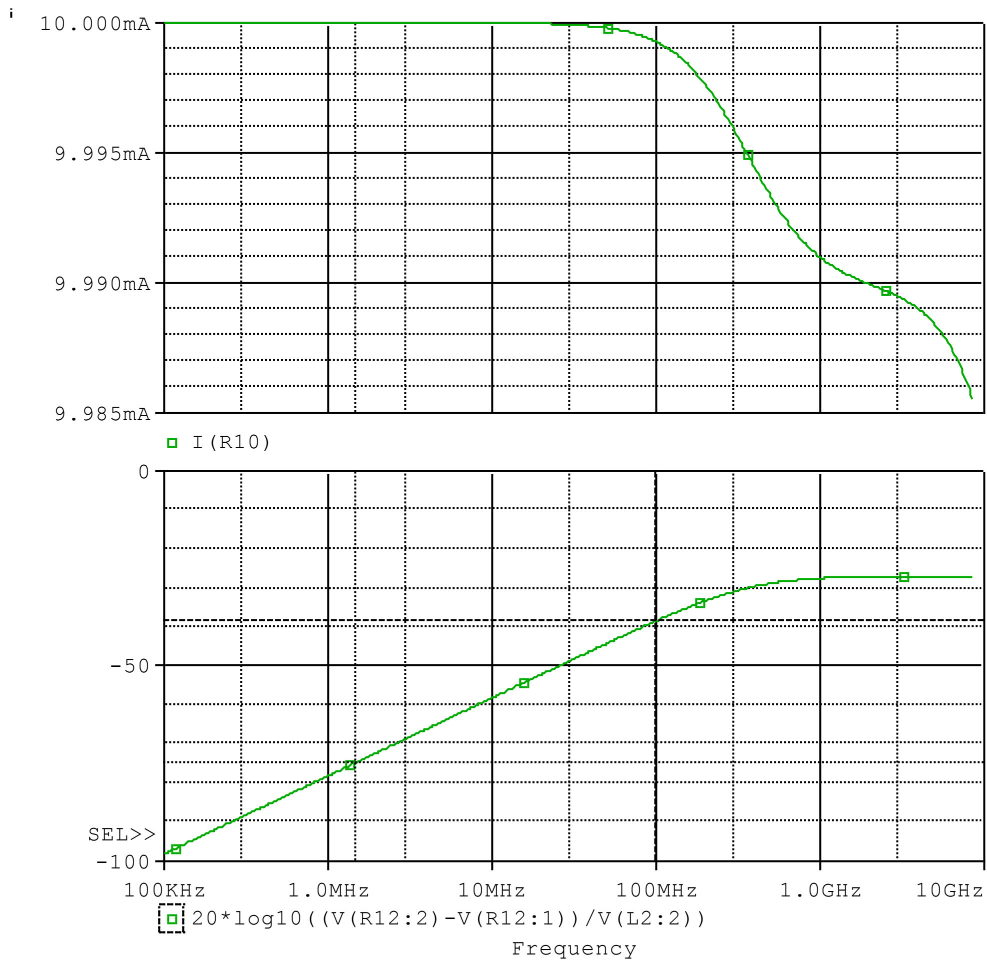

Figure 3-63. Frequency response of current coupling on simplified probe model

The probe’s coupling frequency response decreases after entering GHz. This is due to in high frequency, the impedance of the self and mutual inductance on the trace and probe increases and becomes comparable to 50 ohm. Therefore both the current on the trace and the probe’s response on the 50 ohm termination start dropping. The trace

current might not drop a lot because the mutual inductance is usually relative small. But the probe's coupling frequency response is compressed and flatted out as the self-inductance is relatively large. From the model, there is a tradeoff between the probe's coupling sensitivity and linear coupling bandwidth on the loop size.

3.3.3.6 Cable Loss. The loss of the differential H_z probe needs to be known and the same reason is explained in section 3.2.2.3 with the surface current probe. The S11 measurement result of a differential H_z probe is shown in Figure 3-64.:

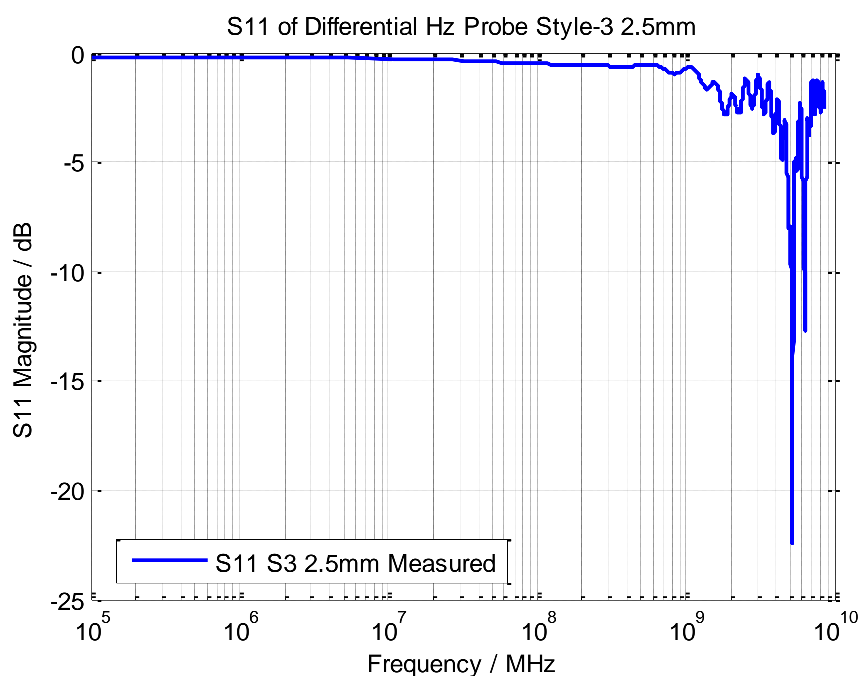

Figure 3-64. S11 result of a differential H_z probe

From the result, the probe's loss is okay up to 1GHz. Higher than 1GHz, dielectric loss and resonance occurs and limits the probe's coupling frequency response.

3.3.4. Simulation Analysis. To better understand and improve the performance of differential Hz trace current probe, its frequency response and parameters related to its coupling mechanism were investigated.

3.3.4.1 Probe Modeling Analysis. The full wave models are created in CST and HFSS. Modeling is based on simplification of the PCB layout, stack-up and tuning of the dielectric constant to curve fit S11 and S21 measurement results. Both models in CST and HFSS have been created as Figure 3-65 shows.

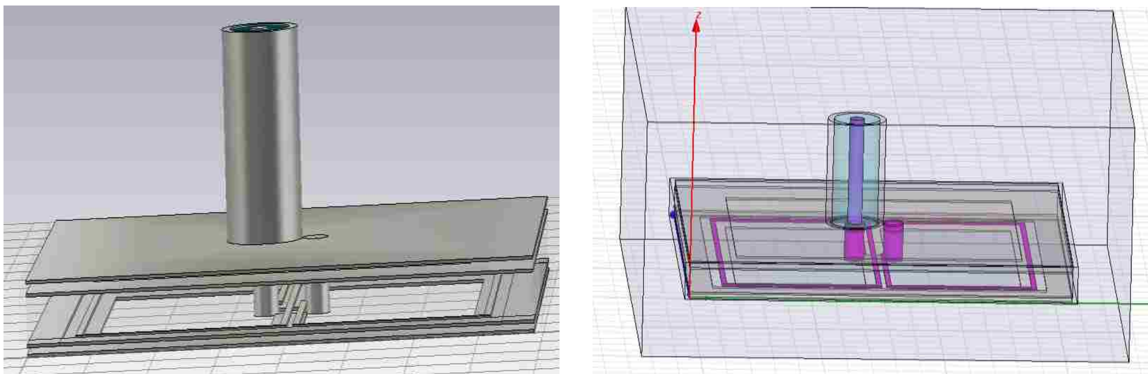

Figure 3-65. The differential H_z probe's CST and HFSS models

A pure PCB probe without common mode chock and ferrties has been made for the simulation results comparison as Figure 3-66 shows:

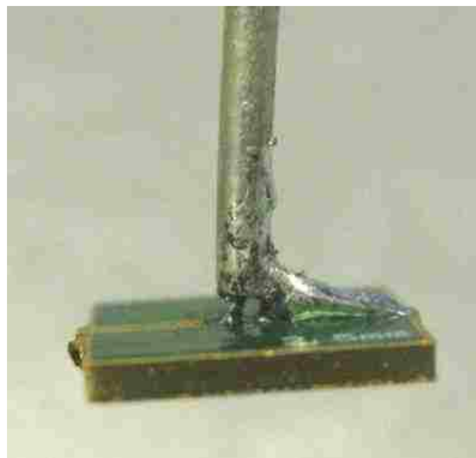

Figure 3-66. Pure PCB probe for model comparison

The simulation and measurement comparison of the probe’s PCB structure is well matched and shown in Figure 3-67:

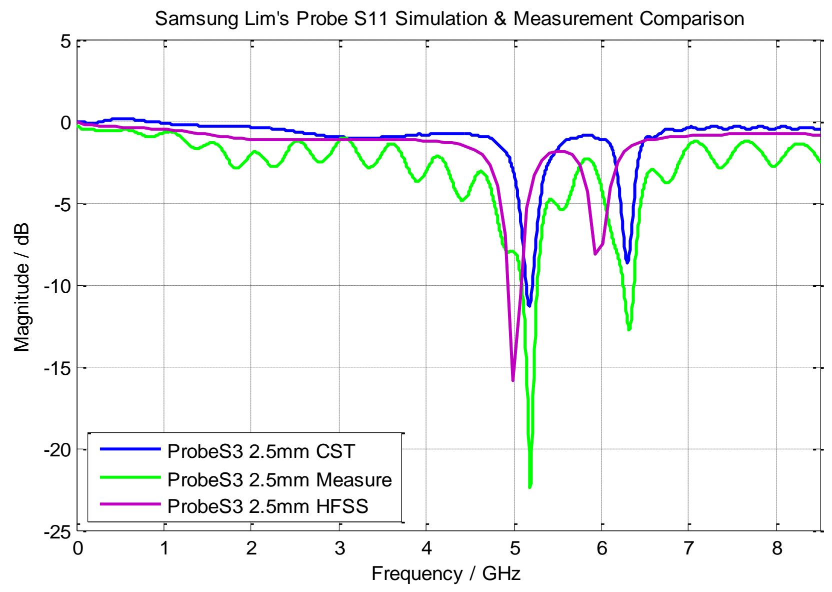

Figure 3-67. S11 comparison for simulation and measurement results

The probe’s coupling mechanism on 2.8 mm 50 ohm microstrip is simulated and matches to the measurement result as Figure 3-68 and Figure 3-69 show:

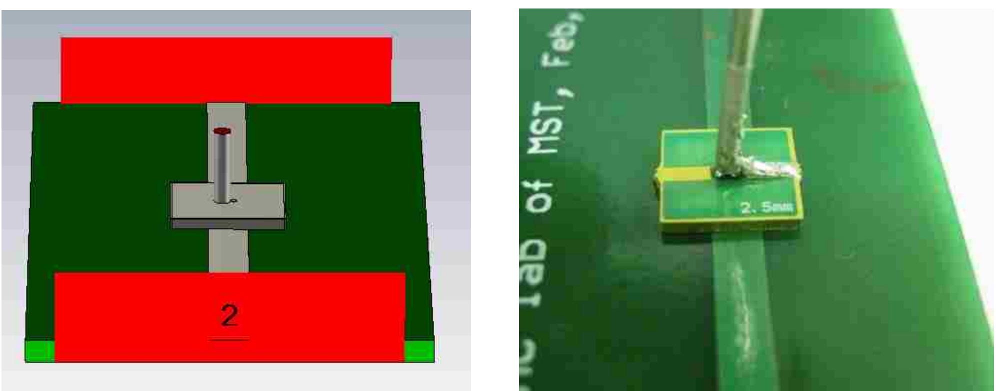

Figure 3-68. Probe’s trace current coupling in simulation and measurement

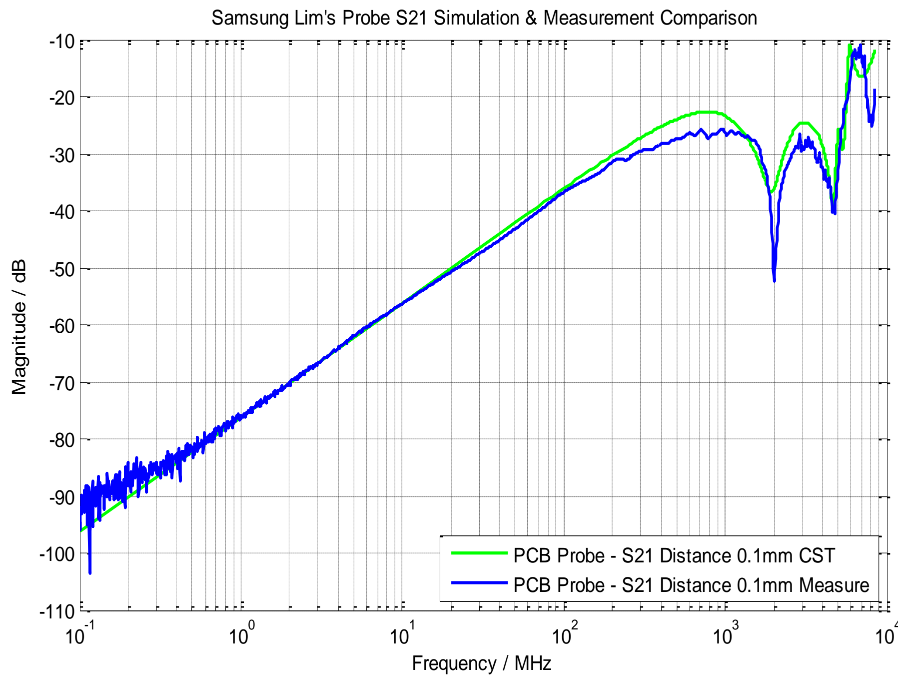

Figure 3-69. Comparison of simulation and measurement coupling response

Then the complete probe (with common mode chock and ferrites) and pure PCB probe's coupling mechanism are compared in measurement as Figure 3-70 shows:

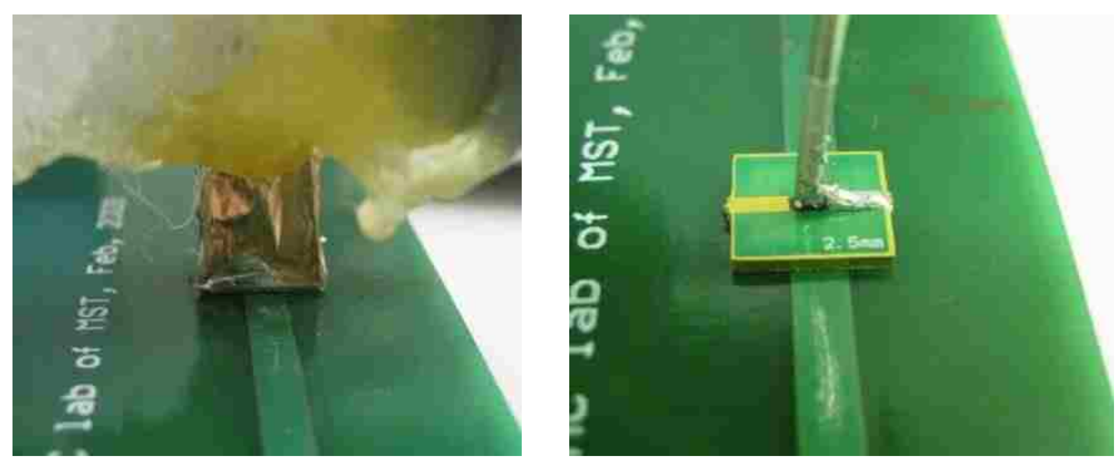

Figure 3-70. Pure PCB loop structure probe Vs complete differential H_z probe

The comparison result is shown in Figure 3-71. From the comparison, the coupling results of the complete probe and pure PCB probe are well matched in 100 KHz to 1 GHz frequency range. At higher frequency, a resonance occurs at 2GHz for pure PCB probe, but does not show up for complete probe. Because the common mode chock and ferrites strongly suppress the common mode current that causes the resonance. Therefore they move the resonance to much higher frequency.

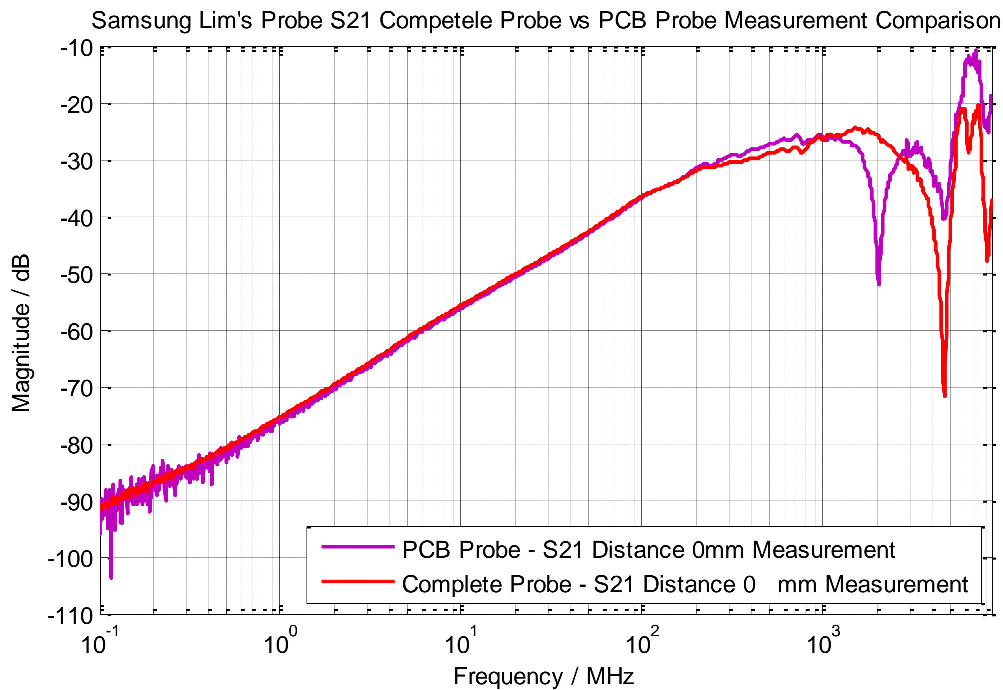

Figure 3-71. Comparison of complete probe and pure PCB probe

Another resonance around 4.6 GHz for the complete differential H_z probe is due to the common mode chock's resonance on its differential current return path as Figure 3-72 shows. This resonance will be the hard limitation of this probe as it is built into the current return path. However, 4GHz is fairly enough for the application of ESD current reconstruction.

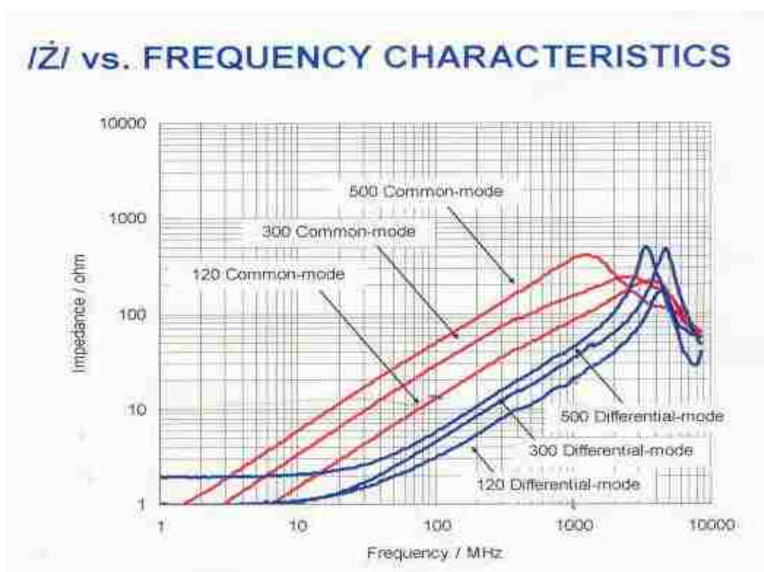

Figure 3-72. Common mode chock datasheet

3.3.4.2 Current Coupling Analysis. Further analysis of the differential H_z probe's trace current coupling mechanism is continued in full wave simulation for the best application of this probe and the preparation of an improved probe design in the future.

3.3.4.2.1 Probe Height (Dz). The height from probe to trace can influence the coupling between the trace and probe. Figure 3-73 shows the probe height Dz:

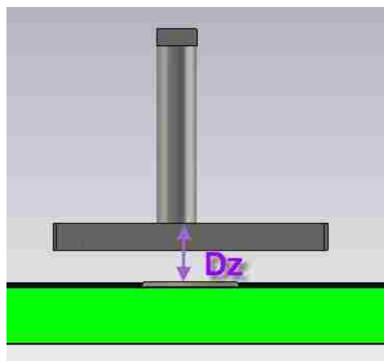

Figure 3-73. The height from probe to the trace (Dz)

The parameters of probe and trace in simulation are fixed as follow: Probe_W = 2.68 mm, Probe_L = 5mm, Probe_CW = 0.5mm, Dx = 0, Trace width = 2.8mm, Trace height = 1.57mm. Figure 3-74 is a view of magnetic flux of the trace current.

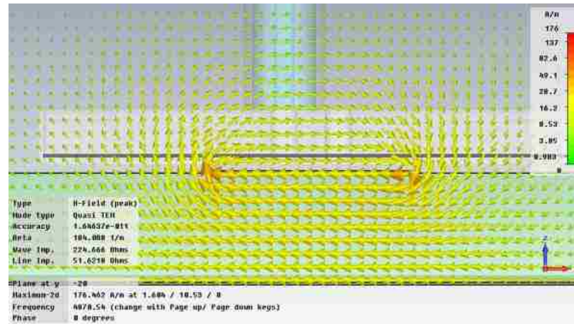

Figure 3-74. Magnetic flux of the trace current

Figure 3-75 shows the probe's coupling frequency responses of trace current, the coupling magnitude drops with height from probe to trace increase. Then 3 frequencies in the linear coupling frequency range are selected for analysis in Figure 3-76.

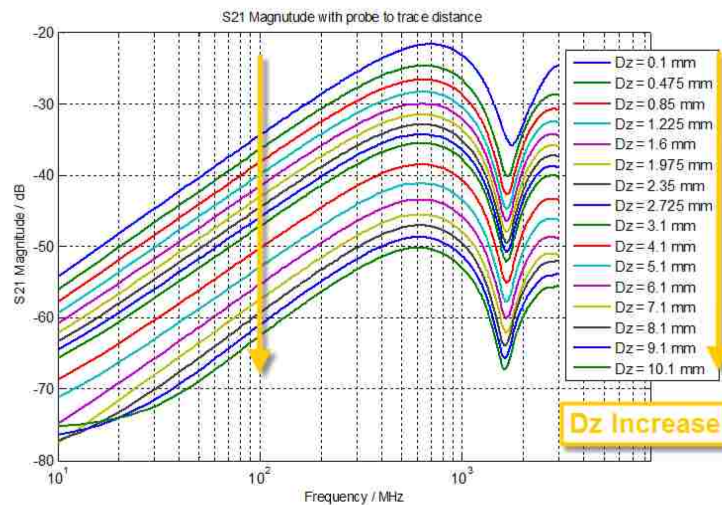

Figure 3-75. Probe's coupling frequency response with different Dz

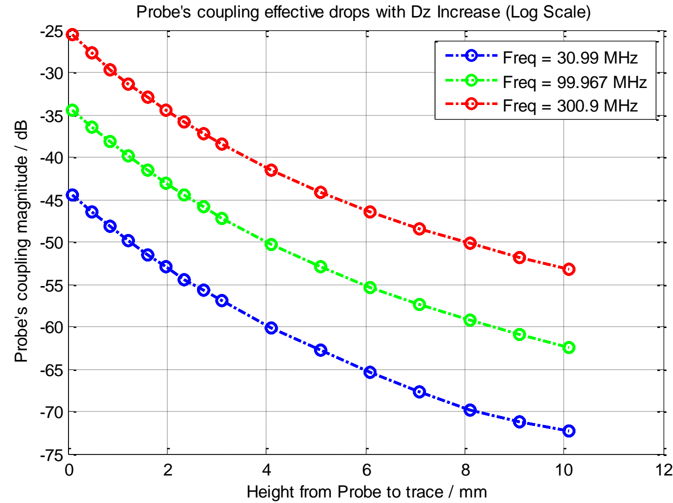

Figure 3-76. Probe's effective coupling drops with Dz increase

From the result, the effective coupling drops with Dz increase is not a function of frequency within the probe's linear inductive coupling range. Then the effective coupling drops with Dz increase is rescaled in linear scale and different curve fit are matched for different height as Figure 3-77 shows:

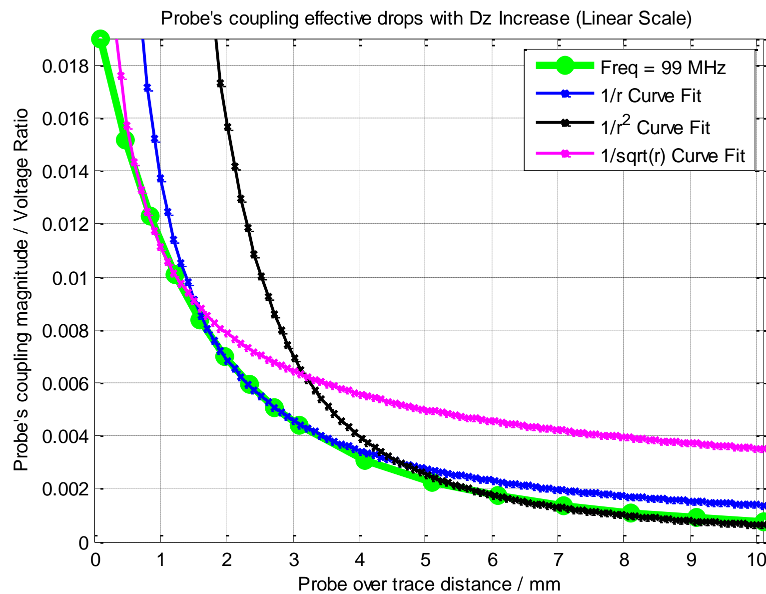

Figure 3-77. Curve fit lines for 100MHz frequency coupling

The probe's coupling response drops with height increase in different fashions at different heights. This depends on the microstrip width and height.

a. When probe is very close to trace, the probe might influence the trace current and no good curve fit was found. The 1/sqrt(r) function has some limited match region. The ln(r) function also doesn't match and is not shown here.

b. When probe to trace height (Dz) > trace to ground height, 1/r curve shows good match from 1.5 mm to 3 mm. Because in this region the trace current cannot be treated as a current element. After integration of many current elements on the trace, a 1/r factor is present. This region is the near-field of the trace.

c. When probe to trace height (Dz) > 5mm, 1/r^2 curve matches the H-field coupling pretty well. This is because when trace is far from the probe, the H-field contribution from trace current is close to a single current element. This region is the far field of the trace.

Therefore, to increase H-field coupling, putting probe as close to trace as possible is very effective.

3.3.4.2.2 Probe Sideway Offset (Dx). The spatial resolution of this probe is influenced by the sideway offset from probe center to trace center (Dx). Figure 3-78 shows the definition of probe's sideways offset:

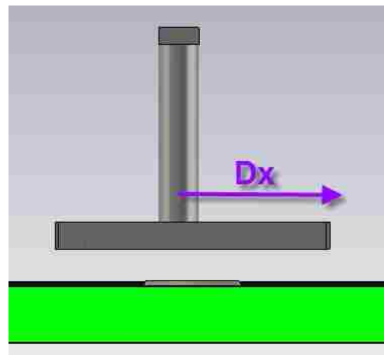

Figure 3-78. Definition of Dx: sideways offset

Simulation analysis of the probe's spatial resolution is conducted with parameters: Probe_W = 2.68 mm, Probe_L = 5mm, Probe_CW = 0.5mm, Dx = 0, Trace_W = 2.8mm, Trace_H = 1.57mm:

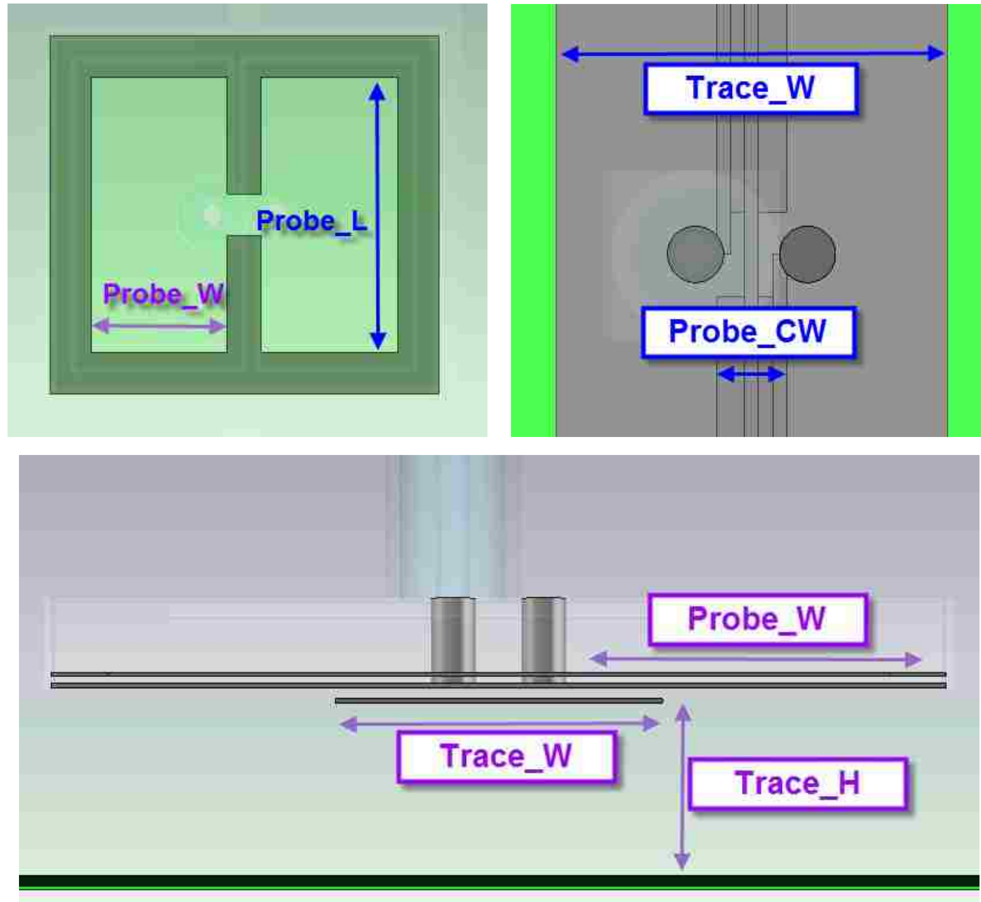

Figure 3-79. To scale drawing of probe and trace parameters

The S21 coupling from trace to the probe is simulated with Dx sweep from -5mm to 5 mm as Figure 3-80 shows. Then the S21 coupling effect of sideways offset for several frequencies is plotted in Figure 3-81.

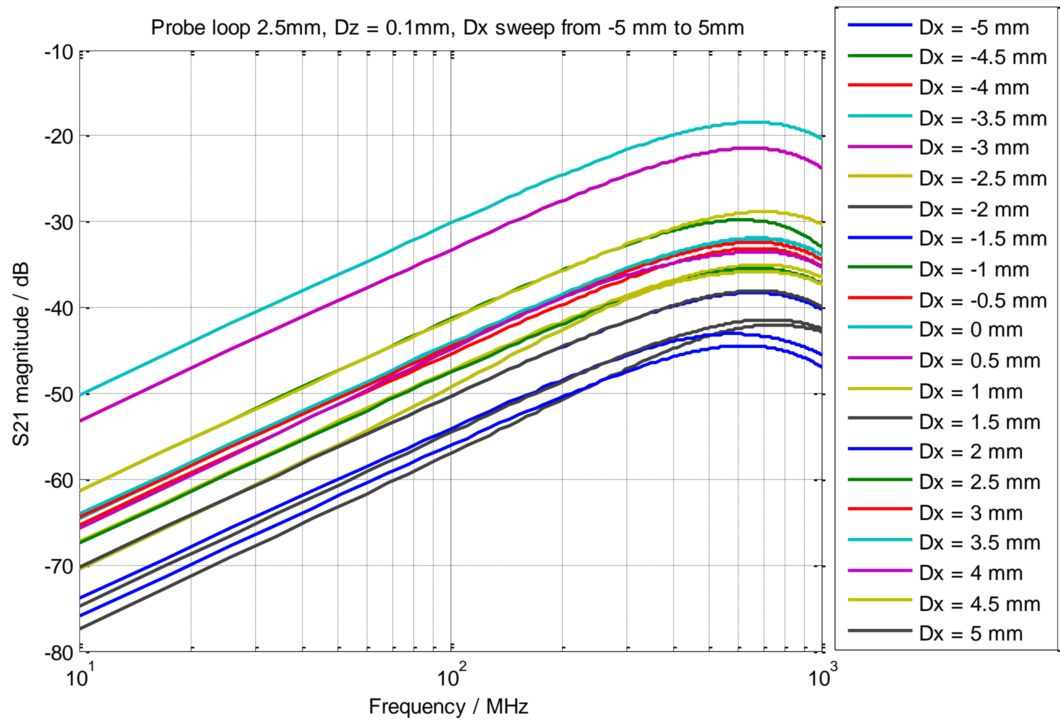

Figure 3-80. S21 as a function of frequency at different sideways offsets (Dx)

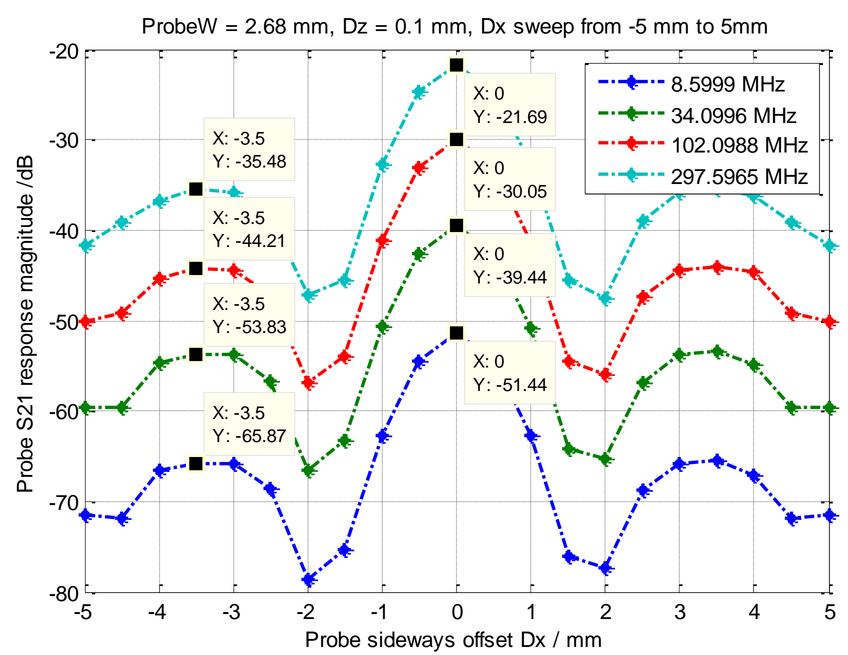

Figure 3-81. S21 magnitude vs sideways offset Dx for several frequencies

Analysis of probe sideways offset effects:

a. The ratio of the main peak to the side peaks is about 14 dB in probe's inductive coupling frequency region

b. The 6 dB down width of the center peak is 1.4mm. This is a small value considering the probe loop width is 2.68mm and the trace width is 2.8mm.

c. The depth of the minimum between the main peak and the side peak in the limited simulation points shows -57 dB and is 27 dB down from main peak, however according to previous S21 magnitude and phase shift analysis (Figure 3-46), minimum is caused by magnetic flux cancel out, and fall down to noise level.

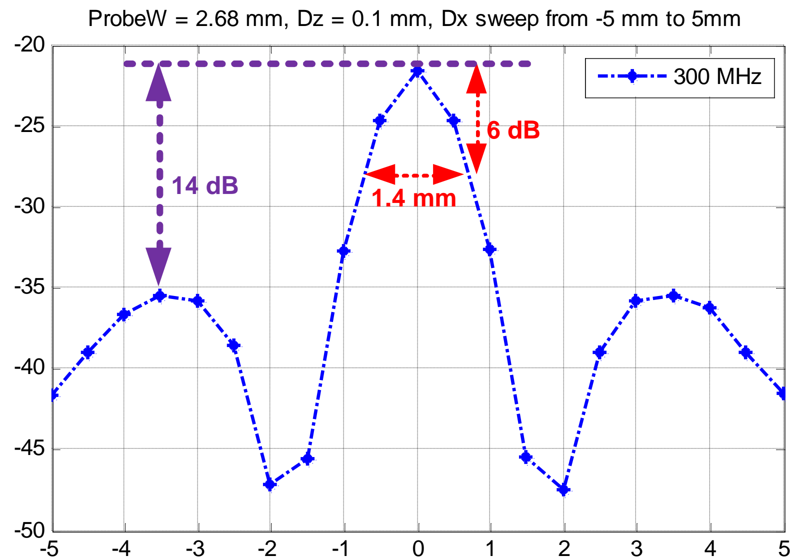

Figure 3-82. S21 magnitude vs. Dx variance @ 100MHz

The probe's spatial resolution depends on the loop width and center shielding width as shown in Figure 3-83. Because 1/2*(Probe_W+Probe_CW) is about the offset distance where the trace's magnetic flux go through loops are canceled out and further offset will cause the magnetic flux goes through loops in opposite directions.

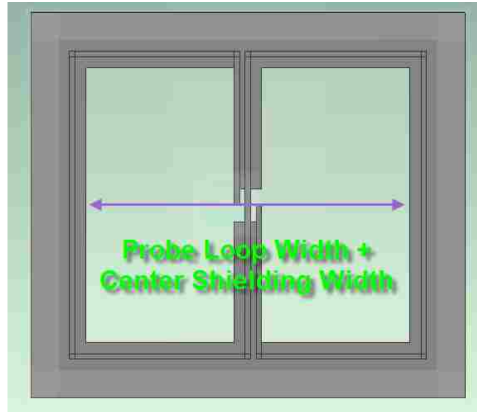

Figure 3-83. Probe loop width + center shielding width

Illustration of this effect is followed by the 3 coupling cases:

a. Maximum coupling when Dx = 0:

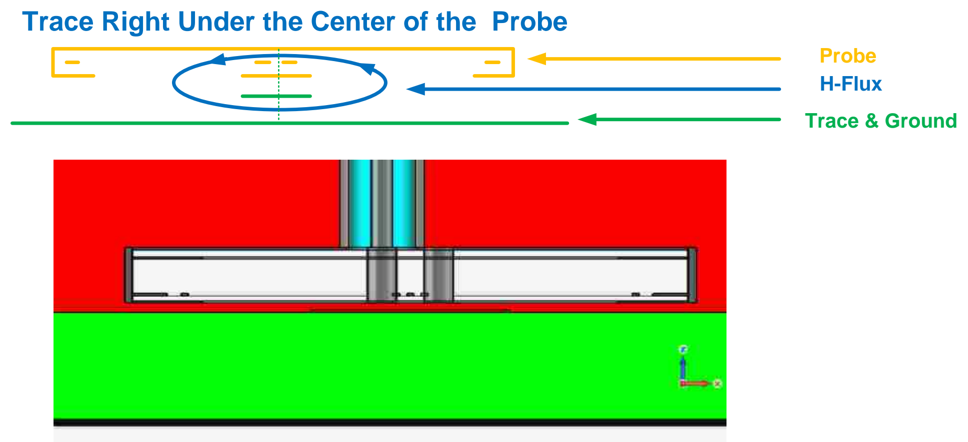

Figure 3-84. To scale drawing when Dx = 0, maximum coupling occurs

b. Minimum Coupling when Dx = roughly 1/2*(Probe_W+Probe_CW):

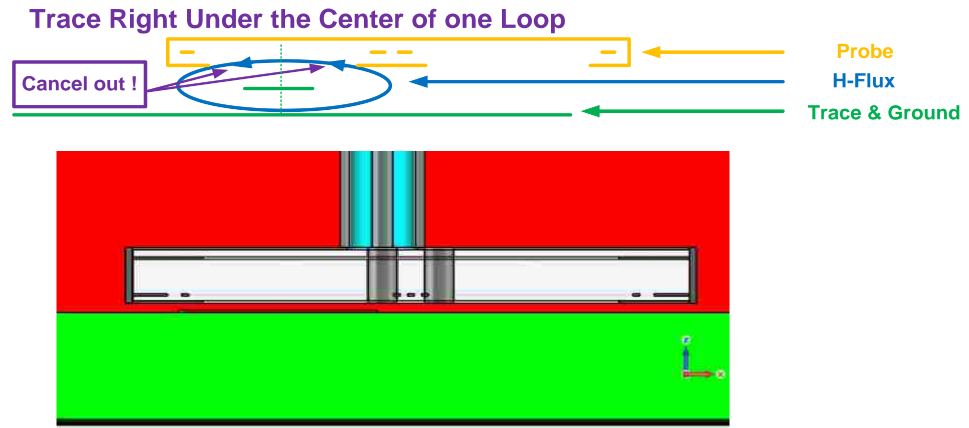

Figure 3-85. To scale drawing when Dx = 1.9 mm, minimum coupling occurs

c. Magnetic flux forced to go opposite direction through loops

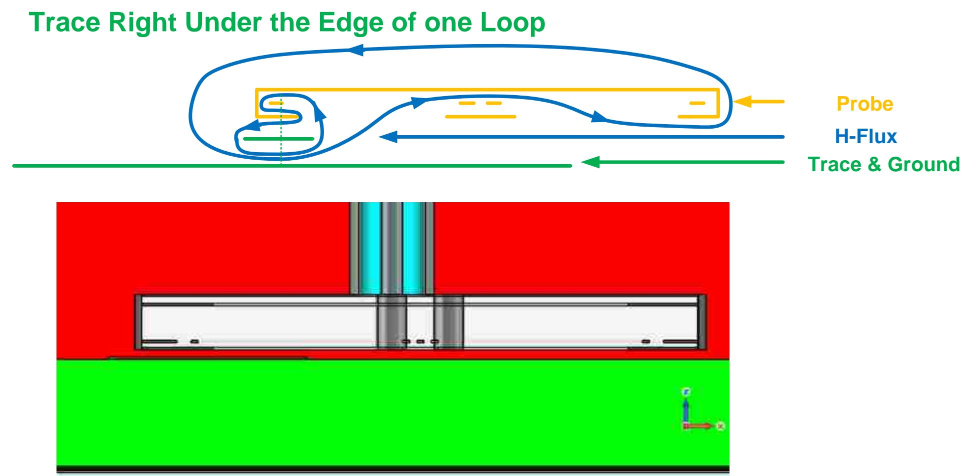

Figure 3-86. To scale drawing when Dx = 3 mm, 180 degree out of phase coupling

Therefore, to increase spatial resolution, the loop width and the center shielding width should be reduced.

A further analysis of probe's spatial resolution related to trace widths is conducted. If the probe's design objective is to reconstruct the trace current on circuit, ideally the probe should have a frequency response that is not a function of trace width, or at least not varies with the trace width a lot. Therefore, the effect of trace width was investigated. In the following simulation, these parameters are fixed: Probe_W = 2.68mm, Probe_CW = 0.5mm, Trace_H = 0.27 mm as Figure 3-87.

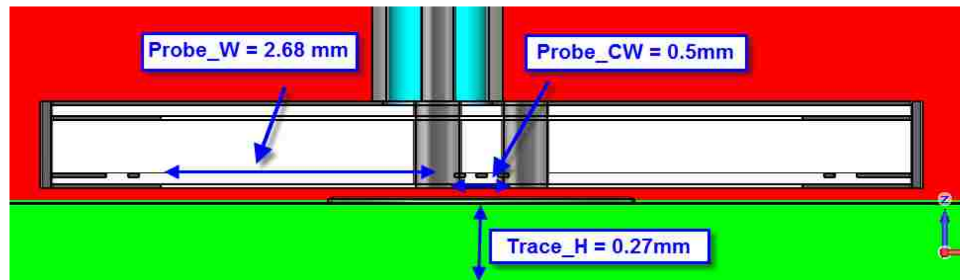

Figure 3-87. To scale drawing of simulation parameters

Then the probe's spatial resolution is obtained for scenarios of Trace_W = 0.1, 0.5 and 2.8 mm at height of 0.1mm. Dx sweeps from 0 to 4 mm with steps of 0.2 mm. The simulated results are shown in Figure 3-88.

From the results in Figure 3-88, there are several interesting points. For 2.8 mm trace, the spatial resolution is pretty flat from Dx = 0 to 1mm.This is because the trace is much wider than the center shielding (2.8>0.5) and even larger than the one loop width. So when the probe sideway offset is from 0 to 1mm, similar amount of magnetic flux close to the trace edges will go through the probe loops as Figure 3-89 and Figure 3-90 shows:

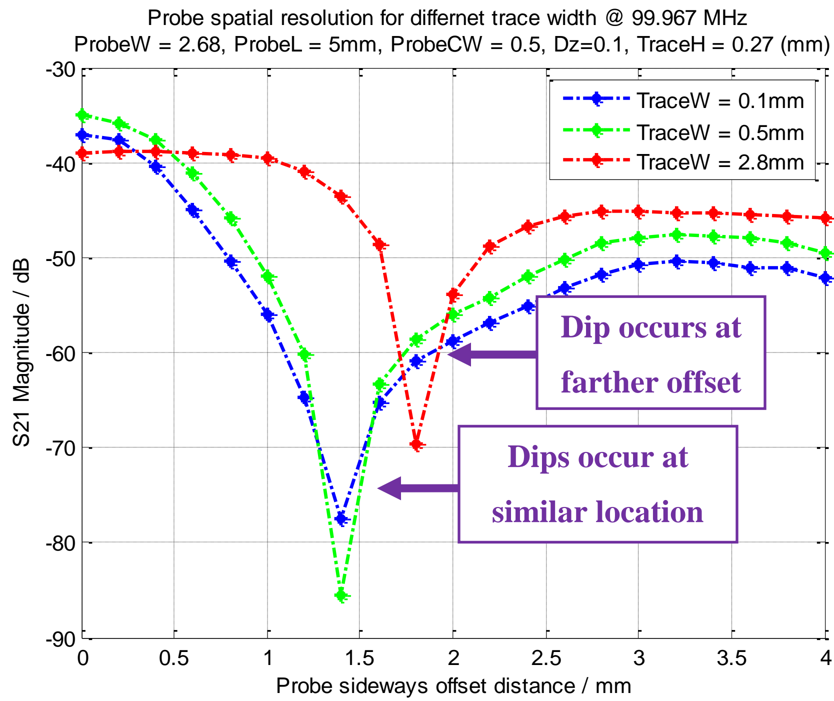

Figure 3-88. Probe's sideway spatial resolution for different trace width

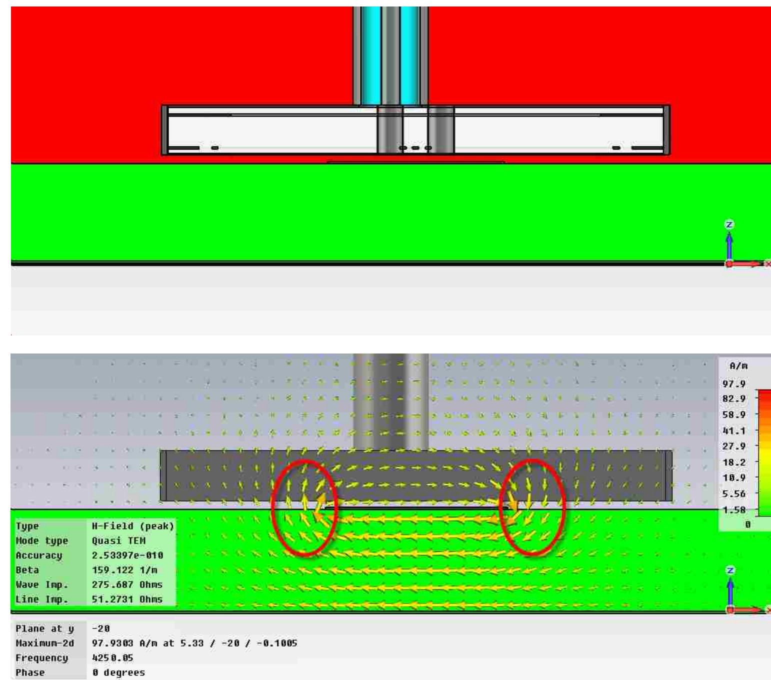

Figure 3-89. Magnetic fluxes crossing the loops concentrated on the trace edges

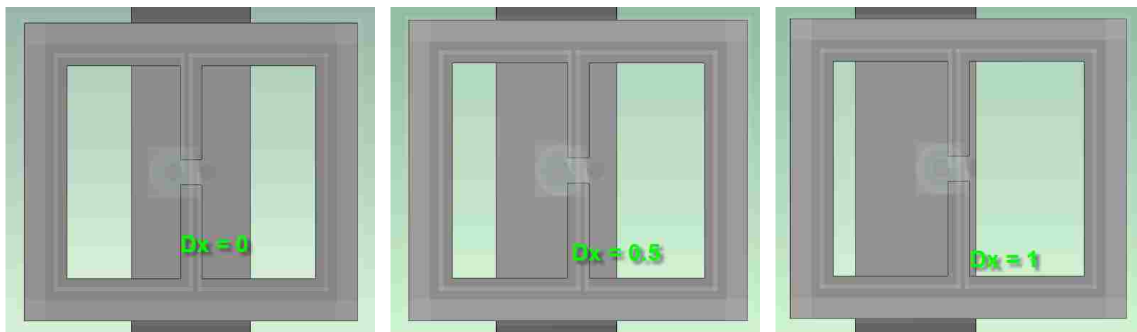

Figure 3-90. Dx varies from 0 to 1 mm when trace width = 2.8mm

For 0.1 and 0.5 mm trace, the coupling drops with sideway offset from beginning. This is because when the trace is equal or smaller than the center shielding (Figure 3-91), as soon as the probe has a little offset, the magnetic flux going through the loops will be blocked by the center shielding and bypass the 2 loops.

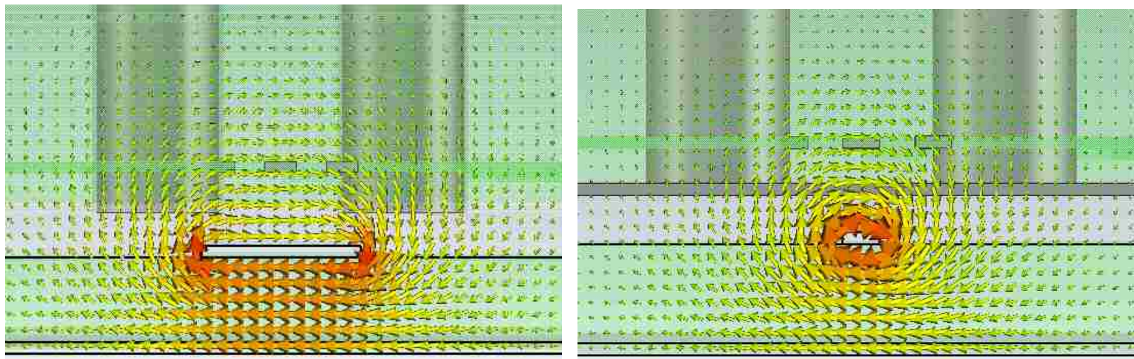

Figure 3-91. Magnetic coupling of 0.1 and 0.5 mm wide trace

For the 0.1 and 0.5 mm trace, the minimum coupling occurs at roughly the same location (Dx = 1/2*(Probe_W+Probe_CW)), where the magnetic flux is roughly canceled

out at that distance. But when the trace width is larger than the loop width (for example 2.8 >2.68), the minimum coupling offset location would shift a distance of (Trace_W-Probe_W)/2, otherwise the edge of the trace so close to the other loop that it will force some magnetic flux going through the other loop as Figure 3-92 shows:

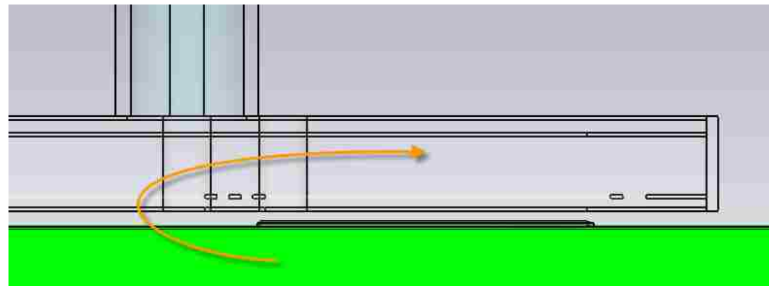

Figure 3-92. Dx = 1/2*(Probe_W+Probe_CW)) when Trace_W> Probe_W

But after further shifted roughly a distance of (Trace_W-Probe_W)/2, the edge of the trace is under the loop and this is the location where most magnetic flux going through and out of the loop right above the trace, as Figure 3-93 shows:

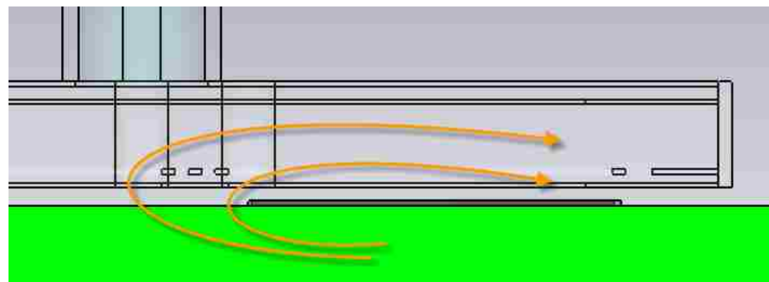

Figure 3-93. Dx = 1/2*(Trace_W + Probe_CW)) when Trace_W > Probe_W

The magnitude of the maximum coupling is not following the order of trace width. The maximum occurs at 0.5mm, then 0.1mm, 2.8mm is the weakest one. This is because when trace width is close to probe center shielding width, the edges of the trace is right under the edges of the two loops and therefore most of the magnetic flux from the trace is covered by the two loops of the probe, as Figure 3-94 shows:

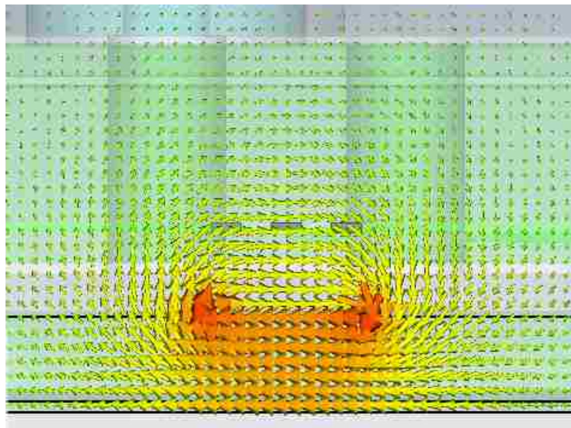

Figure 3-94. Probe_CW = Trace_W = 0.5 mm

When Trace_W = 0.1 mm, certain magnetic flux from trace current goes under the center shielding of the probe as Figure 3-95 shows:

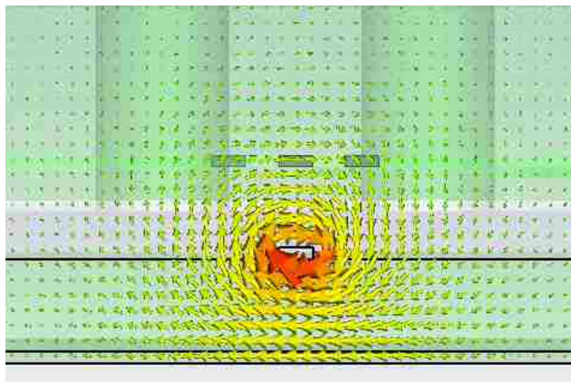

Figure 3-95. Probe_CW = 0.5 mm, Trace_W = 0.1 mm

When Trace_W = 2.8 mm certain magnetic flux is not crossing the loops and in the center region, certain area of the loops has no Hz components as Figure 3-96 shows.

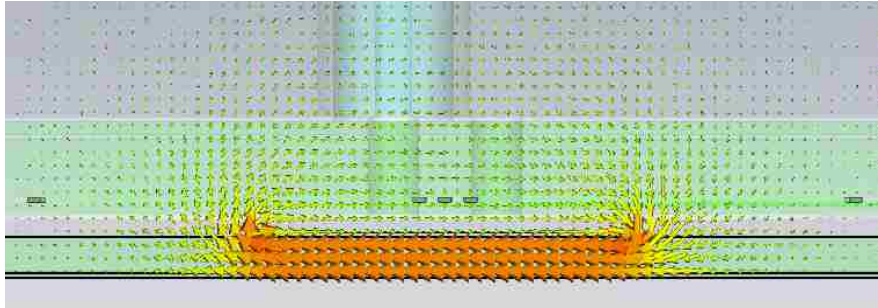

Figure 3-96. Probe_CW = 0.5 mm, Trace_W = 2.8 mm

Height influence for probe sideways resolution:

The probe height will also have some influence on the probe sideways resolution as the magnetic field will be became sparser at higher distance. The probe's spatial resolution for different width 50 ohm traces when Dz = 0.1 mm and Dz = 0.5 mm is shown in Figure 3-97 and Figure 3-98:

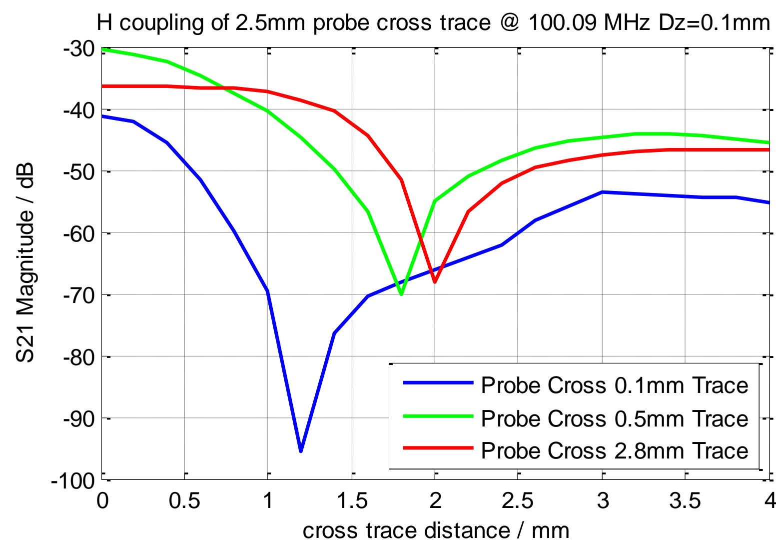

Figure 3-97. Probe spatial resolution for different trace when Dz = 0.1 mm,

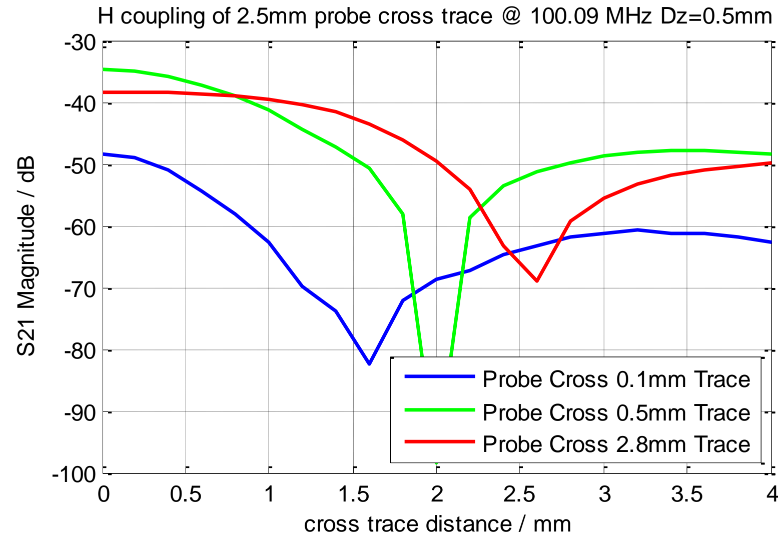

Figure 3-98. Probe spatial resolution for different trace when Dz = 0.5 mm

Therefore moving the probe higher has such influence:

1. Lower the overall coupling responses, especially for narrow traces
2. Lower the probe's sideway spatial resolution a lot.

This indicates that putting the probe closer to the trace also helps increasing coupling sensitivity and spatial resolution.

3.3.4.2.3 Probe Directional Response (Rot). The directional response of a probe reflects how it couples to field or current during rotation, usually from the maximum to the minimum coupling direction. A ideal loop probe has good directional response that follows cosine drop from the maximum to minimum coupling direction. And if a probe's directional response follows cosine drop, the orthogonal measurements probe induced signals such as Vx and Vy can be separately processed and directly mapped to vectors Hx and Hy, or Jx and Jy. However, a real H-field probe, depending on the structure and its coupling mechanism, may not have directional response well following cosine drop. Thus the process of orthogonal measurements data will need to be compensated for the probe's directional response.

For the case of this trace current probe, the orthogonal measurements data can only be compensated when its directional response is symmetry between [0, 90] and [0, -90] and monotone decreasing in [0, 90] (0 is the maximum coupling direction) in its

inductive coupling dynamic range. Figure 3-99 is the differential Hz trace current probe's directional response with parameters: Probe_W = 2.68 mm, Probe_L = 5mm, Probe_CW = 0.5mm, Dx = 0, Trace width = 2.8mm, Trace height = 1.57mm, Dz = 0.1mm, Probe_Rot (rotation degree) varies from 0 to 90:

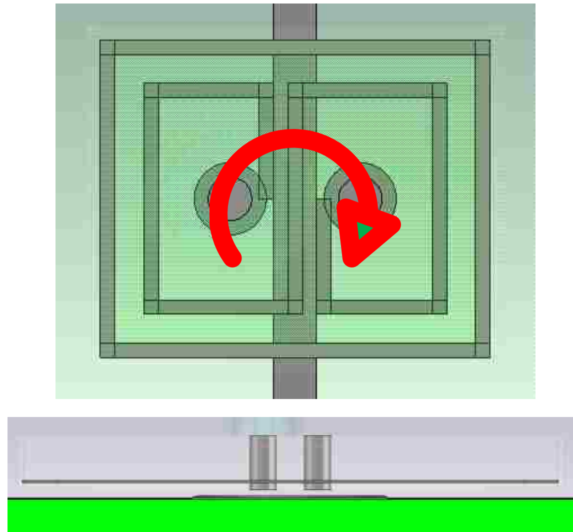

Figure 3-99. Top and side view of the differential H_z probe and trace

The results of S21 coupling from trace to probe are shown in Figure 3-100:

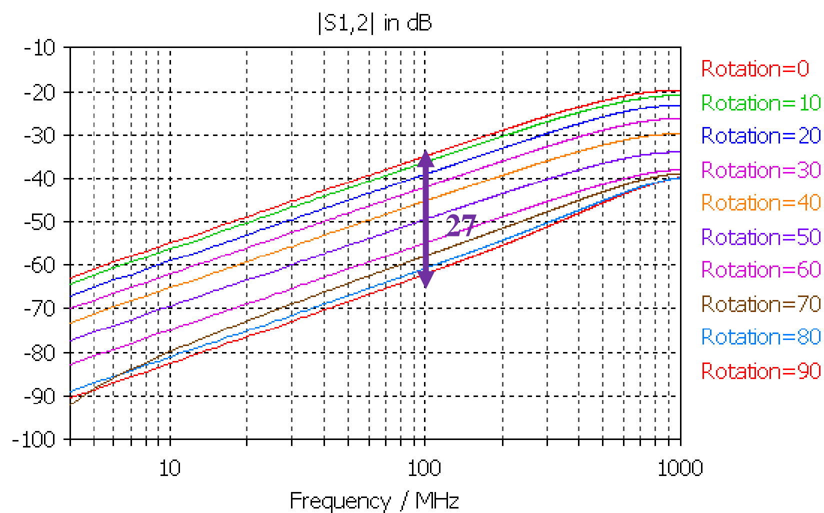

Figure 3-100. Probe's coupling frequency responses during rotation

After plot coupling against rotation degrees, the probe's directional response is shown in Figure 3-101:

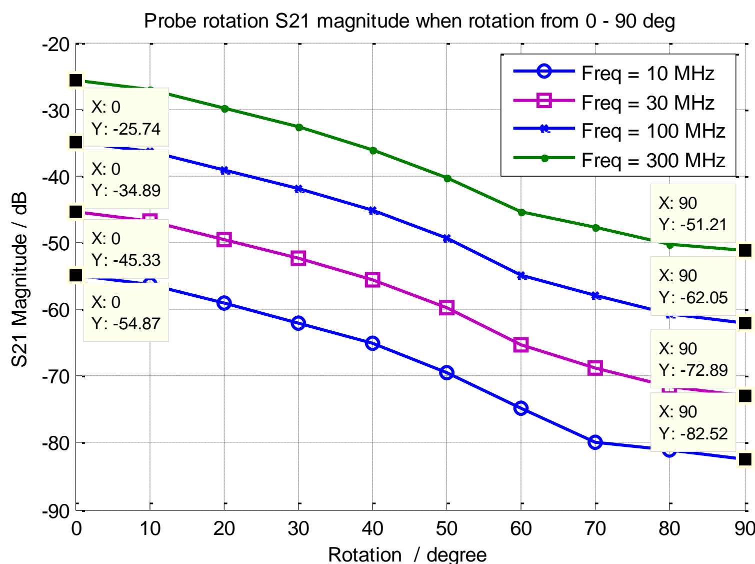

Figure 3-101. S21 magnitude vs probe rotation degree at several frequency points

For this case, the probe has good 90 degree rejection (around 27 dB). However, when the probe loop become smaller, both the probe's sensitivity and directional response became worse.

Another simulation set is conducted with these parameters: Probe_W = 0.5 mm, Probe_L = 1mm, Probe_CW = 0.5mm, Dx = 0, Trace_W = 0.5 mm, Trace_H = 1.57mm, Dz = 0.1mm, Probe_Rot (rotation degree) varies from 0 to 90 degree. The scale drawing of the simulation setup is shown in Figure 3-102 :

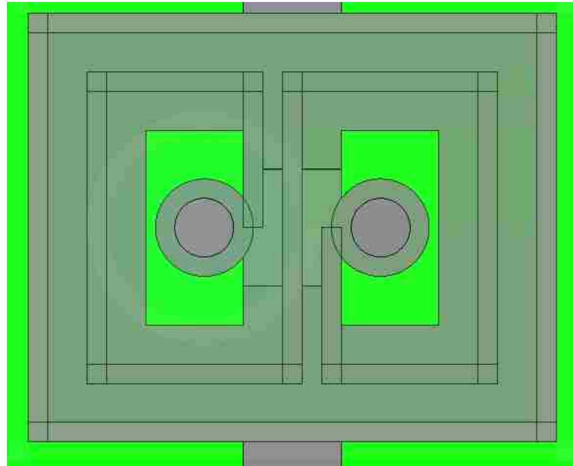

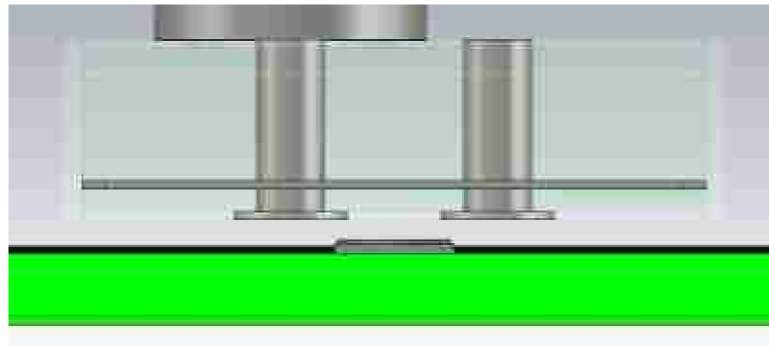

Figure 3-102. To scale drawing of differential H_z probe and trace

The smaller probe’s coupling responses during rotation is plotted as Figure 3-103 shows:

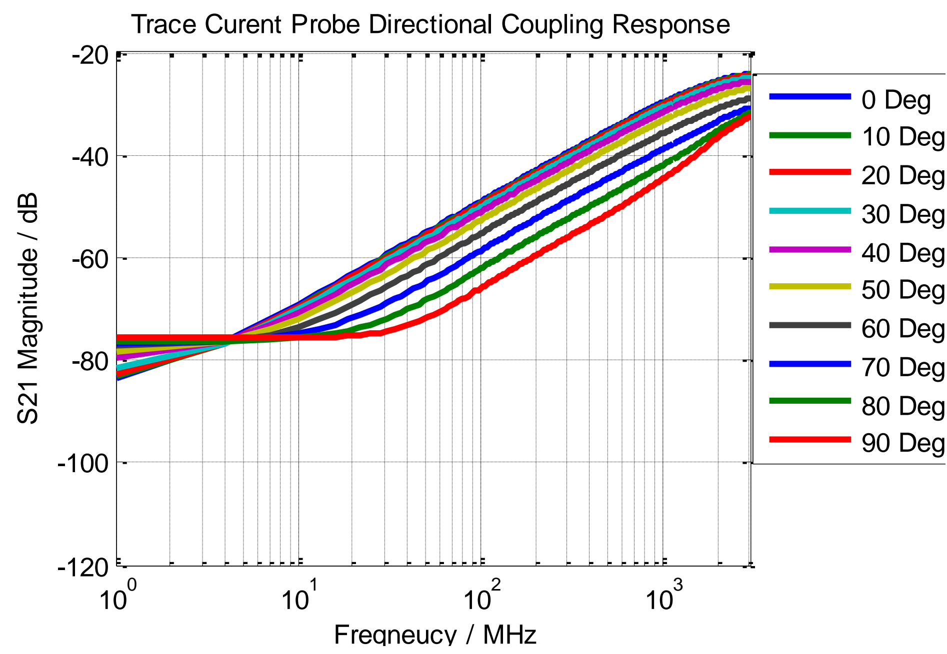

Figure 3-103. Probe's coupling frequency responses during rotation

The normalized directional response is plotted as Figure 3-104 shows.

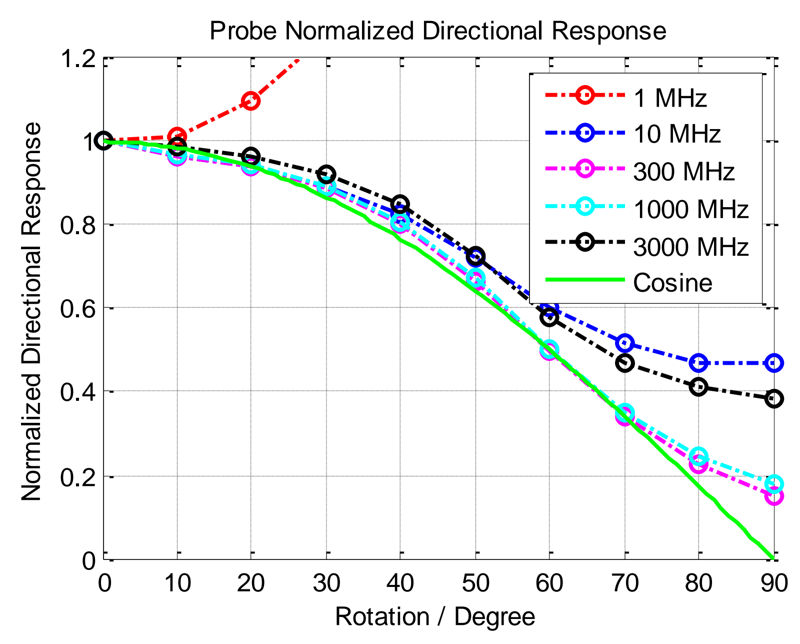

Figure 3-104. Probe's normalized directional response in several frequencies

It shows although the probe's coupling frequency response at maximum coupling orientation is good from 1MHz to 2GHz, the directional response is only good from 50MHz to 1GHz after some degree rotated (40 degree in this case), both high and low frequency coupling shows coupling compression and orthogonal coupling rejection is less than 20 dB. The coupling compression is partially due to the E-field coupling from the unshielded vias as Figure 3-105 shows:

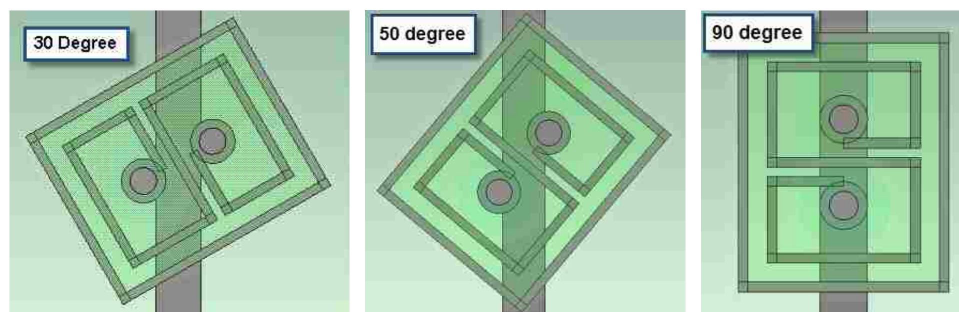

Figure 3-105. Probe's E-field coupling of unshielded vias increase during rotation

The orthogonal coupling rejection is due to trace current inductive coupling into the "vias' loop" as Figure 3-106 shows. After the probe is 90 degree rotated, the two differential loops canceled the H-flux through them, but the "vias' loop" is just rotated into its maxim coupling orientation. When the probe's differential loops become smaller, the "vias' loop" remains the same size and tens to influence probe's directional response.

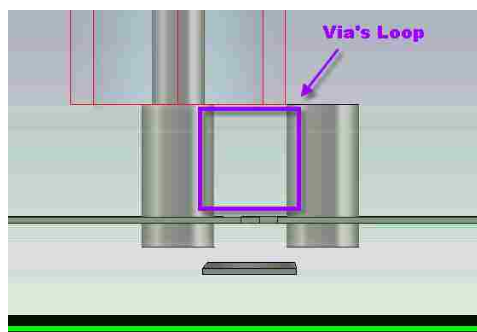

Figure 3-106. The via's loop from this differential H_z probe

3.3.4.2.4 Probe SPICE Model. For a summary of the modeling analysis, a complex SPICE model of the probe's coupling response is shown in Figure 3-107:

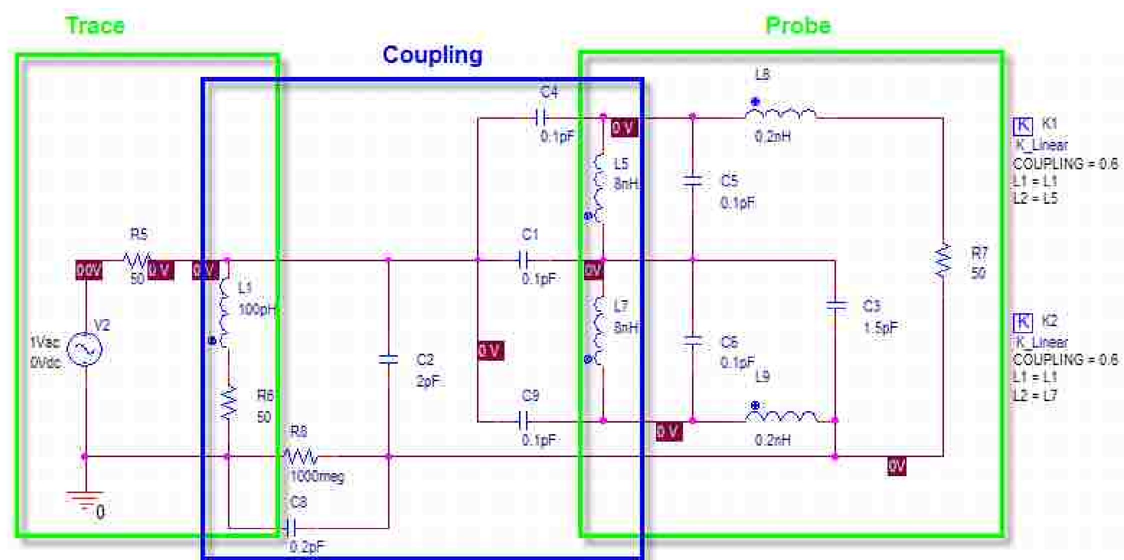

Figure 3-107. SPICE model of the differential H_z probe and coupling mechanism

In the circuit model two in-phase inductors (L5 and L7) couples to the trace current, representing the two differential turn loops. C5 and C6 represent the capacitive coupling between vias and loop traces near the probe center. L9 and L8 represent the inductance of the two vias. C1 represent the capacitive coupling between exposed loop and the trace underneath. C2 represents the trace capacitive coupling to the probe shielding. C3 represents the capacitive coupling between the trace of loop and the shielding (the loop was designed to be very close to bottom layer). C8 represents the capacitive coupling between trace ground and probe shielding. C4 and C9 represent the E-field coupling between trace and two vias.

In this model, it shows the coupling mechanism between a 2.5 mm wide loop differential probe and a 2.8 mm trace. The comparison of full wave model, circuit model and measurement are shown in Figure 3-108:

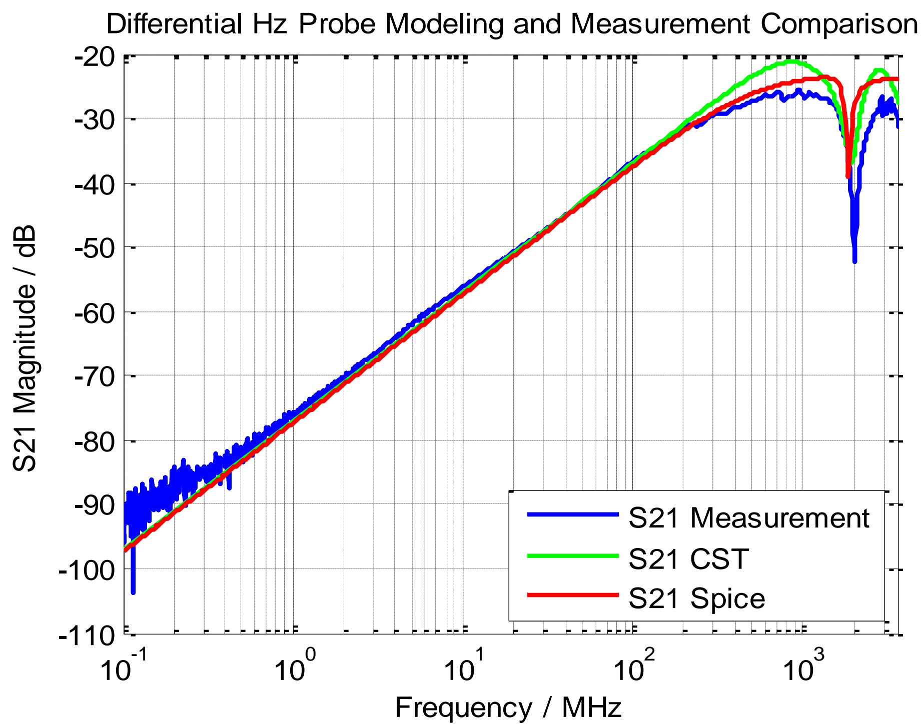

Figure 3-108. Comparison between SPICE, full wave models and measurement

4. CURRENT RECONSTRUCTION SCANNING METHODS

To capture the injected ESD current, the magnetic field is measured by a probe close to the surface of the PCB. An ESD pulse is injected into the PCB (injection to ground plane is the following case) and the magnetic near-field components at one location is captured by probes respectively. Then the probe is moved to next location and another pulse is injected for measurement. Such step is repeated until a sufficient number of locations have been measured. The timing of measurements on all locations should be well synchronized.

For the injected plane surface current reconstruction, due to the close proximity of the shielded loop probe to ground plane, the surface current density J approximately equated to the magnetic field component H, which can be recovered by orthogonal scanning data process and probe factor compensation. For the coupled trace current reconstruction, the differential H_z probe is used to measure the trace current with rejection of injected plane current coupling.

There are a couple of choices for setting up the measurements. The first method is using an ESD injection source, such as ESD generator or transmission line pulser (TLP), and a real-time oscilloscope with H-field probe to capture the transient current. The signal synchronization is done by trigger output from ESD generator or TLP. Another method is to use a network analyzer (NWA) to measure frequency domain coupling (S21) between injection port and probe port in frequency domain, and then do a time domain transform to get the time domain results.

4.1. TIME DOMAIN SCANNING METHOD

For ESD current injection and reconstruction, the most directly setup would be a ESD source and probe connected to time domain instrument. The block diagram and scanning setup will be described first, then the scanning raw data will be shown and analysed.

4.1.1. Block Diagram and Scanning Setup. Figure 4-1 shows the block diagram of time domain current reconstruction scanning method:

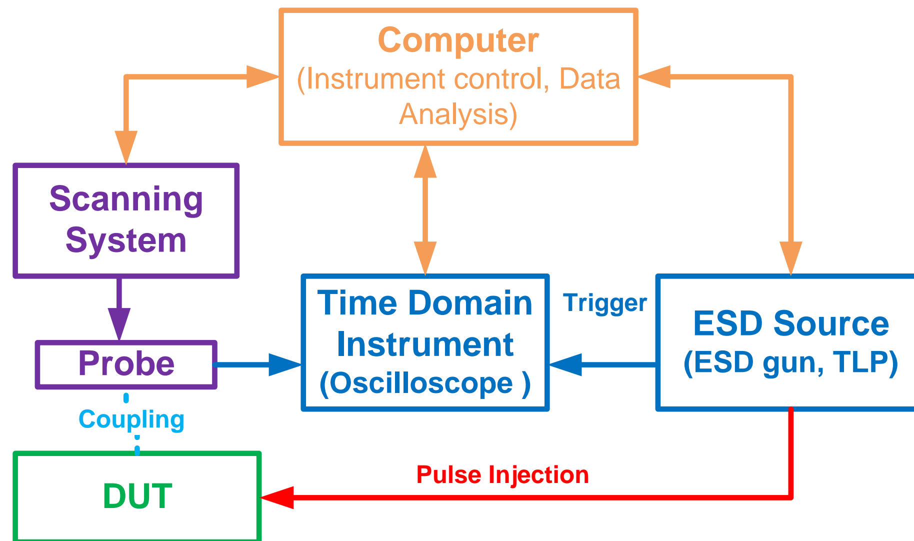

Figure 4-1. The block diagram of time domain scanning method

The scanning system is controlled by a computer which allows flexible adaption to other instruments. The process of the scanning program is:

Move probe to location

Start ESD pulsing

Take data from time domain instrument and check signal level:

If oscilloscope is not well scaled, improve scale and measure again

If oscilloscope is well scaled, record the data and go to next location

All recorded data is time referenced on the trigger out from the ESD Source, so the current spreading on the PCB can be visualized by processing data into frames and plotting them as a function of time.

The time domain current reconstruction scanning method performed in the following case is using a Transmission Line Pulser (TLP) as excitation source because it is easier to model and simulate than an ESD gun. Figure 4-2 shows the current reconstruction scanning setup using a TLP and an oscilloscope:

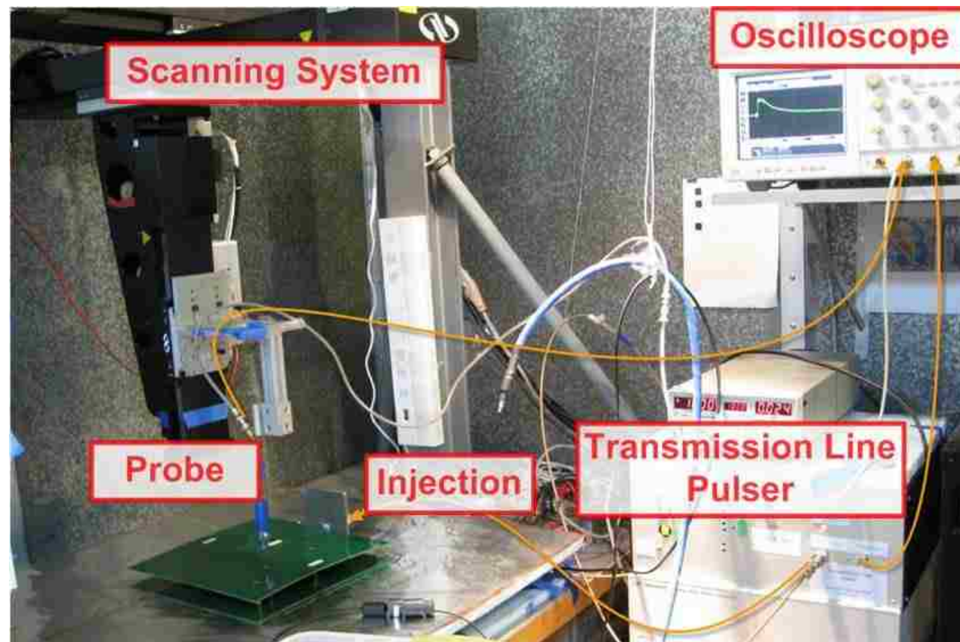

Figure 4-2. TLP and oscilloscope scanning setup

In the setup, the ESD current is injected from the right middle edge (x =300mm, y = 150mm) of the PCB at the ground plane. From the injection location, current spreads over the ground layer as Figure 2-1and Figure 2-4 showed, and couples to the 3 traces. All traces are terminated by matched loads. A shielded vertical-loop probe will measure the current spread on the surface of the PCB with 2 orthogonal directions (Hx and Hy components separately). In this way, one set of orthogonal scanning data will be created for post processing of complete current vector.

The oscilloscope records data after receiving a trigger from the TLP. Providing the TLP repeats well all measurements are "synchronized" and show the current spreading when plotted as a function of time.

4.1.2. Scanning Raw Data Analysis. Plotting the captured data over the DUT picture frame by frame allows a pretty good illustration of the injected current spreading on the PCB. The scanning raw data with probe oriented in parallel to X-axis is shown in Figure 4-3:

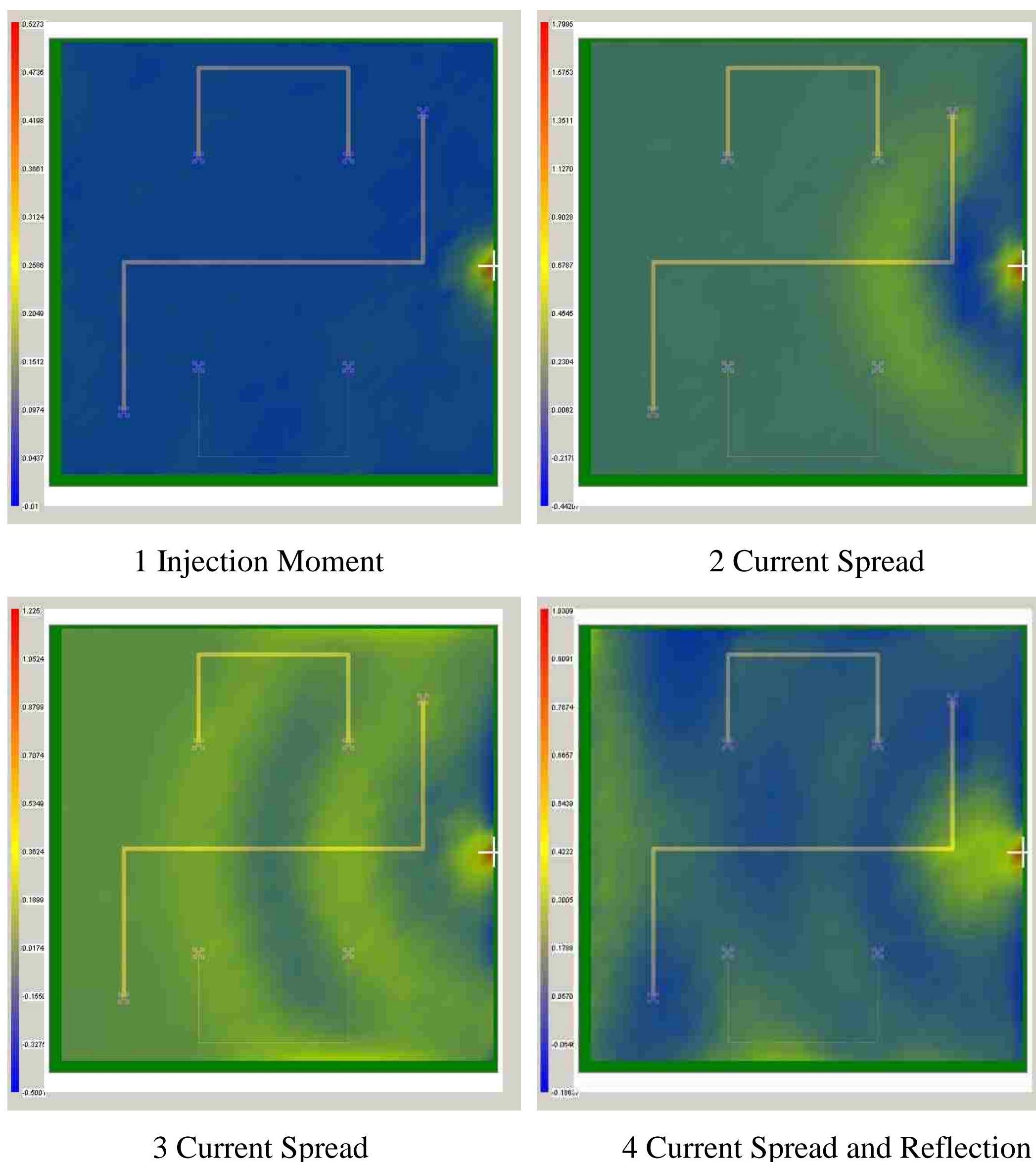

1 Injection Moment 2 Current Spread

3 Current Spread 4 Current Spread and Reflection

Figure 4-3. Movie frames of time domain scanning raw data (X-orientation)

The first frame shows a very large current density at the injection moment. It spreads in a circular fashion across the board (frame 2 and frame 3). The figures above illustrate only Hy field component (related to Jx) on the top side of the PCB. The PCB is connected to a large ground plane via SMA male to male connectors on its bottom side. Parts of the current will flow on the bottom side. After the current reaches the edges of the board, reflected waveform shows up in frame 4.

Due to the shape of the injection waveform from the TLP has some ringing in the rising edge and sometime thereafter, the fact that the probe signal approximately reflects the time derivative of the current density and the DUT structure has resonance at high frequency (especially 500MHz and 1GHz), a series of injections taking place when the raw data is plotted into frames. After the raw data is deconvoluted to obtain the current density this effect should be reduced.

The coupled trace current is hardly visible from this raw data as Figure 4-4 shows.

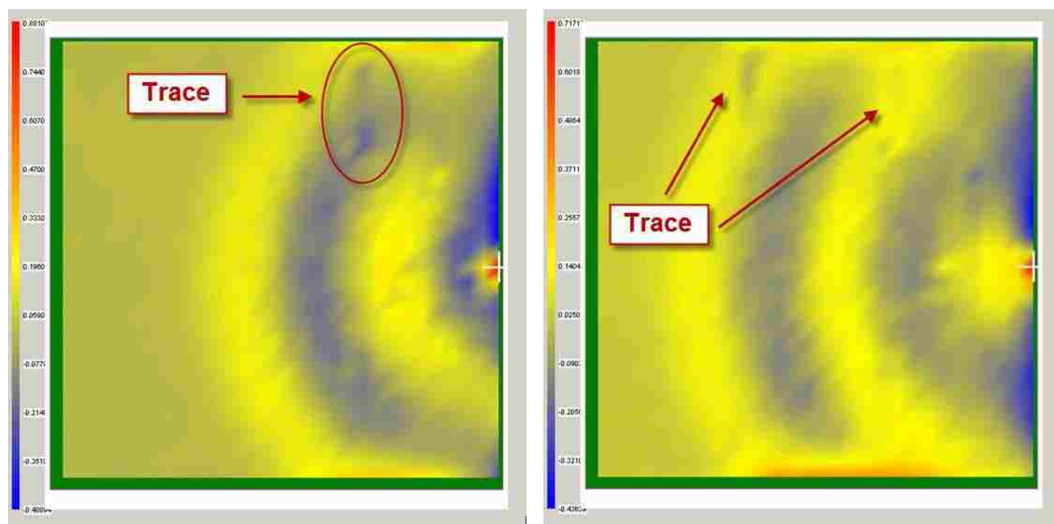

Figure 4-4. Movie frames with coupled trace current hardly visible

For a number of reasons the coupled trace current is not visible here. First, the probes used are not designed to suppress the magnetic field of the current density on the ground plane; instead they are designed to measure exactly the current on the ground plane. Second, the scanning resolution is 10mm x 10mm, thus few data points are close to the traces (trace is 2.8 mm wide).Therefore designing spatial probes with suppression to ground plane current but couples to trace current is necessary to visualize the coupled trace current.

Another scanning raw data plot with probe coupling oriented to Y-axis is shown in Figure 4-5:

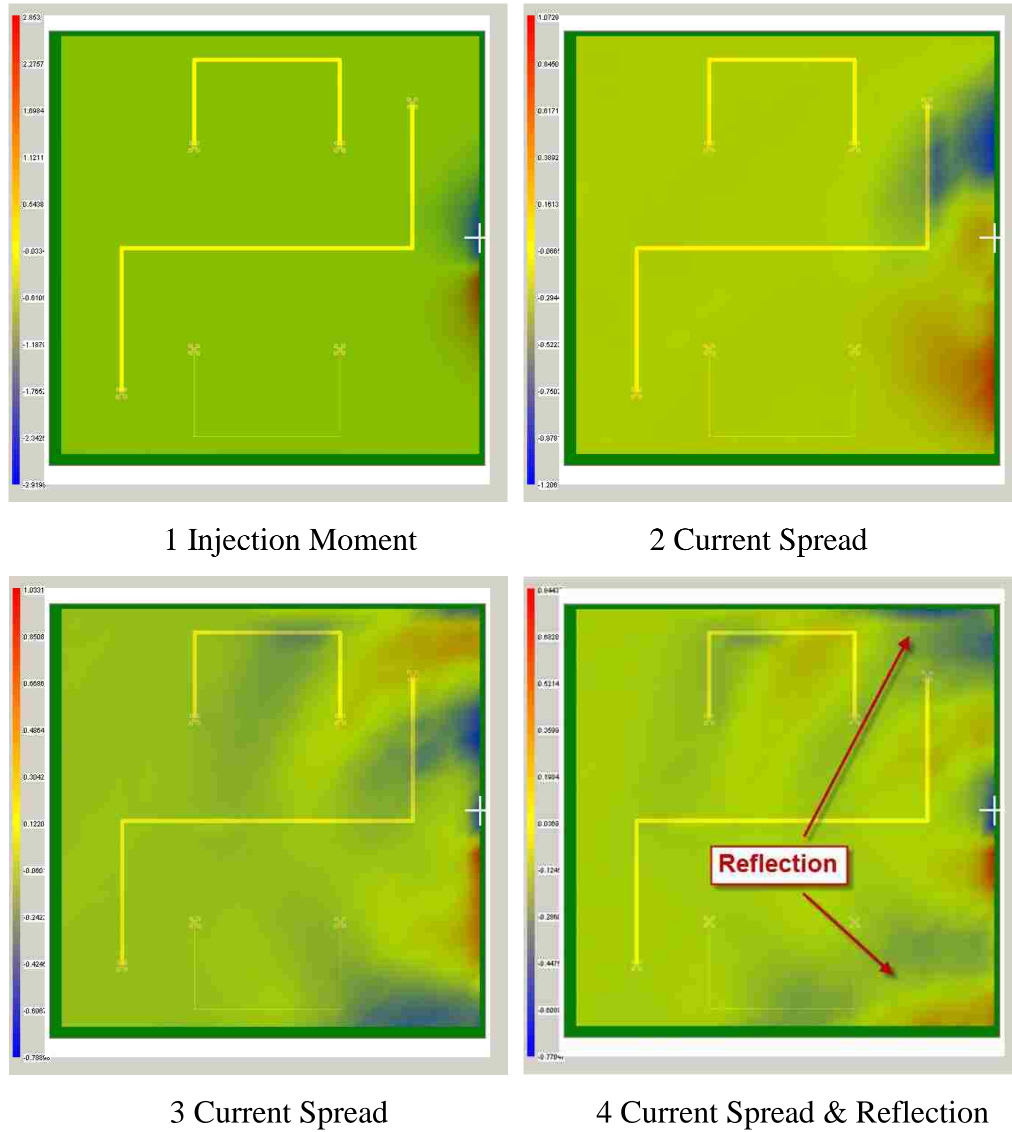

1 Injection Moment 2 Current Spread

3 Current Spread 4 Current Spread & Reflection

Figure 4-5. Movie frames of time domain scanning raw data (Y-oriented)

The raw data movie frames show the Hx component (related to Jy). The injected current flows in the up-down direction as frame 1 shows. Other frames show the current

spreading with circular fashion and the reflections occurs at the PCB edges. It is visible that the spreading circles are in 2 colors (blue and red). This is because the current flowing in opposite directions couples reverse amplitude (positive and negative) for the same vertical-loop probe orientation.

From the initial scanning result, there is an indication of lack of perfect symmetry. This is because the probe is not perfectly aligned or 90 degree rotated. Also the probe is handmade. In the future, PCB designed E-field shielded loop probe will provide higher accuracy and reproducibility. And probe rotator should also be added for precise 90 degree rotation. Overall, the TLP and oscilloscope scanning raw data gives a good result.

4.2. FREQUENCY DOMAIN SCANNING METHOD

When the test setup is linear with respect to current, it is not forced to use a high voltage ESD source as injection. A network analyzer with time domain transformation can be used for excitation and receiver instrument instead.

4.2.1. Block Diagram and Scanning Setup. The setup of the frequency domain scanning method is very similar to the time domain method.

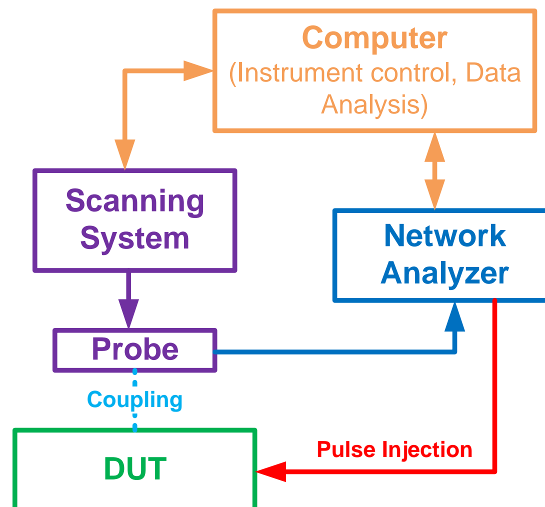

Figure 4-6. The Frequency domain scanning method

The setup injection port is connected to network analyzer port 1 and the probe is connected to the network analyzer port 2. Then the S21 is measured and transformed to the time domain. To improve the signal noise ratio, a 20 dB low noise amplifier is added in front of the receiving port with frequency response calibrated.

Figure 4-7. Network analyzer scanning setup

For a linear system a network analyzer measurement has many advantages over a direct time domain measurement in this case:

- It has better repeatability, unlike TLP using a high voltage relay (mechanical device) to produce pulses, and the relay also wears over time
- It has better dynamic range than oscilloscopes, so more details can be visualized during the injected or coupled current decrease over time
- It is easier to check the field coupling, validate the probe performance, setup mechanical stability in frequency domain
- The probe's coupling frequency response can be compensated within the network analyzer calibration step, then the recorded signal reflects the current directly
- the signal noise ratio can be improved by adding amplifiers on both the injection or receiving ports, and their frequency response can also be compensated within the network analyzer calibration step

- The injected by a network analyzer is cleaner than TLP, for example a step signal with no ringing or overshoot. Figure 4-8 shows the voltage waveform comparison:

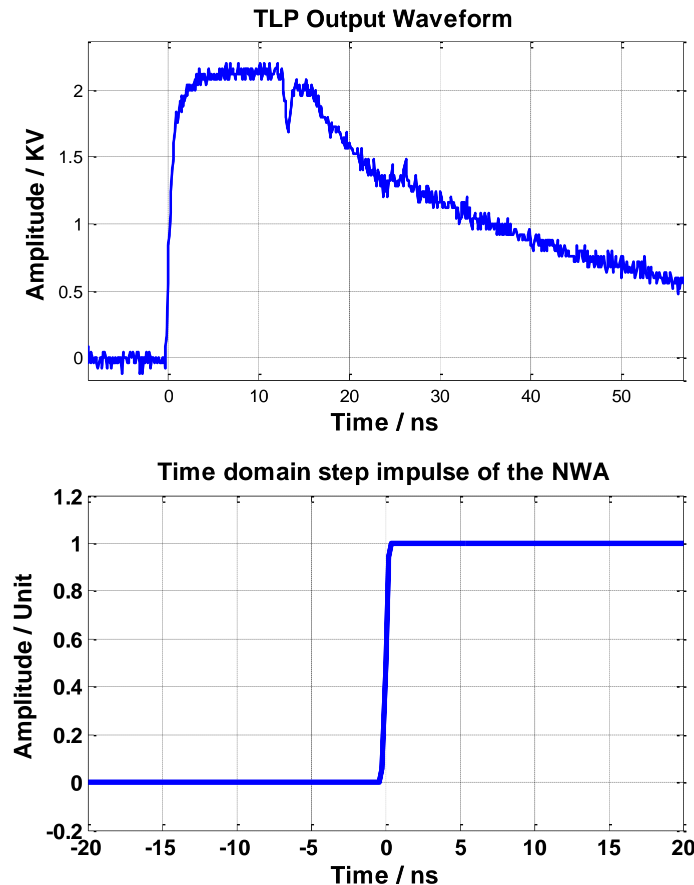

Figure 4-8. TLP and NWA time domain waveforms

- If the time domain transform is done at post process (after a scanning of S21 frequency domain data), the excitation signal can be arbitrary waveforms, not just several types from the network analyzer instrument.
- This method is normally safer for both device under test (DUT) and receiver instrument than high voltage injection methods.

However, since the method only works for linear system, any nonlinear effects such as current caused by voltage breakdowns won't be able to be captured. And this method usually requires an additional low noise amplifier at receiver or a power amplifier at injection to increase signal noise ratio as the frequency domain instrument setup has pretty weak injection signal and itself has noise, especially at low frequency.

4.2.2. Scanning Raw Data Analysis. For the network analyzer time domain transform setup, a normalized step function is generated as Figure 4-8 shows. Because the injected current will roughly follow the voltage waveform and the loop probe coupling is roughly the derivative of the excitation, a single pulse is expected in scanning raw data. Plotting of the captured raw data with probe oriented in parallel with X axis is shown in Figure 4-9:

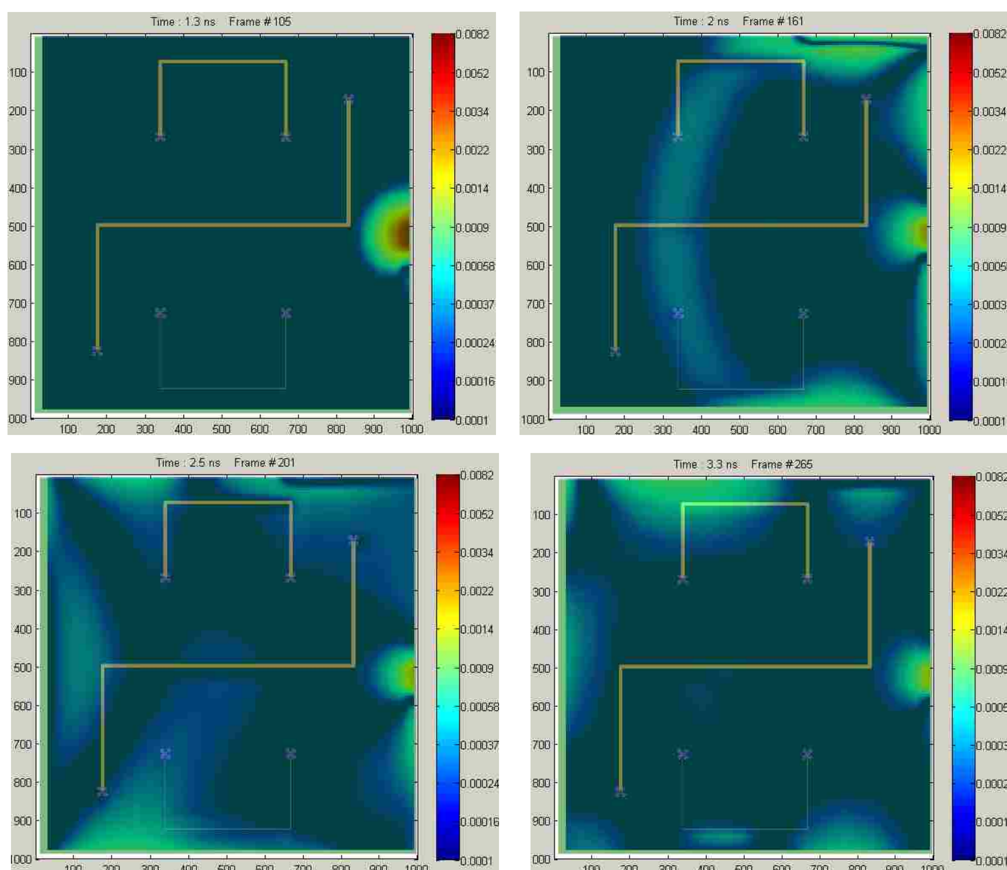

Figure 4-9. Movie frames of frequency domain scanning raw (X-oriented)

Comparing to previous TLP and oscilloscope raw data movie frames, the raw data shows much clearer outline due to better waveform shape. The reflected current waves are also more visible in details due to the better dynamic range of network analyzer.

Another set of movie frames of scanning raw data with probe oriented in parallel with Y-axis is also shown in Figure 4-10; the visualization scale is log scale so the absolute value of raw data is taken, then plot in log scale.

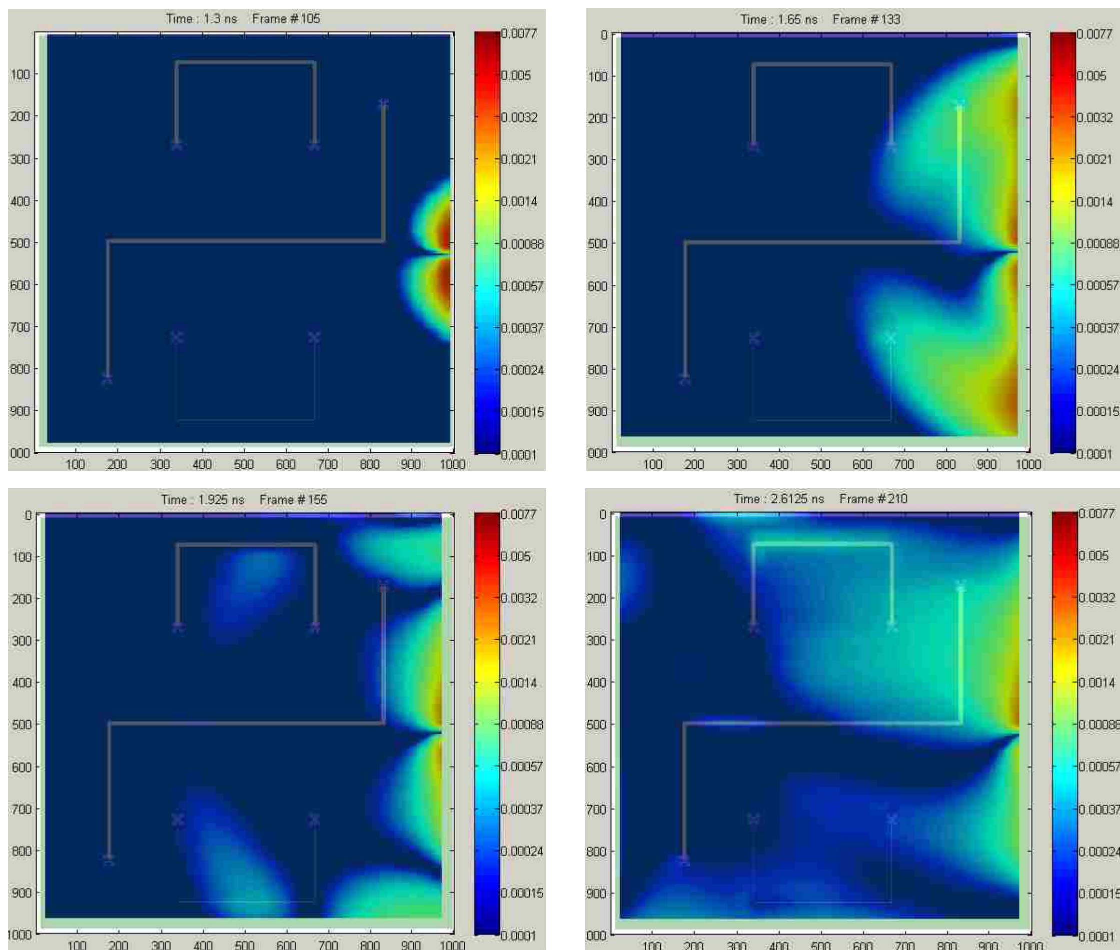

Figure 4-10. Movie frames of frequency domain scanning raw data (Y-oriented)

Overall, the raw data of the network analyzer is better than that of the TLP and oscilloscope scanning setup in excitation waveform and dynamic range. However to get this method work, the network anlayzer scanning setup should have enough coupling

bandwidth and dynamic range to cover the main spectrum of the transient magnetic field, the measurement setup should be very stable in this bandwidth, otherwise one frequency error will ruin the overall time domain data.

4.3. SCANNING DATA PROCESS

After the near-field scanning data is recorded, further process of the data is needed to visualize the current spreading on the scanning area. The main process would be the probe frequency response and directional response compensations to get the corrected complete current spreading vector. In addition, for the frequency domain scanning data, one can implement arbitrary waveform excitation to instantly get different sets of current spreading results.

4.3.1. Probe Frequency Response Compensation.

4.3.1.1 Deconvolution Methodology. In mathematics, deconvolution is an algorithm-based process used to reverse the effect of convolution on recorded data. In general, the object of deconvolution is to find a solution of a convolution equation of the form:

$$f * g = h$$

Usually, h is the recorded signal, and f is the signal that we wish to recover, but has been convolved with a transfer function g when we recorded it. The function g represents the transfer function of an instrument or a driving force that was applied to a physical system. If we know g, then we can perform the deterministic deconvolution.

For a loop probe, the H-field strength is the signal that we wish to recover, expressed as f in the equation above, the induced loop voltage is the recorded signal, expressed as h in the equation above. Using a network analyzer we can measure and calculate the frequency response of the probe, which would be represented by g in the equation above. Then the deconvolution can be performed in principle. However, deconvolution is often an instable process, thus many details of the process need to be considered to obtain a meaningful result.

The overall process can be divided into 3 steps:

1. Prepare recorded probe signal for FFT, which includes removing data offset, extending data and doing FFT.

2. Calculate the frequency response compensation function for probe, which includes modeling and matching the probe's coupling factor, generating frequency compensation function by inversing frequency response, adding appropriate high and low pass filters.
3. Compensate the data by frequency domain multiple, then do an inverse FFT.

The probe frequency response compensation process is shown in Figure 4-11 :

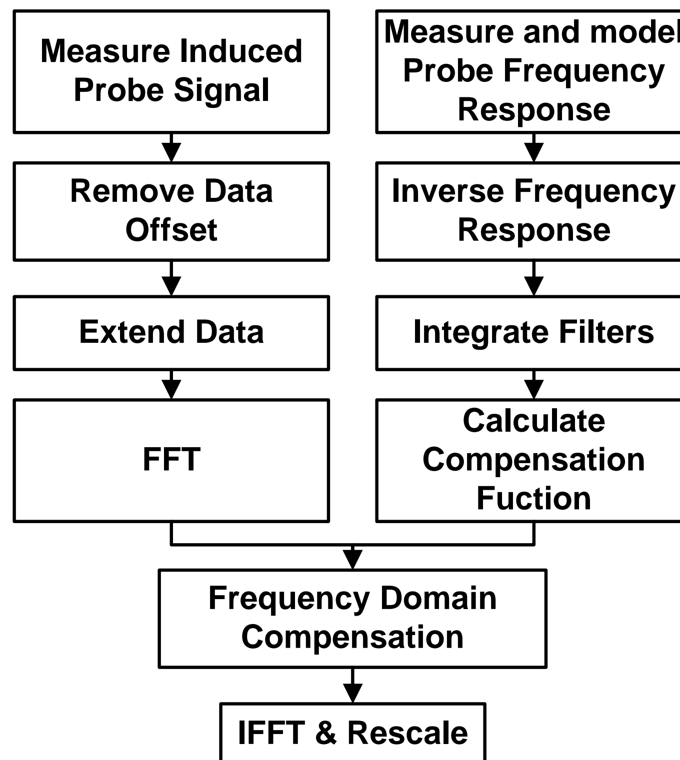

Figure 4-11. Probe frequency response compensation flow chart

4.3.1.2 Surface Current Probe Compensation. Below is an measurement example of the decovolution process for the surface current probe. The experimental setup is below:

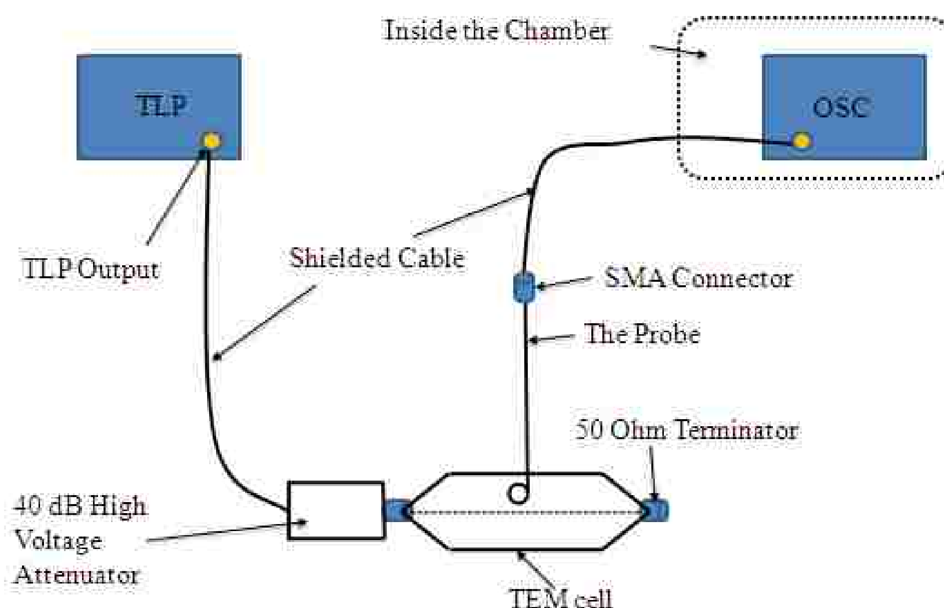

Figure 4-12. Experimental setup of measuring H-Field strength in the TEM cell

The excitation signal comes from transmission line pulser (TLP). After a 40 dB attenuator, the attenuated signal will generate TEM field in the TEM cell. The probe is orientated in its maximum coupling direction. The induced loop voltage on the probe will go through a well shielded cable and be recorded by a fast real-time sampling oscilloscope inside a chamber. Using well shielded cables and putting the oscilloscope inside a chamber are critical to reduce the electromagnet field direct coupling from the TLP to the oscilloscope. The result is to recover the transient field strength in the TEM cell from the signal recorded by the oscilloscope, as Figure 4-13 shows:

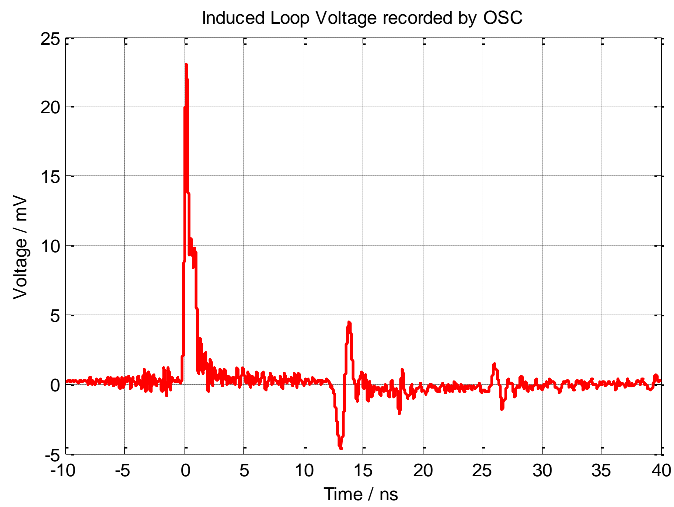

Figure 4-13. Measured induced loop voltage on probe

The above signal will be removed offset and extend with zeros to form a 2^N series for FFT. The coupling can be modeled as a circuit as below Figure 4-14:

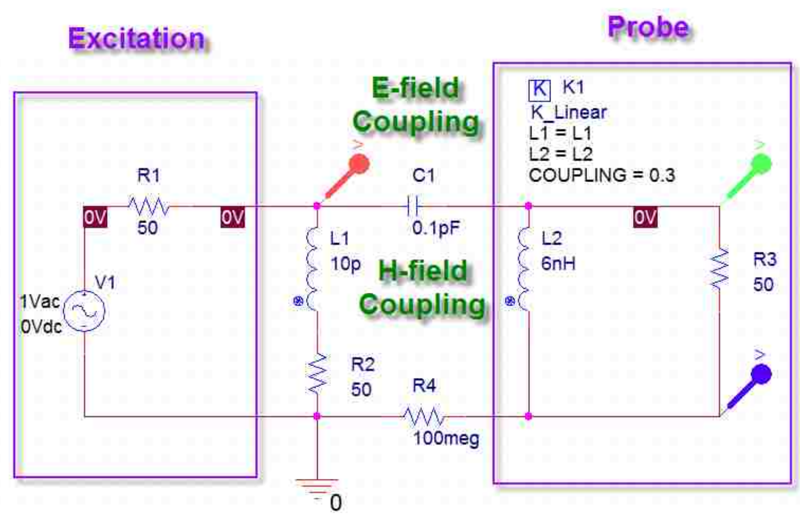

Figure 4-14. Circuit model of field coupling

The coupling factor of the circuit model plus the cable loss (1/2*S11) measured is matched with the S21 measurement result during probe coupling factor characterization, as Figure 4-15 shows.

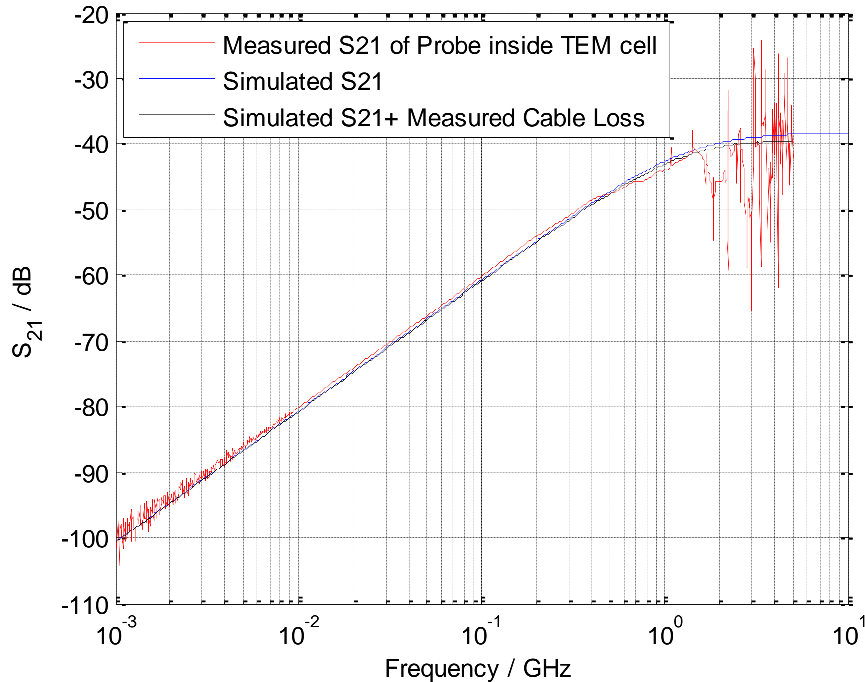

Figure 4-15. Comparison of S21 between measured and simulated coupling factors

Then a circuit model is created to generate the compensation function. For the equivalent circuit in Figure 4-14, the parameters are (in MATLAB Code):

```
L_trace_1 = 10e-12;                  % 10pH
L_loop_1  = 6e-9;                    % 6nH
K1 = 0.3;                            % Coupling factor
M1 = K1*sqrt(L_trace_1*L_loop_1);  % Mutual Inductance
```

The frequency response of the circuit is calculated as below:

```
s  = 2*pi*j*f;
FR = 50.*s*M1./(50 + s*L_loop_1+s*M1)./(50 + s*L_trace_1+s*M1);
```

Then, the effect of the probe cable loss (1/2*S11) needs to be taken into account:

```
FR1 = FR.*(10.^(cable_loss/20));
```

The frequency compensation function of the probe is done by inversing the frequency response as below:

```
CFR1 = 1./FR1
```

Then, to get a better result by suppressing both the high frequency resonance and low frequency noise, both high pass and low pass filters are modeled and added to the frequency compensation function as below:

```
% set a 1 order highpass filter
R_highp = 5;
C_highp = 5e-12;
highpass = s.*R_highp.*C_highp./(1+s.*R_highp.*C_highp);
% set a 1 order lowpass filter
R_lowp = 25;
C_lowp = 10*1e-9;
lowpass = 1./(1+s.*R_lowp.*C_lowp);

CFR2 = CFR1.*highpass/.*lowpass;  % can add more orders
```

Finally the probe's frequency compensation function with filters is completed and a plot of all the compensation functions during this process is shown in Figure 4-16 :

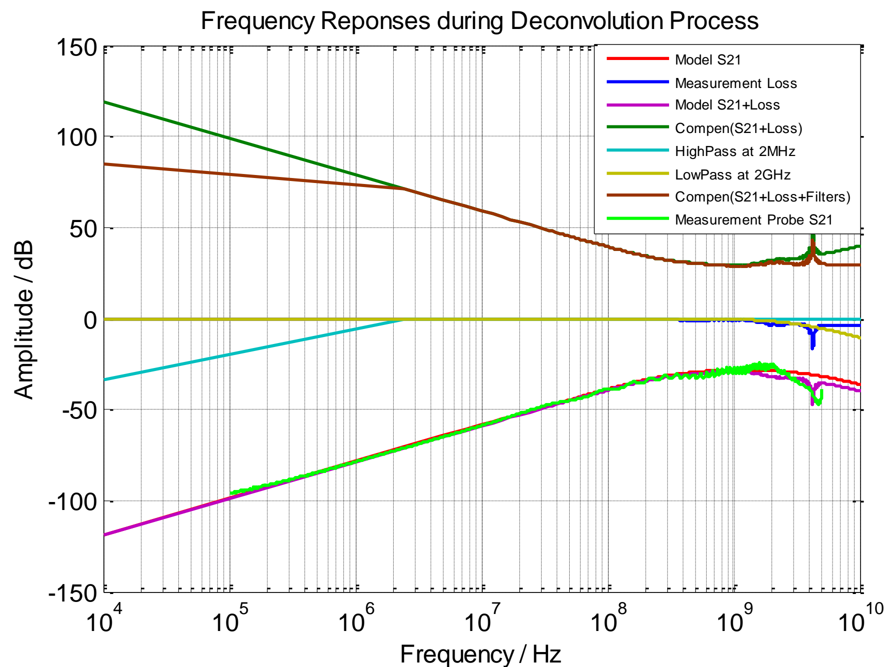

Figure 4-16. The created compensation functions during deconvolution

Now the field strenght can be recoverd by frequency domain multiplication of recorded probe voltage signal (after FFT) and compensation function, then do an IFFT. Figure 4-17 shows a comparison of field strength recovered from measured induced probe voltage and field strength measured directly:

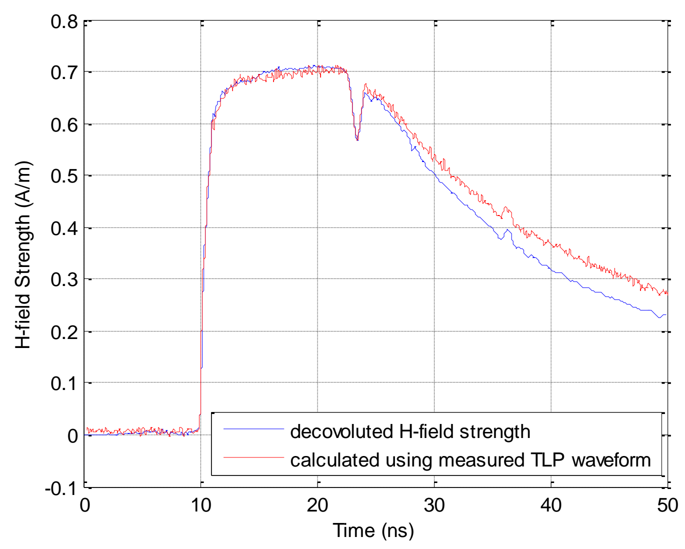

Figure 4-17. Comparison of recovered field strength and measured field strength

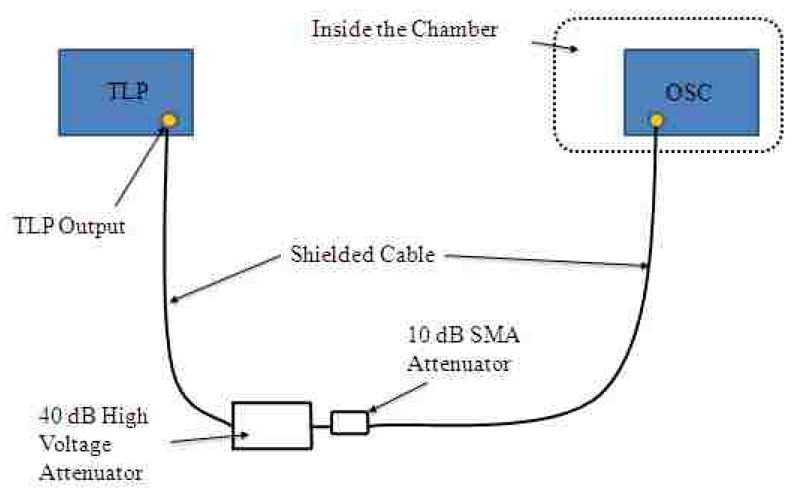

Figure 4-18. Experimental setup for measuring voltage of the TEM cell

4.3.1.3 Trace Current Probe Compensation. The deconvolution process of differential Hz probe is similar to shielded loop probe, but the recover object is trace current (Ampere). Therefore the calibration process is to measure the coupling frequency response on a matched trace as Figure 4-19 shows:

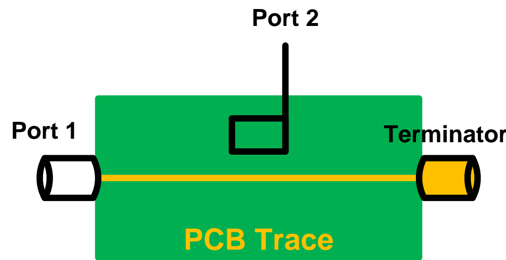

Figure 4-19. Trace current probe calibration method

Since the field around trace current is not uniform, the handling (probe orientation, height and offsets) of the probe during measurement should be well controlled for maximum coupling, the best way is to do calibration with a scanning system. The measurement result is shown in Figure 4-20:

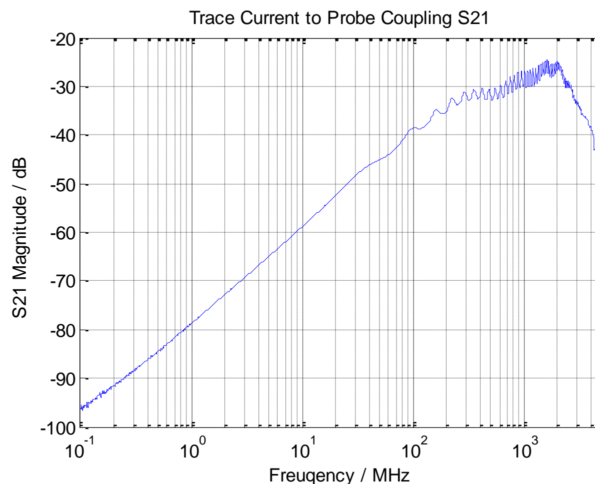

Figure 4-20. Probe frequency coupling response of a differential H_z probe

Then the probe loss is measured as the same setup as shielded loop probe, the result is shown in Figure 4-21:

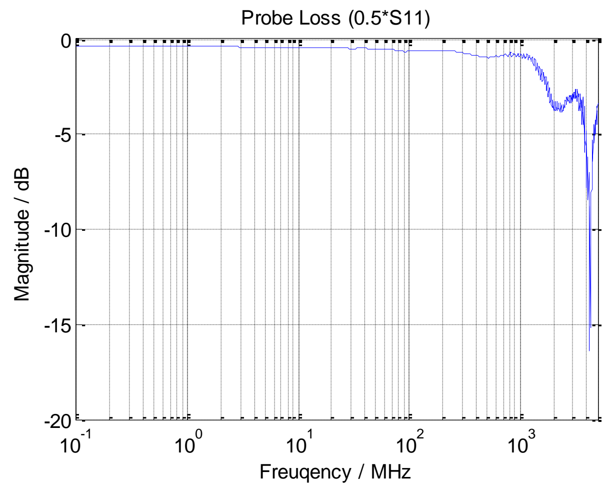

Figure 4-21. Probe loss of a differential H_z probe

The compensation functions during this process are shown as below:

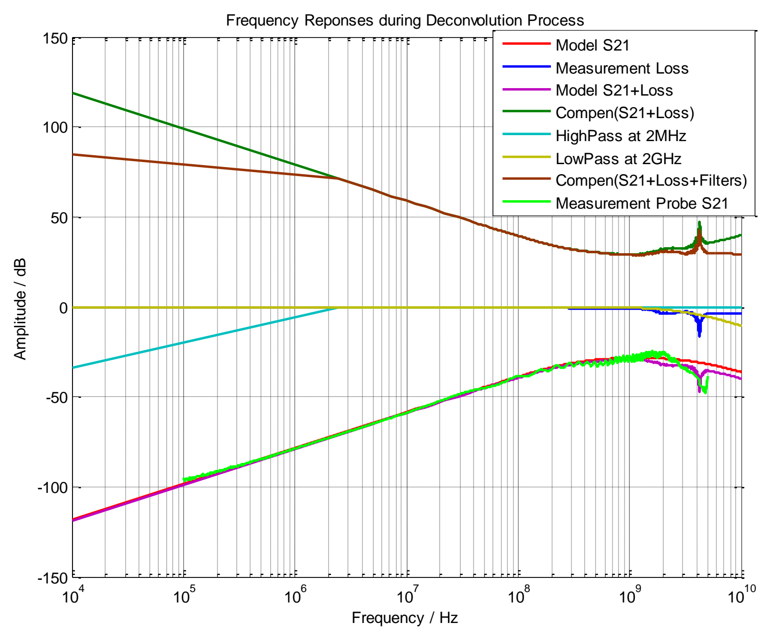

Figure 4-22. The created compensation functions during deconvolution

Figure 4-23 shows the coupled voltage signal when using a differential Hz probe to measure a matched trace current, the excitation signal is a normalized step function:

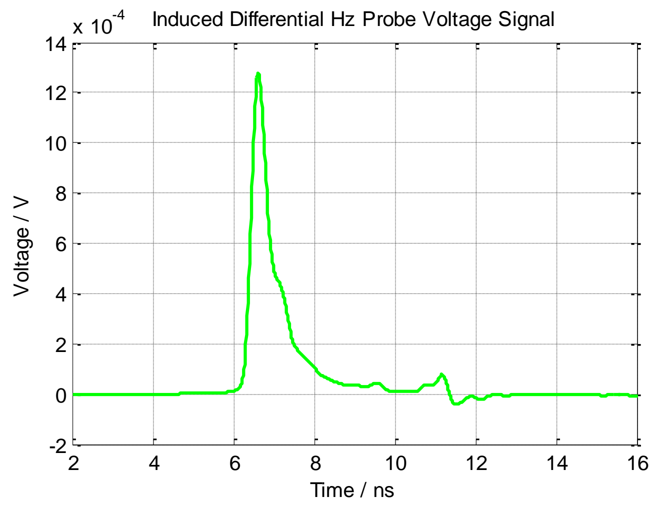

Figure 4-23. Measured differential Hz probe voltage signal

Then, the compensated current from probe signal and the directly measured current is shown in Figure 4-24 :

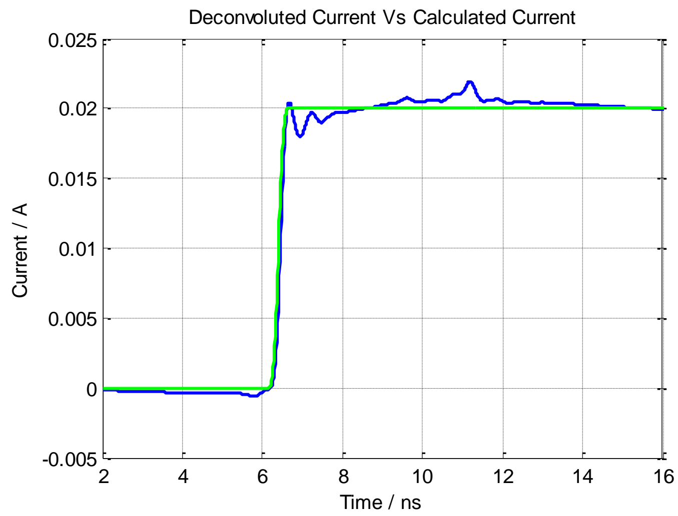

Figure 4-24. Comparison of deconvoluted current and measured current

4.3.2. Probe Directional Response Compensation. The directional response of a probe reflects how it couples to field or current during rotation, usually from the maximum to the minimum coupling direction.

A shielded single loop probe usually has good directional response that follows cosine drop from the maximum to minimum coupling direction. If a probe's directional response follows cosine drop, the orthogonal measurement signals such as Vx and Vy can be separately processed and directly mapped to vectors Hx and Hy, or Jx and Jy.

A shielded trace current probe, depending on the coupling mechanism, may not have good directional response that follows cosine drop. Thus the process of orthogonal scanning data needs to compensate for its directional response.

The directional response of a probe is only compensable in its linear dynamic range, or inductive coupling range. Figure 4-25 shows a trace current probe with deficient directional response. The linear region is from 50 MHz to 1 GHz. The normalized directional response of the probe is shown in Figure 4-26. The 90 degree rejection is less than 20 dB, which suggests certain common mode coupling exists.

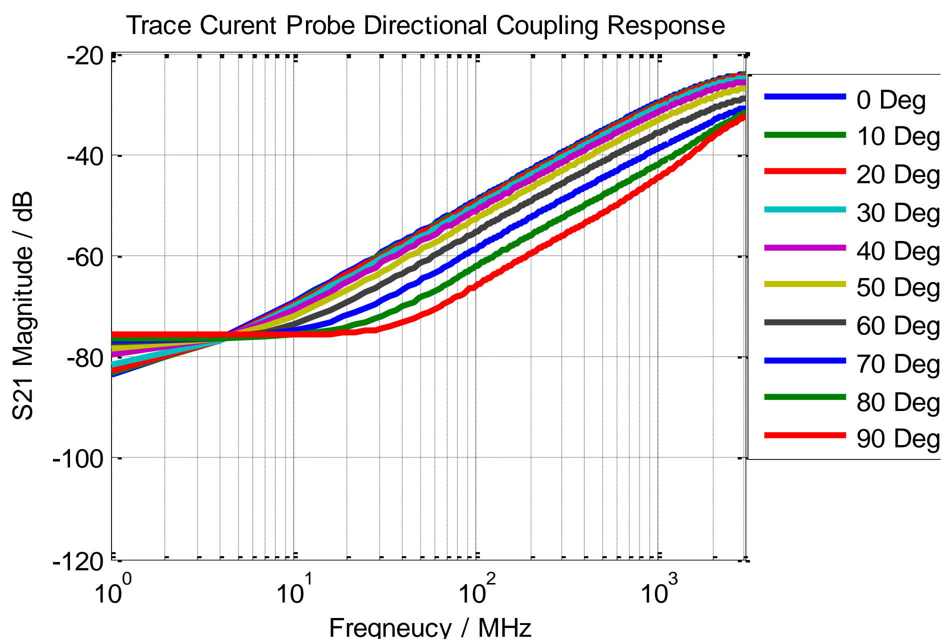

Figure 4-25. Probe with deficient directional frequency response

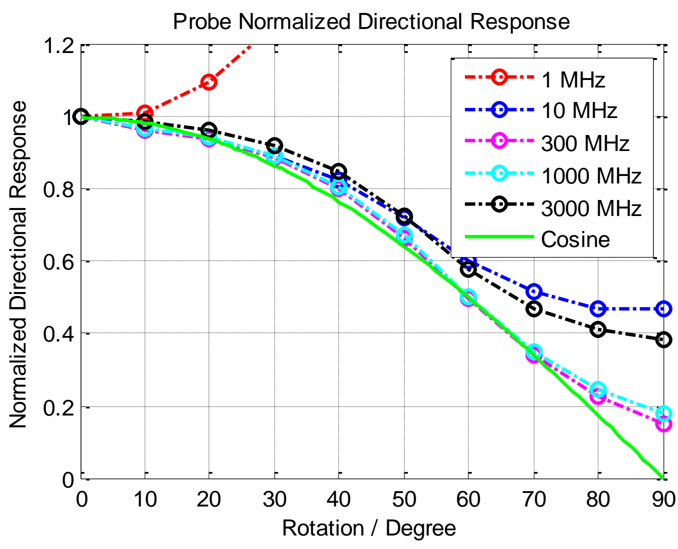

Figure 4-26. Probe's normalized directional response in several frequencies

The coupling frequency responses of a probe with better directional response are shown in Figure 4-27.

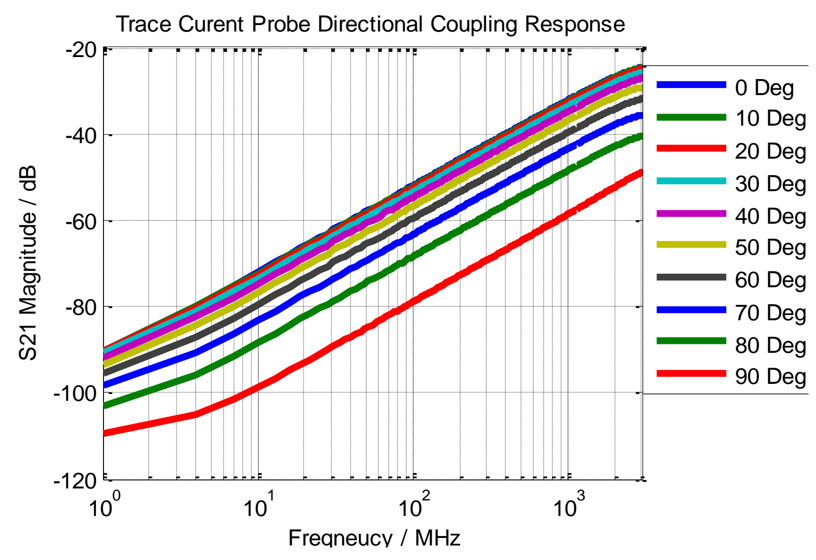

Figure 4-27. Probe with better directional frequency response

The probe has wider inductive coupling dynamic range (from 5MHz to 3GHz) with good directional response. In addition, its normalized directional responses in this range are shown in Figure 4-28.

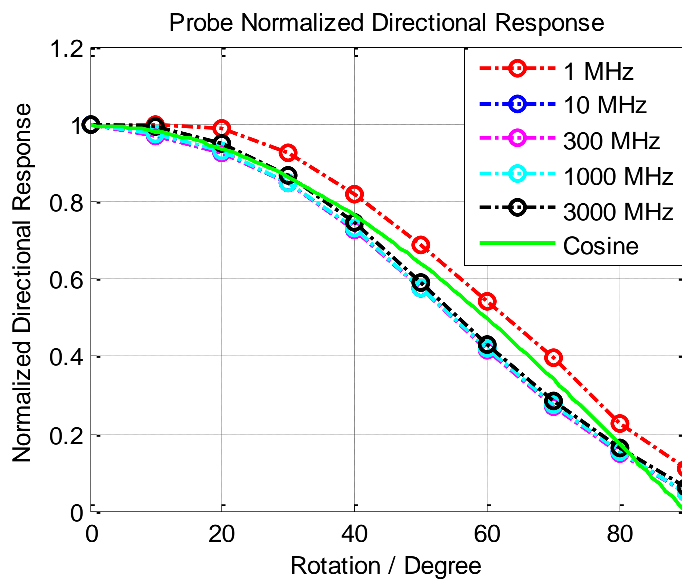

Figure 4-28. Probe's normalized directional response in several frequencies

The orthogonal scanning data can be compensated if its directional response is symmetry between [0, 90] and [0, -90], and also monotone decreasing in [0, 90] (0 degree is the probe's maximum H-field coupling direction and the probe is well shielded against E-field coupling). Suppose an orthogonal data set of Vx and Vy is measured from scanning using this probe as Figure 4-29 shows.

The trace current under the probe is θ degree from the X-axis positive direction and 90-θ degree from the Y-axis positive direction. The process to calculate I and θ from Vx and Vy is to find the measured local Vx/Vy ratio in the calibrated and interpolated Vx/Vy curve as the Figure 4-30 shows.

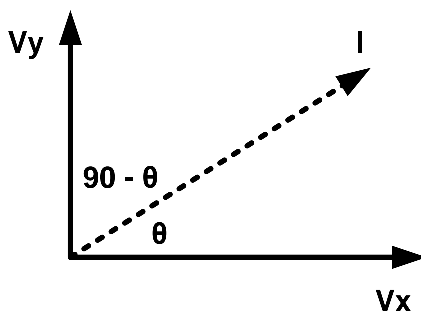

Figure 4-29. Commonly measured orthogonal data set

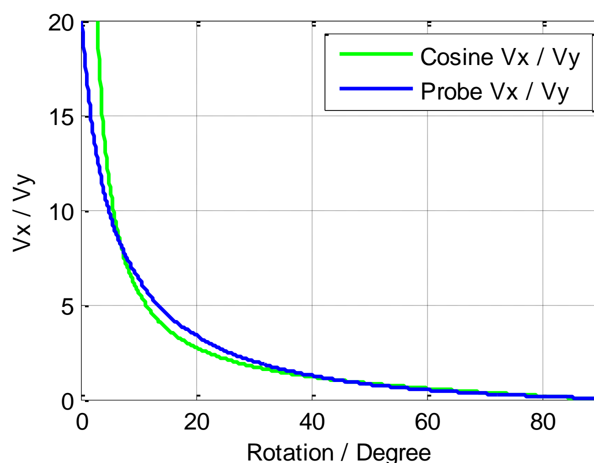

Figure 4-30. Probe's Vx/Vy monotone decreasing curve

Since the probe's normalized directional response is monotone decreasing, the Vx/Vy curve is also monotone decreasing. Therefore, there is a one-to-one correspondence relation between the Vx/Vy and θ. Then the maximum coupling response vector V can be calculated from the probe's normalized directional response as Figure 4-31 shows and the trace current vector I can be recovered from frequency response deconvolution process.

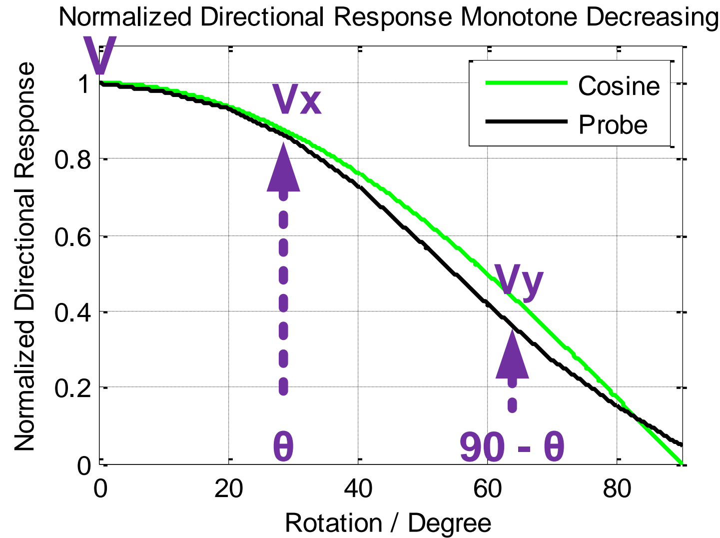

Figure 4-31. Relations of Vx, Vy and V on the normalized directional response

In this way, the current vector I can be completely recovered as long as the probe's normalized directional response is symmetry between [0, 90] and [0, -90], and also monotone decreasing in [0, 90]. The common mode h-field coupling maximized at 90 degree direction won't be added into the recovered vector I.

4.4. CURRENT SPREADING VISUALIZATION

After the raw data or the processed data are finished, the visualization of the data is important since this gives the most directly illustration of all data for the current spreading analysis.

4.4.1. Current Magnitude Visualization. As the magnitude of the injected surface current density or coupled trace current is the most interested value for the current reconstruction scanning results, the visualization of the magnitude is studied.

4.4.1.1 Linear Scale Image. The most directly illustration method is to plot the magnitude of time domain signal at each location in a 2D image as Figure 4-32 shows:

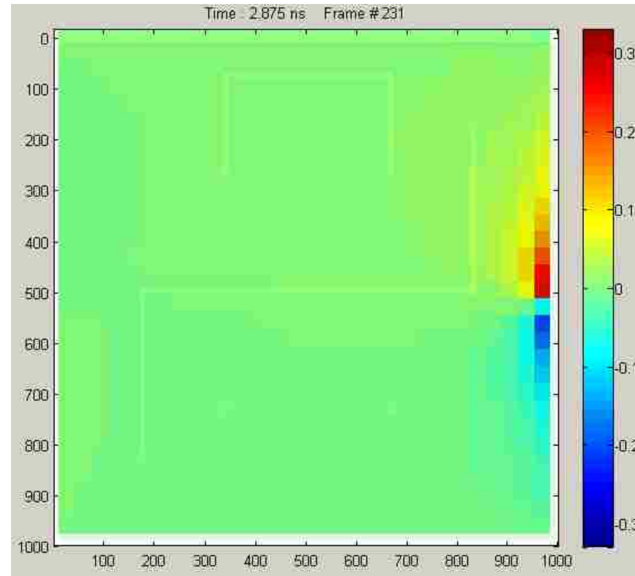

Figure 4-32. 2D image of compensated Jy component

In the above figure, the color mapping of the figure is scaled to the maximum of the overall scanning data in the event duration, and is symmetry in positive and negative value. However, this scale is good for comparing 2D field over time, but many details is hardly visible, especially after the injected current spreads for a while and the current density or magnetic field strength is too weak.

Another type of visualization – linear floating scale, which sets the maximum and minimum color map according to the real-time 2D max and min, is better for analyzing the details after the current density drops a lot from injection moment. A comparison of the of linear fixed and linear floating color mapping scale after current density at the same moment after current density drops is shown in Figure 4-33:

However, even in the floating scale, many details of the scanning data might not observable, especially when the current density on a frame contains data span over several order of magnitude. The advantage of linear scale is the positive and negative are very observable.

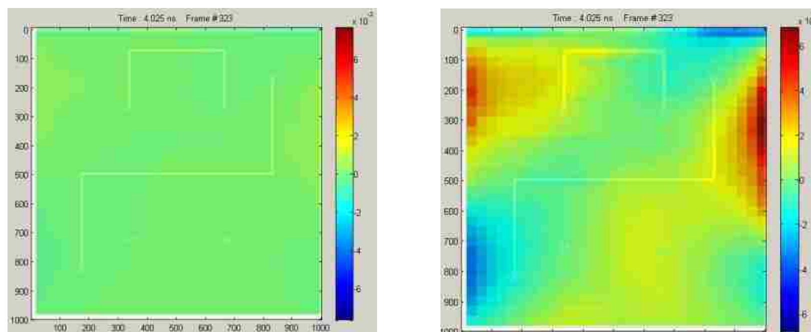

Figure 4-33. Comparison of linear fixed and floating scale

4.4.1.2 Log Scale Image. To better observe the scanning data in more details, the log scale visualization method is implemented by taking the absolute data value and map it into log scale. One important factor of this color mapping method is the minimum mapping should higher than the noise level, otherwise the mapping of noise level signal is largely “zoomed” and the mapping of useful data is squeezed onto the upper corner of the color bar.

Figure 4-34 shows the same data with different log scale color mapping factors. The min color mapping value of left figure is relatively too low and causes most of the data in this image to be too red. The right figure shows another image with minimum color mapping value just above the noise level and therefore the data is illustrated in better color mapping. However, the drawback of this method is the loss of polarity information during visualization.

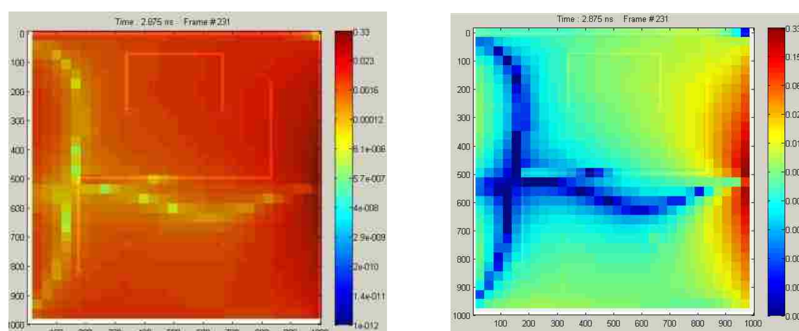

Figure 4-34. 2D images of scanning data with different log scale color map factor

4.4.2. Current Vector Visualization. The complete current spreading vector can be illustrated as arrows with its length showing the current magnitude or density and its direction showing the current flowing directions. This would be the most informative visualization method for current spreading vectors as Figure 4-35 shows:

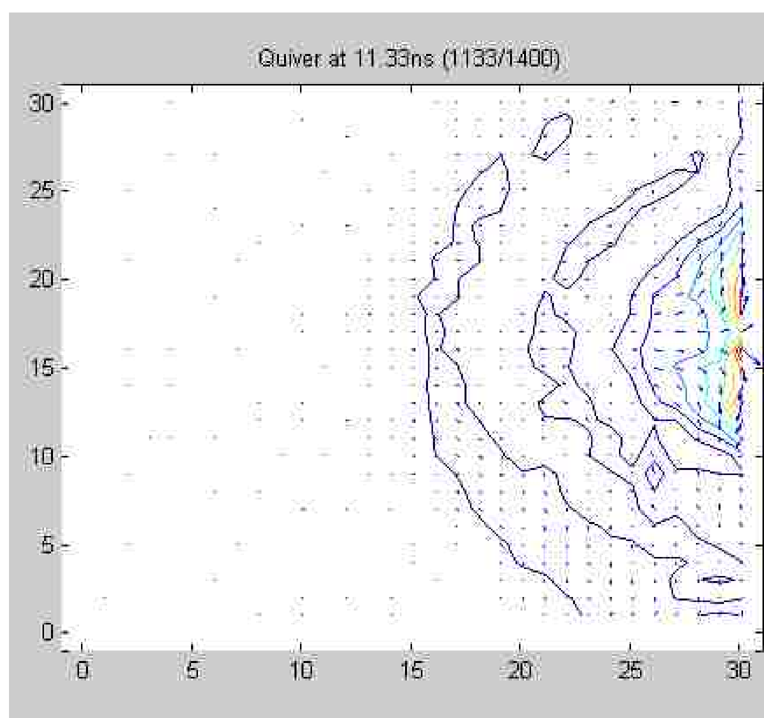

Figure 4-35. Vector visualization of current reconstruction scanning data

However, the only vector visualization method might not looks as nice as the color mapping images as when the resolution gets higher, the length of current vectors in the figure are forced to be smaller and looks like a lot of points not arrows, especially when the magnitude of the current spreading vectors are cover several orders of magnitudes. A better way of showing the current spreading vector might be combining the vector arrow (normalized the magnitude so it only shows current flowing directions) with magnitude log scale color mapping image.

4.4.3. Linear Interpolation of Image. Sometime, the scanning points of the a area is spare, but the current spreading is linear for the scanned structure so that a linear interpolation view can help recognize some small details relations as Figure 4-36 shows.

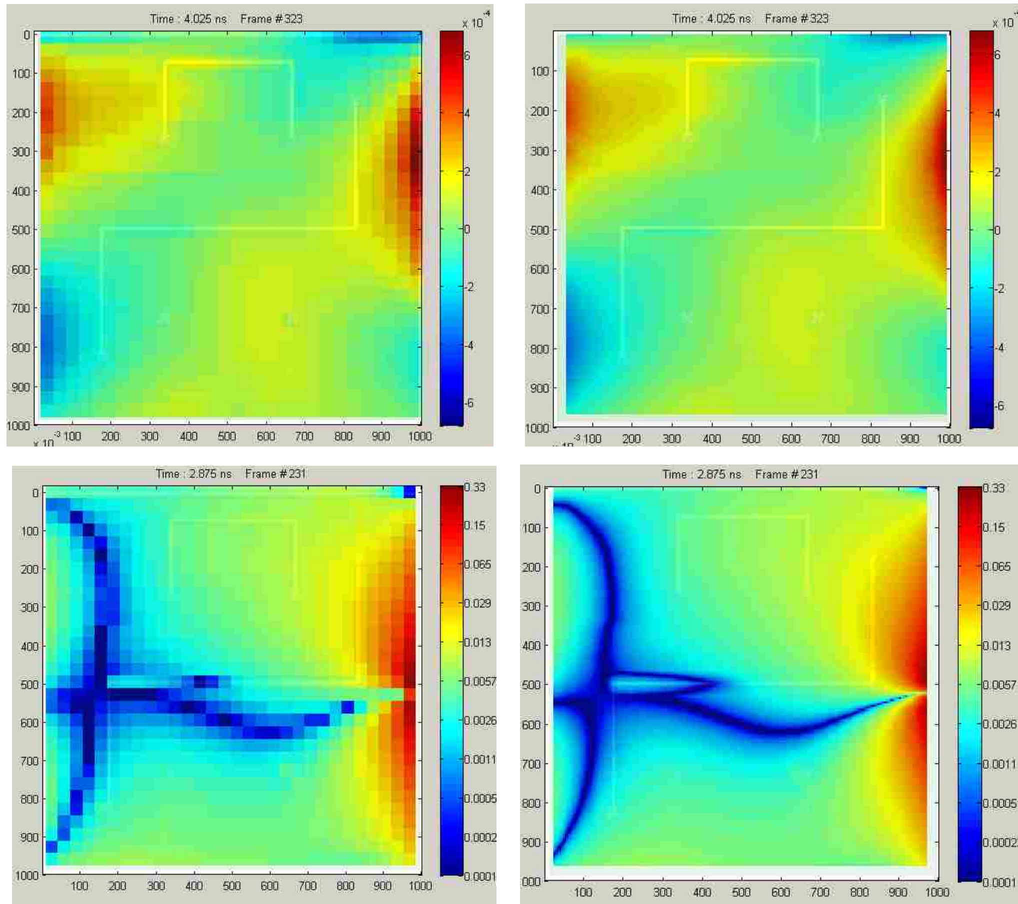

Figure 4-36. Linear interpolation effect of scanning data

The figures on the left side show the directly scaled data image, and the figures on the right side show the interpolated scaled data image. The interpolated image not only just looks smoother, but also shows the field over the trace (on the left center of the board) very well.

4.4.4. Current Reconstruction Viewer (GUI). To better analyze the scanning data, a graphic user interface with probe factors compensation, 2D current spreading visualization, time domain signal hold on comparison is designed for current reconstruction data analysis as Figure 4-37 shows:

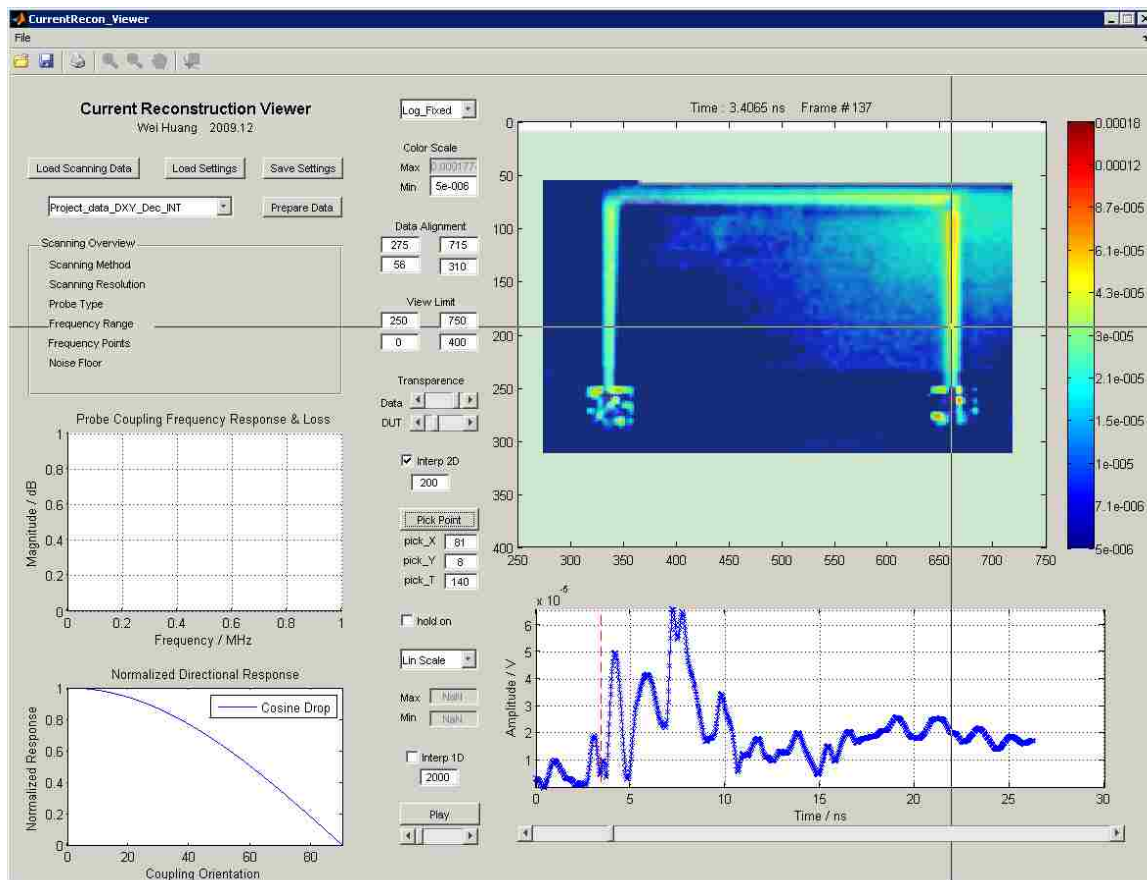

Figure 4-37. Current reconstruction viewer (GUI)

.

5. SCANNING RESULTS SIMULATION VERIFICATION

5.1. CURRENT RECONSTRUCTION STRUCTURE MODELING

To better analyse the injected current spreading and field coupling mechanism on the PCB current injection structure, and also verify the validation of reconstructed current spreading results from near-field scanning, a full wave model of the structure is created. The top view of the full wave model is shown in Figure 5-1:

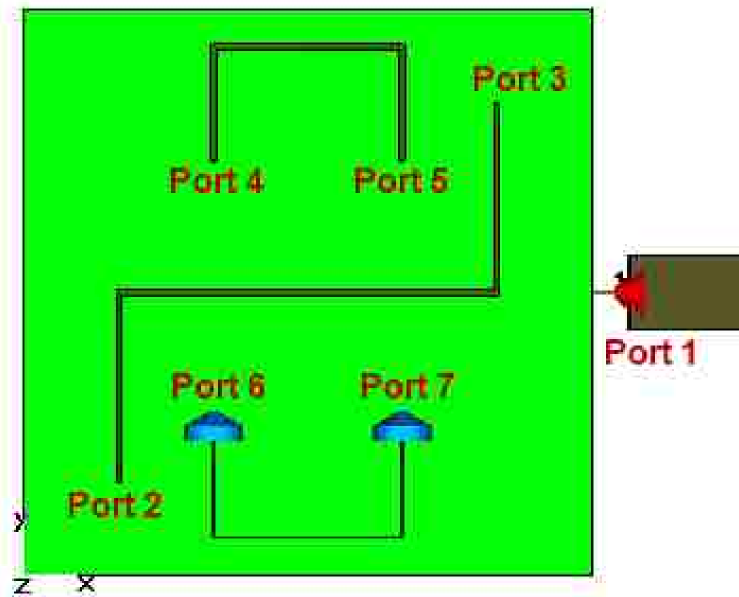

Figure 5-1. Top view of the PCB current injection model

To simulate the current injection event on the structure, the reflection coefficient (S11) of the injection port and the coupling factors between SMA ports and injection port (S21 – S71) of the model needs to be matched precisely with measurement results.

To quickly simplify and model an existing structure, a good ways is starting from instant measurement inspections, not directly model. For modelling of the excitation port, several suspected influence factors on the excitation port are listed and the investigations of their influence on S11 are done in Table 5.1:

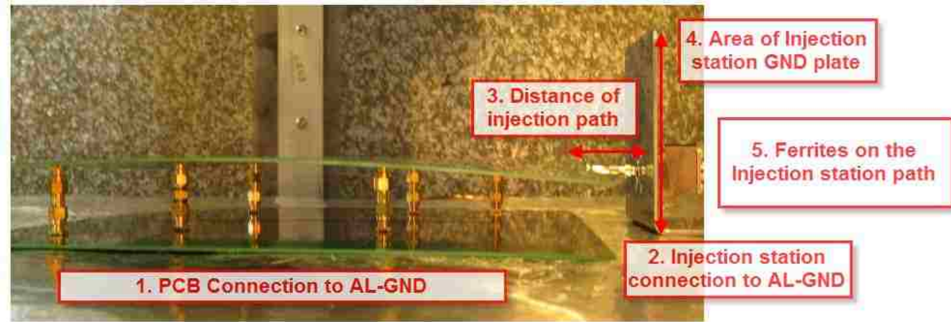

Figure 5-2. Suspected influence factors for excitation ports

1) Connection between PCB and GND
2) Connection between injection structure and GND
3) Length of the injection pin
4) Size of the injection station GND plate
5) Ferrites influence on the injection cable
6) Free space around the structure
7) Free space near the excitation port

Table 5.1. Measurement results of suspected influence factors for simulation

#	Influence	Indication
1	Huge	Need very good contact in measurement
2	Huge	Need very good contact in measurement
3	Somehow	Need precisely modelled in simulation
4	Huge	Need precisely modelled in simulation
5	Little	Few common mode on excitation port, simulate mode 1 is okay.
6	Little	10 cm space around the structure should be enough
7	Somehow	Need enough free space around the injection structure in simulation

From the investigations, the size of the injection pin and the shape of the injection structure are measured precisely for modelling; the large current return ground is

modelled as PEC boundary and the contacts are fortified in measurement, enough free space is left around the excitation port as Figure 5-4 and Figure 5-4 show:

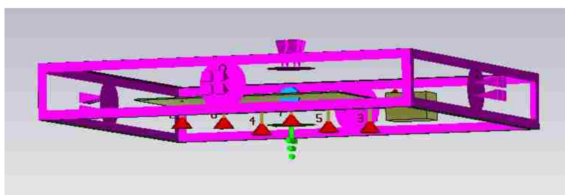

Figure 5-3. Boundary of the PCB ESD structure model

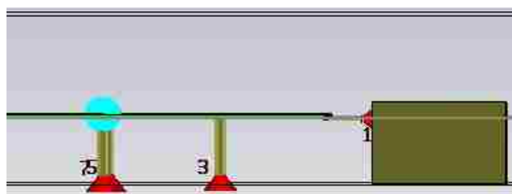

Figure 5-4. Free space around the excitation port

The S11simulation result matches measurement result as Figure 5-5 shows:

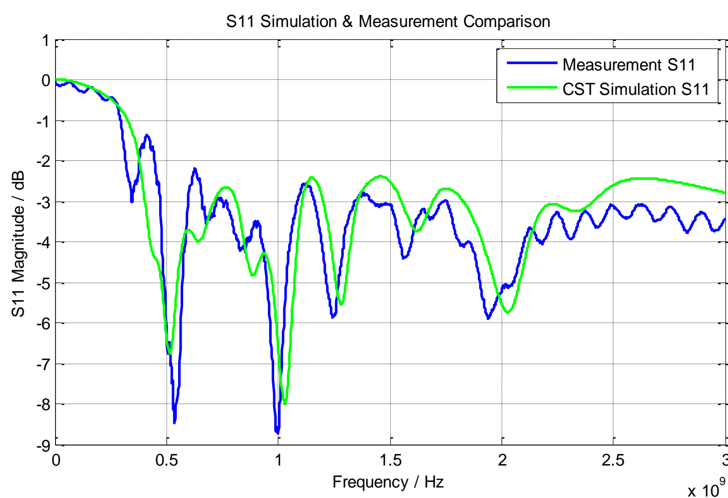

Figure 5-5. Frequency domain verification of excitation port on the structure

In the same way, the coupling frequency responses of other ports are verified in both frequency domain and time domain simulation as Figure 5-6 and Figure 5-7 shows:

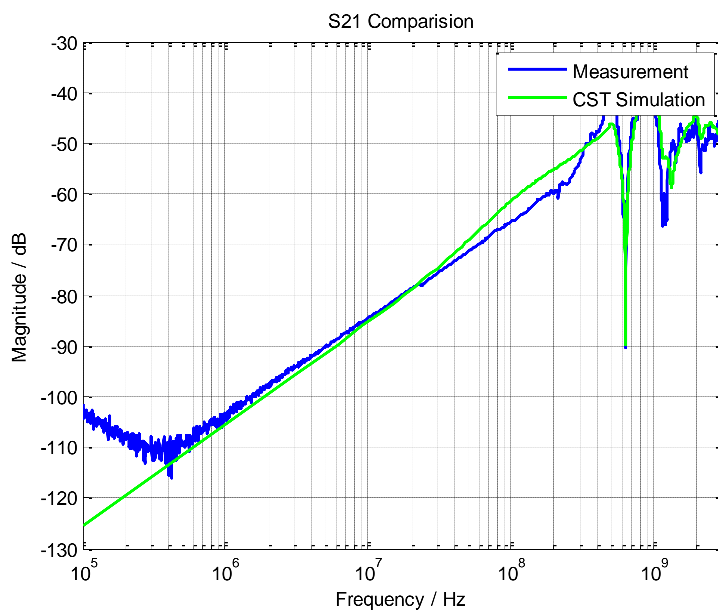

Figure 5-6. Frequency domain verification of port 2 coupling on the structure

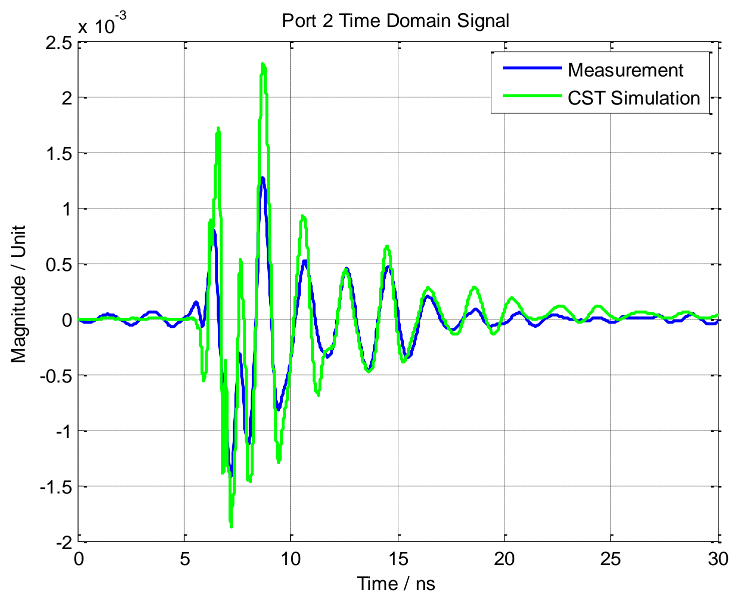

Figure 5-7. Time domain verification of port 2 coupling on the structure

After the verification of all the ports as previous shows, a well modelled PCB ESD structure is ready for numerical field coupling and current spreading analysis. Figure 5-8 to Figure 5-11 show the injected surface current spreading and H-field simulation results of the model:

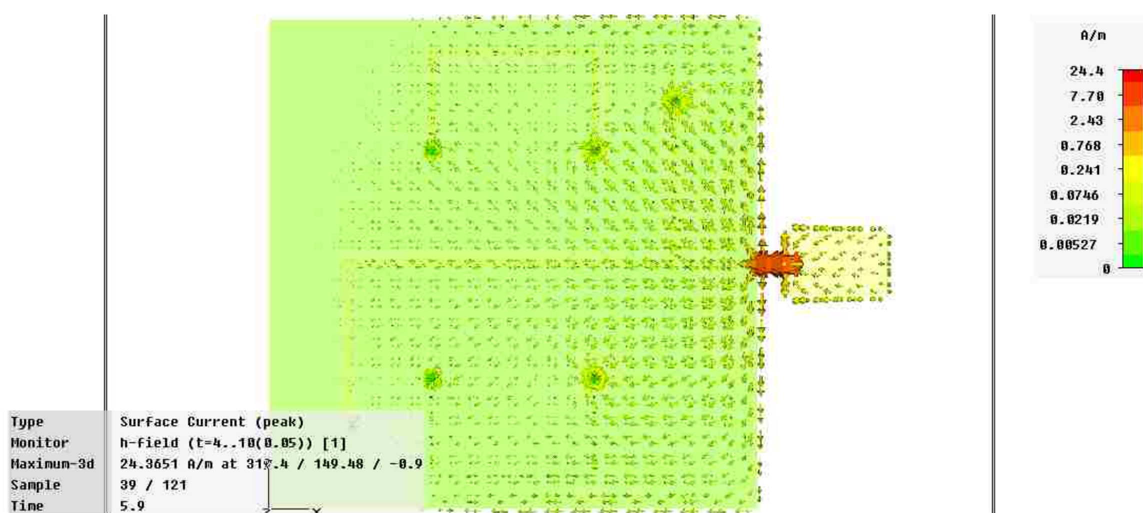

Figure 5-8. Simulated surface current on PCB ESD structure – top view

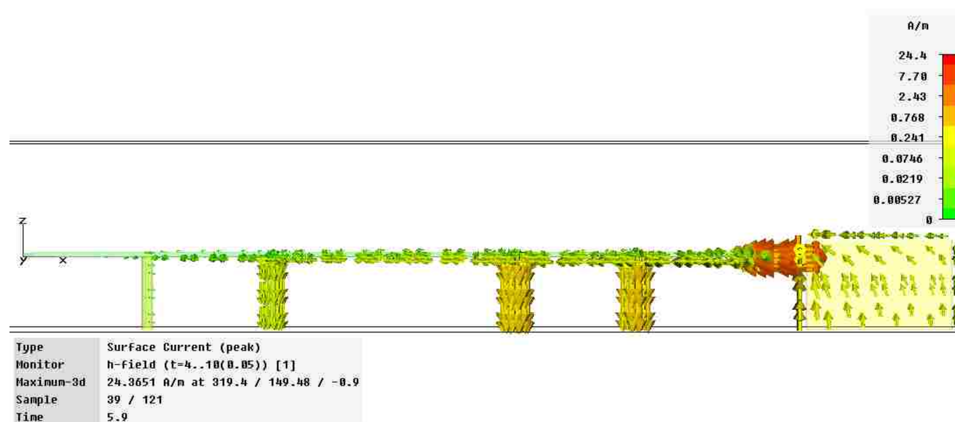

Figure 5-9. Simulated surface current on PCB ESD structure – side view

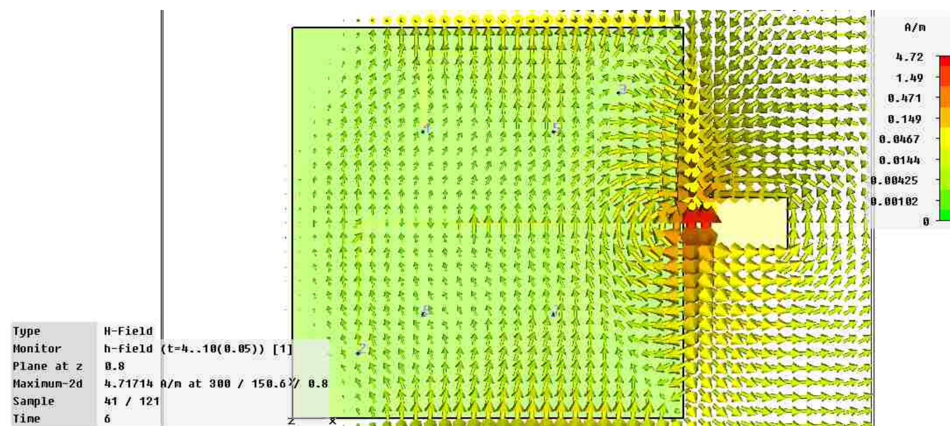

Figure 5-10. Simulated H-field on top side of PCB ESD structure

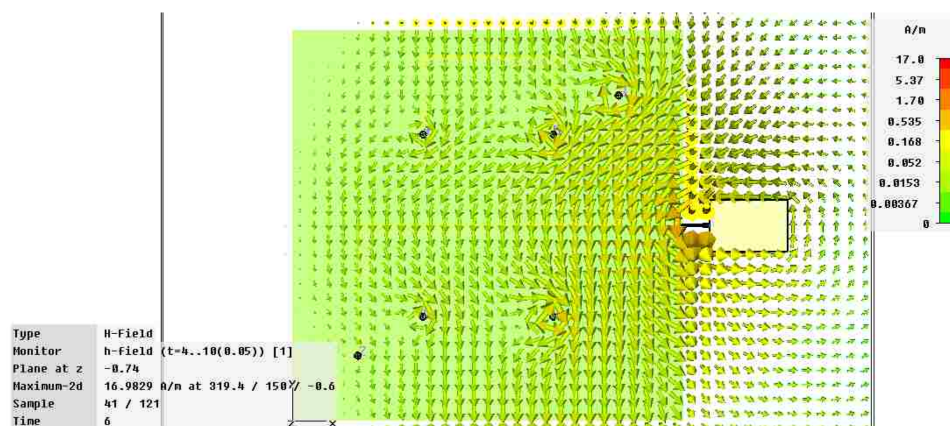

Figure 5-11. Simulated H-field on bottom side of PCB ESD structure

The modeling of the ESD current injection structure is finished and can be used for current spreading and field coupling analysis and verification of reconstructed current spreading results from near-field scanning.

5.2. RECONSTRUCTED SURFACE CURRENT VERIFICATION

First, verification of how well local H field components reflect the current density on the ground plane is simulated in CST. The comparison between field Hy and current density Jx is compared below:

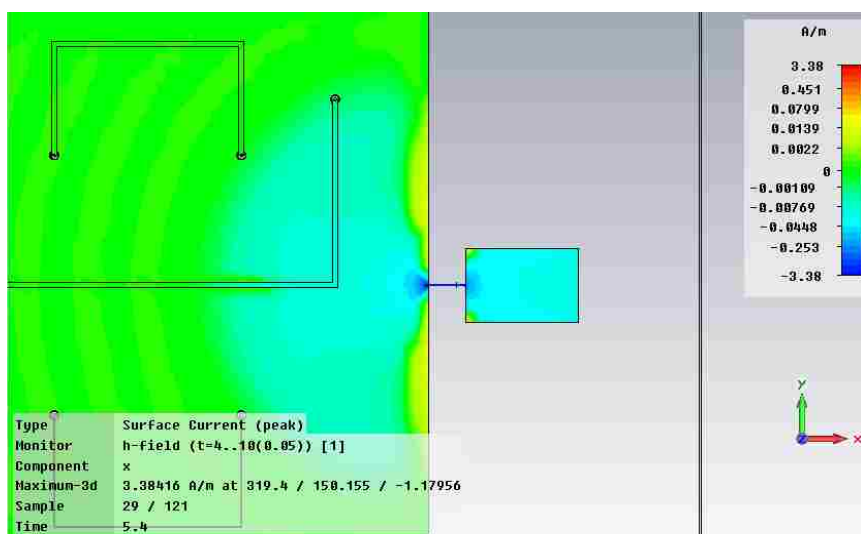

Figure 5-12. Simulated current density J_x distribution on top of the ground plane

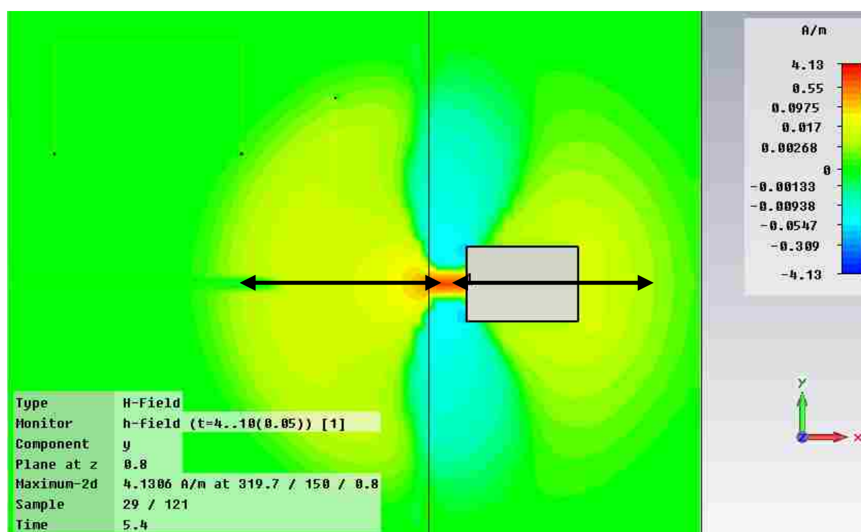

Figure 5-13. Simulated field H_y distribution on top of the ground plane

From the comparison, Hy reflects Jx in the distribution in general. For the same distance from the injection rod, the field coupling drops with $1/r^2$ in space while the current density drop with 1/r along plane surface. Therefore after propagating over a distance, H-field from surface current density will dominate the local H-field.

Further investigation on the local field components at different height also indicates the Hx components are very close to each other at heights of 0.5 mm to 4.65 mm as Figure 5-14 and Figure 5-15 shows. Therefore the field measurement at 0-5 mm height over the PCB won't influence the result much.

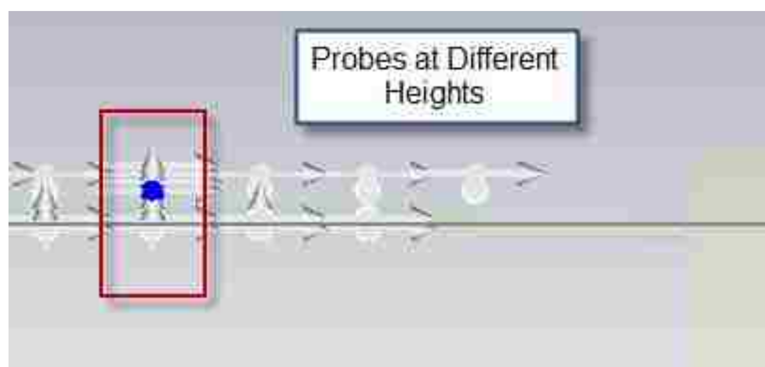

Figure 5-14. Probes at different heights over the ground plane

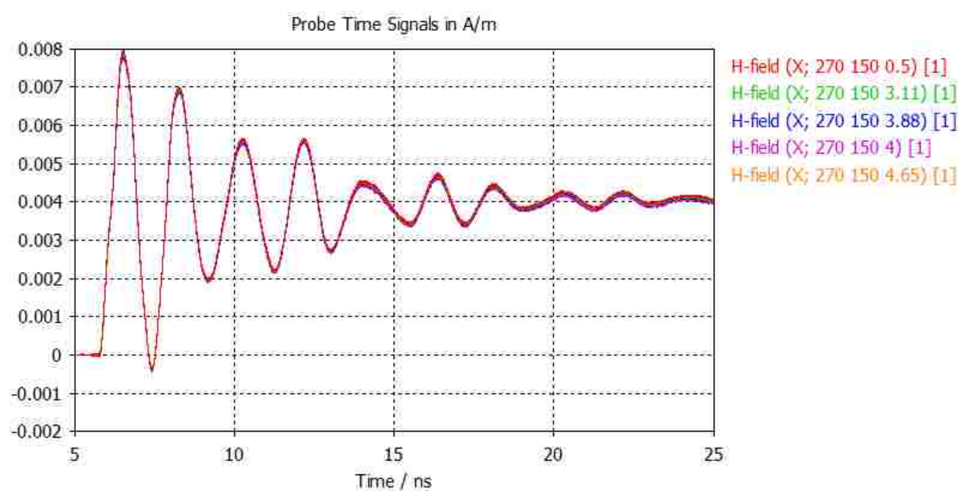

Figure 5-15. Comparison of H_x component over ground plane with different heights

Then, the CST simulated surface current Jx and current reconstruction scanning recovered correspondence are shown in Figure 5-16 and Figure 5-17:

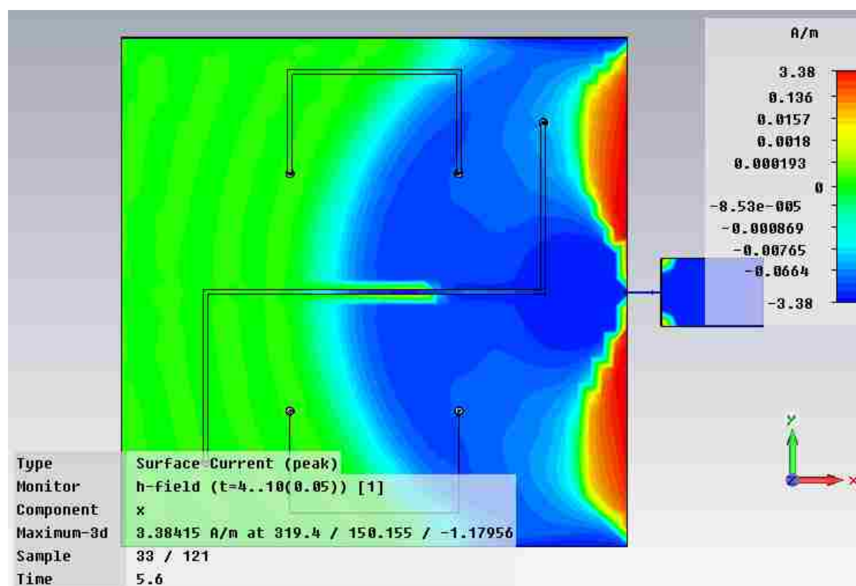

Figure 5-16. Jx from CST simulation

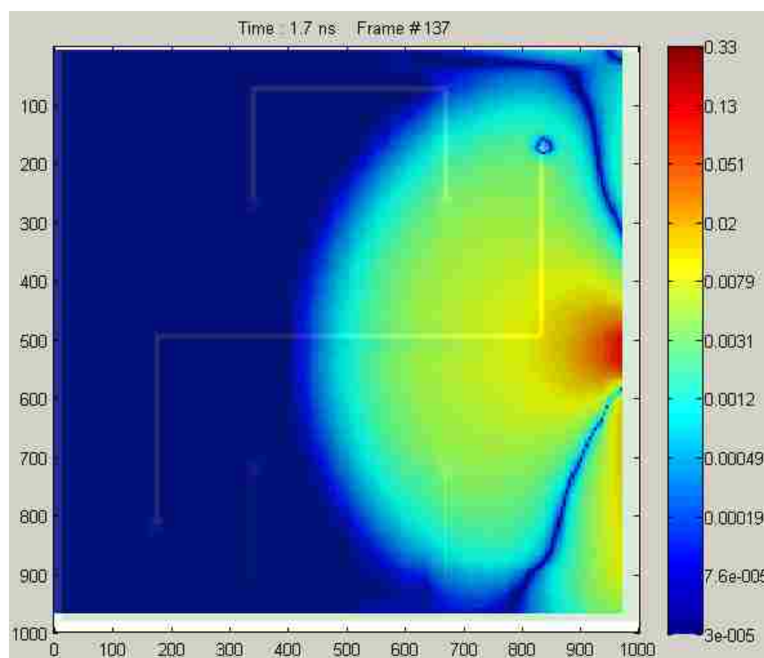

Figure 5-17. Jx from current reconstruction near-field scanning

The reconstructed surface current Jy and CST simulated correspondence are shown in Figure 5-18 and Figure 5-19:

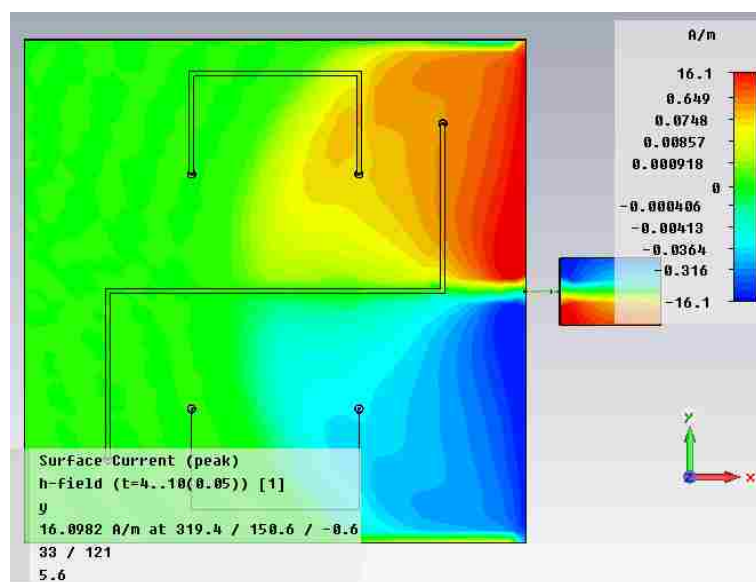

Figure 5-18. Jy from CST simulation

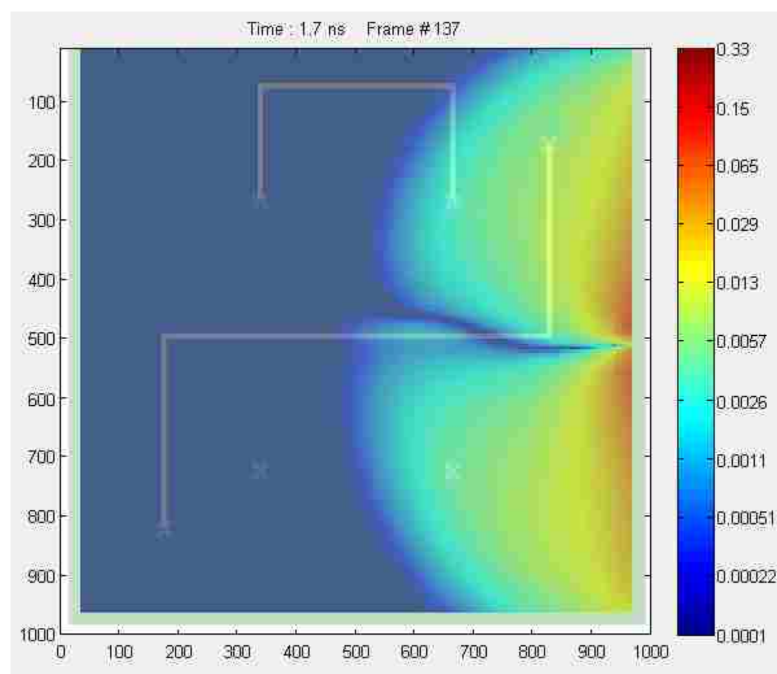

Figure 5-19. Jy from current reconstruction near-field scanning

These figures show the results of the scanning reconstructed data matches the full wave simulation results. The visualization methods of the simulation software and measurement are different so their images are different. A more precise validation of the scanning result is comparing the local scanning result and the simulated result in time domain. The Jx (Hy) component at 30mm away from the injection location is compared in simulation and measurement; the results are well matched in time domain as Figure 5-20 and Figure 5-21 show:

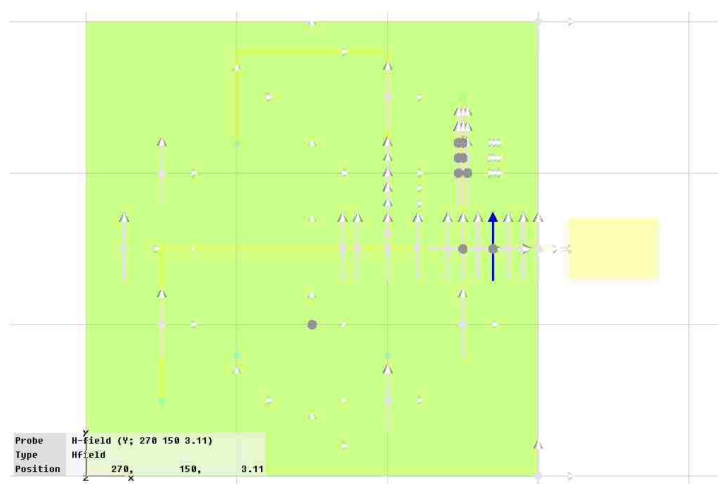

Figure 5-20. H-Field probe location in CST simulation

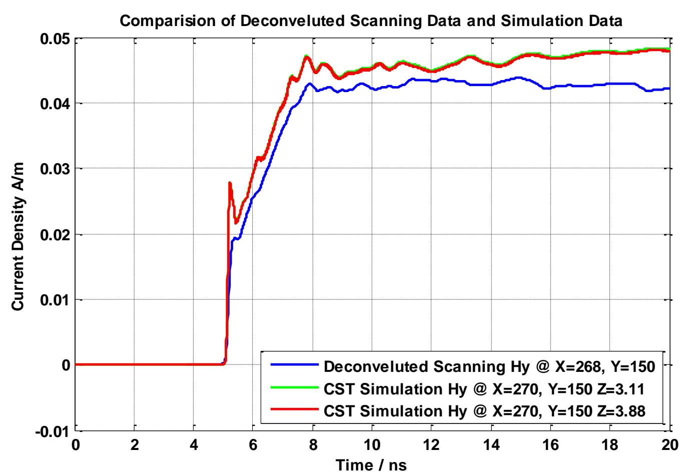

Figure 5-21. Comparison of reconstructed scanning result and simulation result

At this point, the methodology of reconstructing surface current density from magnetic near-field scanning is completed and validated.

5.3. RECONSTRUCTED TRACE CURRENT VERIFICATION

To validate the probe's response to coupled trace current, its sideway offset response to coupled trace current during ground plane current injection is observed at location as Figure 5-22 shows:

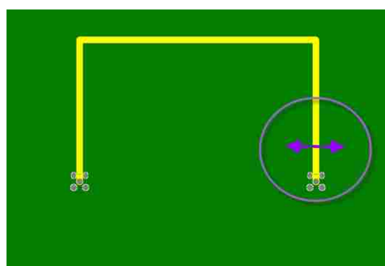

Figure 5-22. Position where sideway offset coupling response is measured

When scanning a probe across a trace with its maximum coupling direction couples to the trace current, the sideway offset response tells how well the probe couples to the trace current with rejection to the surface current on the ground plane. The local magnetic field coupling at trace cross section is shown in Figure 5-23:

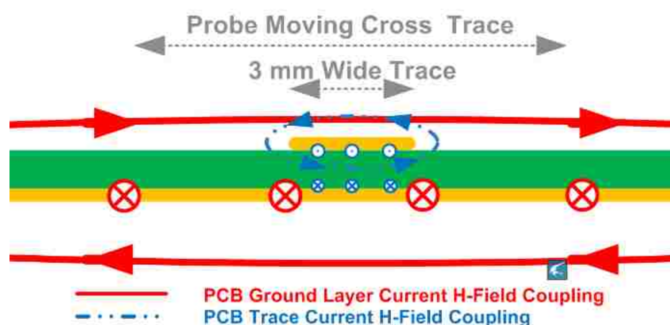

Figure 5-23. The local magnetic field coupling at trace cross section

The result of comparison between shielded horizontal loop probe, shielded vertical-loop probe and differential H_z trace current probe is shown in Figure 5-24:

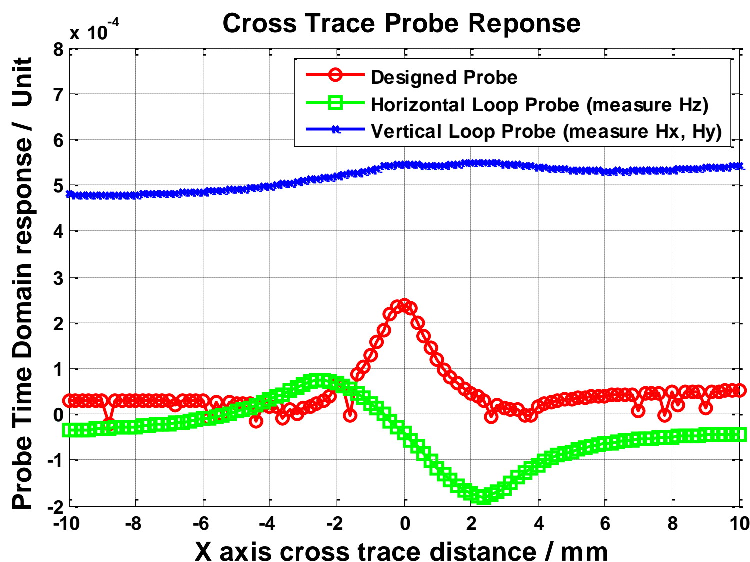

Figure 5-24. Comparison of different probes in sideways offset response

From the comparison result between the 3 different types of probes, the vertical-loop probe which has no rejection to the ground plane surface current coupling is overwhelmed by the magnetic field of the ground plane current, the horizontal loop probe with rejection to ground plane current coupling (H_x and H_y) components tells the coupled trace, but it shows two maximum coupling position at two sides of the trace. The differential Hz probe shows the best sideway coupling response with its high sensitivity and spatial resolution. Another set of scanning comparison over a 0.15 mm wide trace is shown in Figure 5-25. The differential H_z probe shows the best coupling response to trace current.

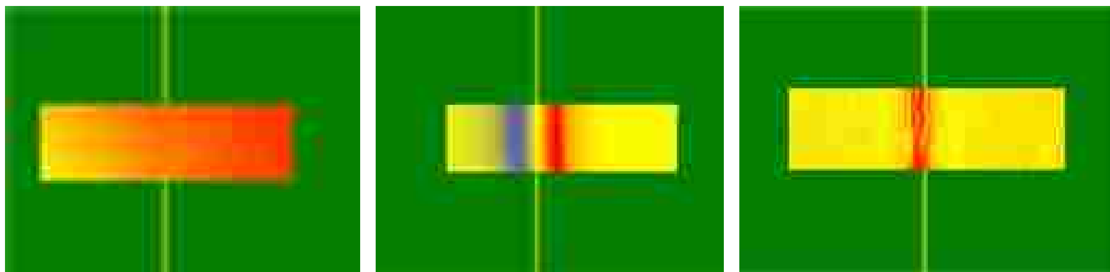

Figure 5-25. Comparison of different probes in scanning area

. A simulation of the magnetic field components above the PCB after ground plane current injection shows the detailed field distribution and couplings. Figure 5-26 shows the Hx component and Figure 5-27 shows the Hy component over the PCB, they are dominated by surface current coupling. Figure 5-28 shows the Hz component over the PCB and trace current coupling dominates H_z components in PCB center. These indicate the H_z component scanning measurement is the only possible scanning method for capturing the trace current.

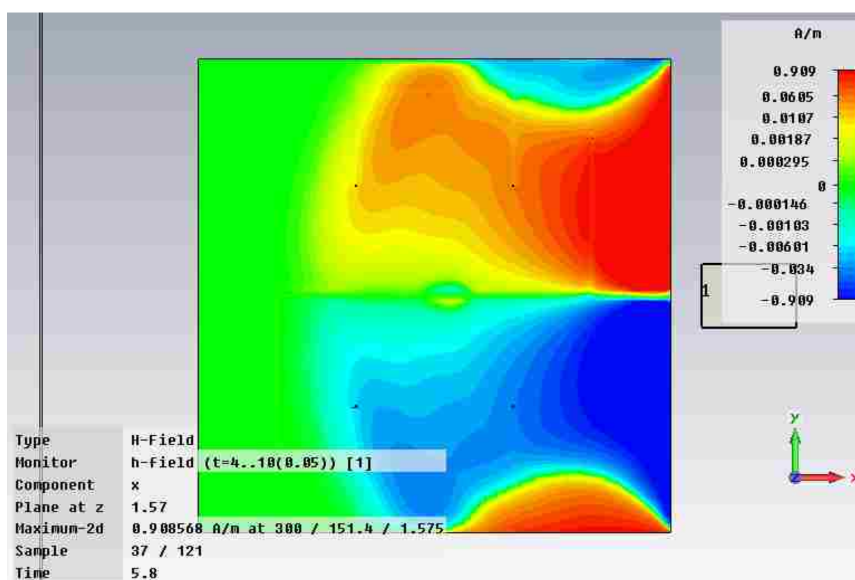

Figure 5-26. Hx components over the PCB after ground plane injection

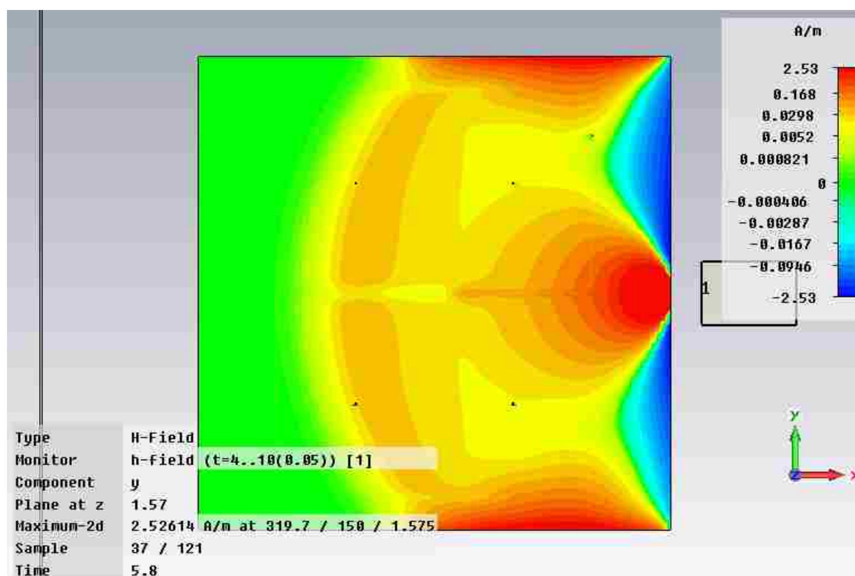

Figure 5-27. Hy components over the PCB after ground plane injection

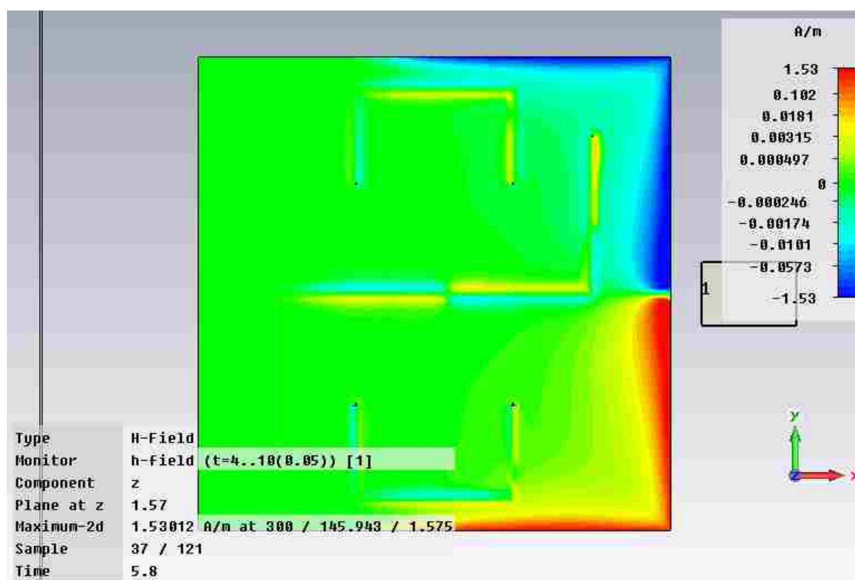

Figure 5-28. Simulation analysis of the field components over PCB

However, even the H_z components measurement method is not working for all cases or areas. When the injected plane surface current reaches edges, current will bounce

back or flip to the other side and bring strong Hz components near the edges. Some of them will influence the local Hz components as Figure 5-29 shows and the coupled trace current might not be measurable at these locations.

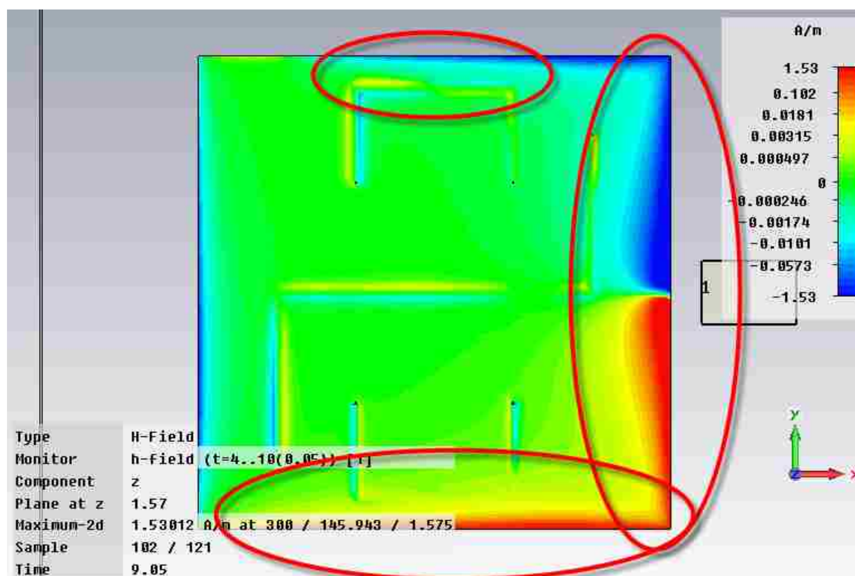

Figure 5-29. Hz components dominated near board edges

Then the local field influence from differential Hz current probe is also investigated. The field probes for the simulation analysis of differential Hz current probe's effect in influencing local field components is shown in Figure 5-30.

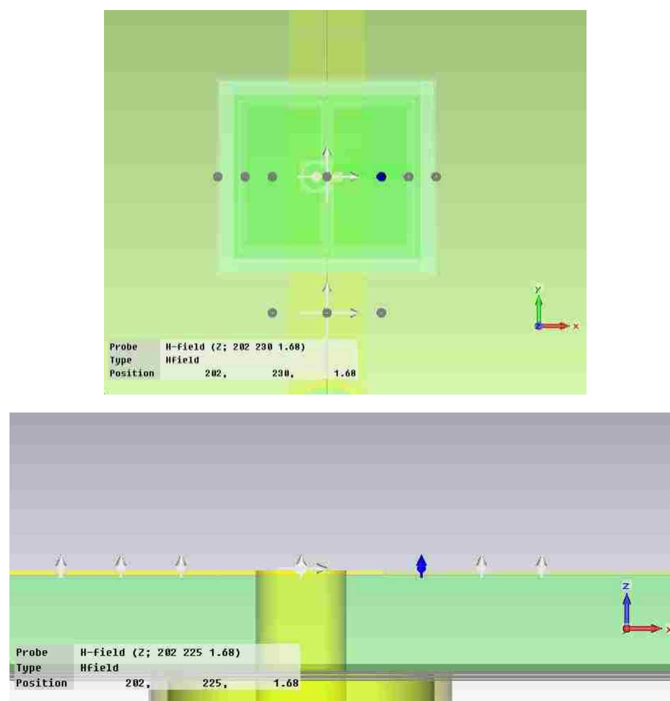

Figure 5-30. Hz probe locations under differential Hz probe in simulation

The local Hz field distribution of the same current injection structure with or without differential Hz probe is simulated; two frames of the Hz field map at the same time is compared in Figure 5-31:

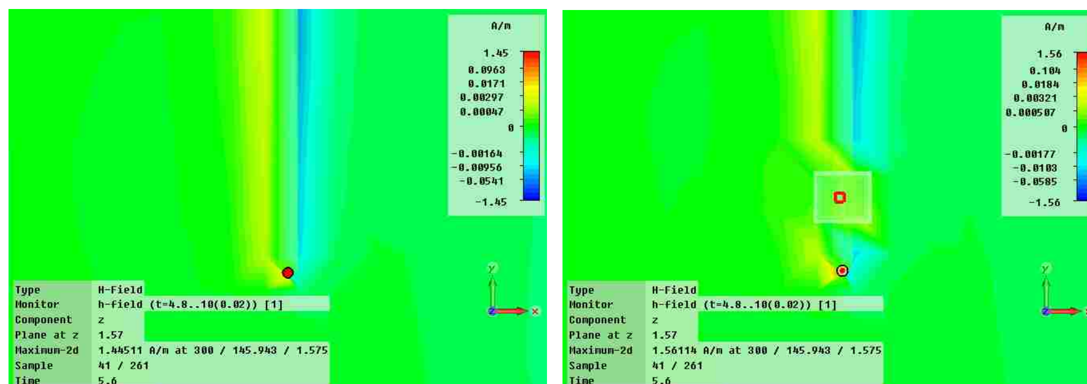

Figure 5-31. Comparison of local Hz with or without differential Hz probe

From the comparison, the Hz field distribution is changed locally right under the differential Hz probe. A time domain comparison of the two cases (with or without differential Hz probe) is shown in Figure 5-32:

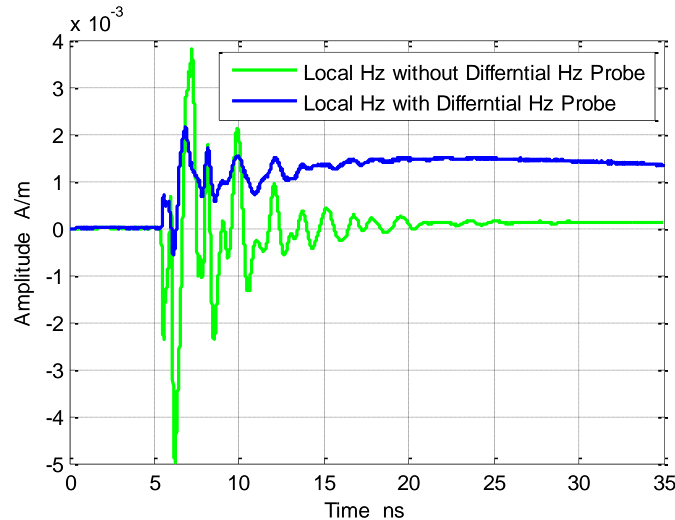

Figure 5-32. The local H_z of cases with or without differential H_z probe

Such result indicates that the differential Hz probe's influence on the local field component is pretty strong. However a comparison of trace port current with or without differential Hz probe in Figure 5-33 shows that the influence on the trace current is not very strong because most of the coupling geometry around the trace was not changed:

The analysis of local Hz component in this case is illustrated in Figure 5-34. After putting a metal object above a trace, it's nearby local E field and H field are changed. The H field from injected plane surface current is pushed two the sides of the metal and field goes along the surface of the metal as the middle picture illustrated. If a differential Hz probe is put over a trace, the same effect happens. Such effect changes the original Hx or Hy component from injected plane surface current into new Hz components and couples into the probe loops together with the trace current Hz field components.

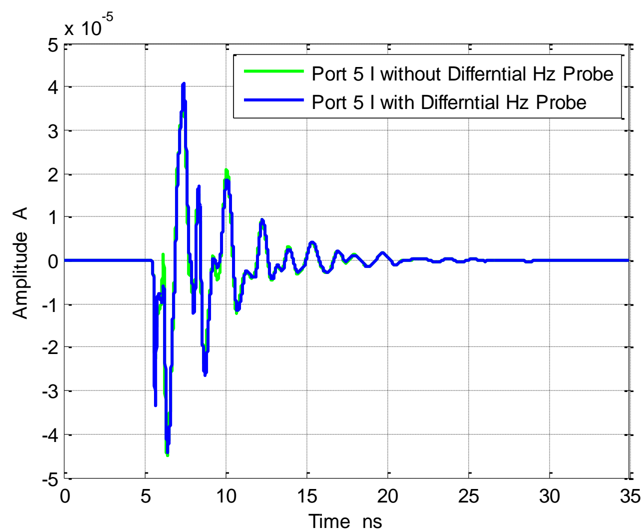

Figure 5-33. Comparison of port current with or without differential H_z probe

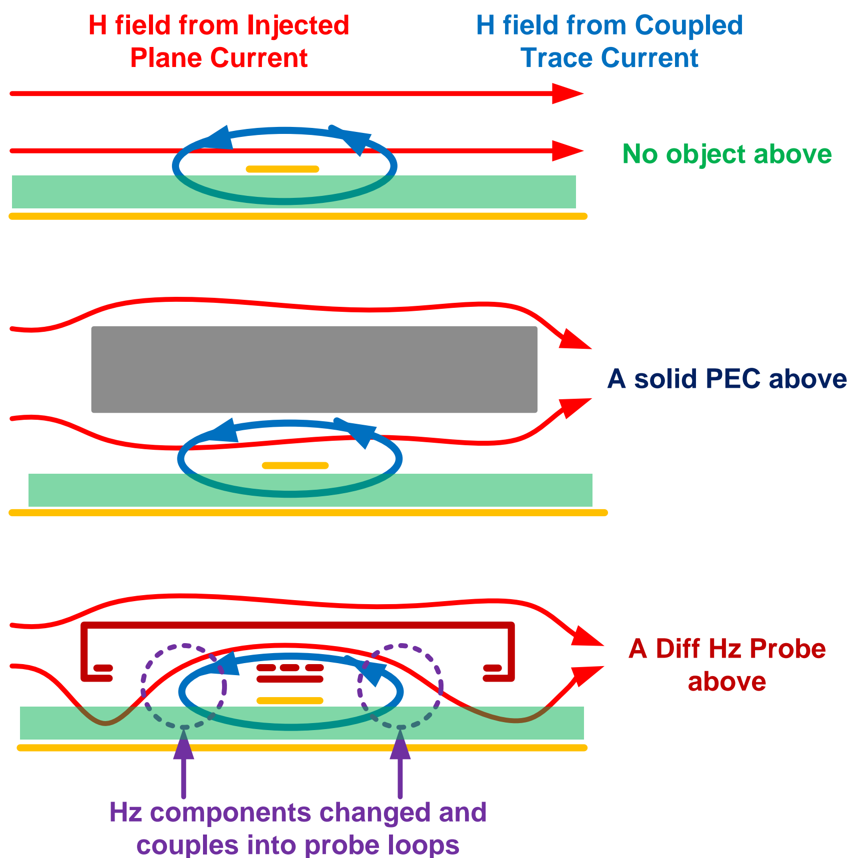

Figure 5-34. Local H_z component changes after putting a differential H_z probe

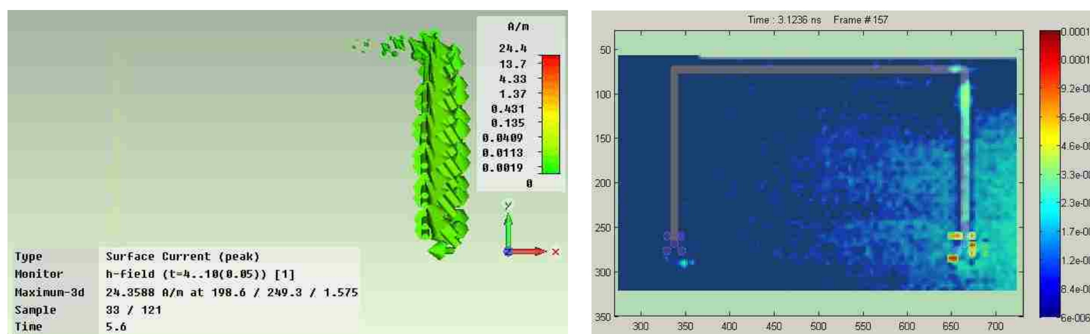

Frame 1 (0 ns)

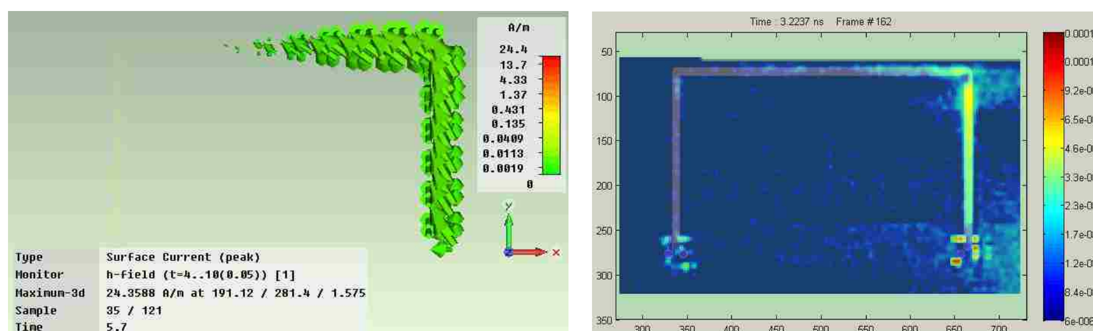

Frame 2 (after 0.1 ns)

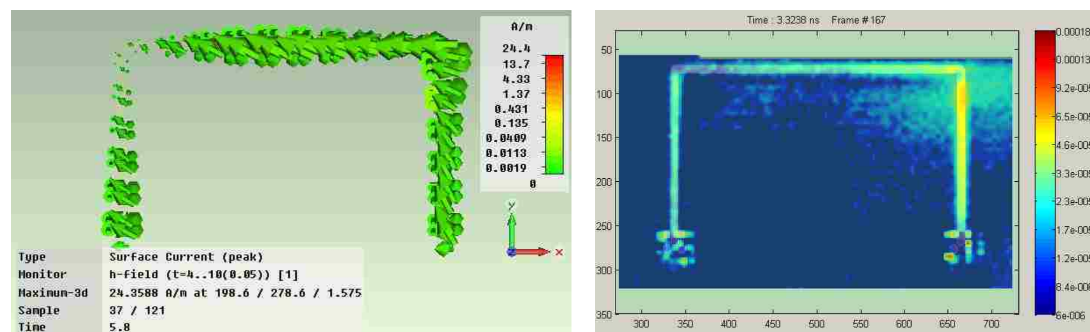

Frame 3 (after 0.2 ns)

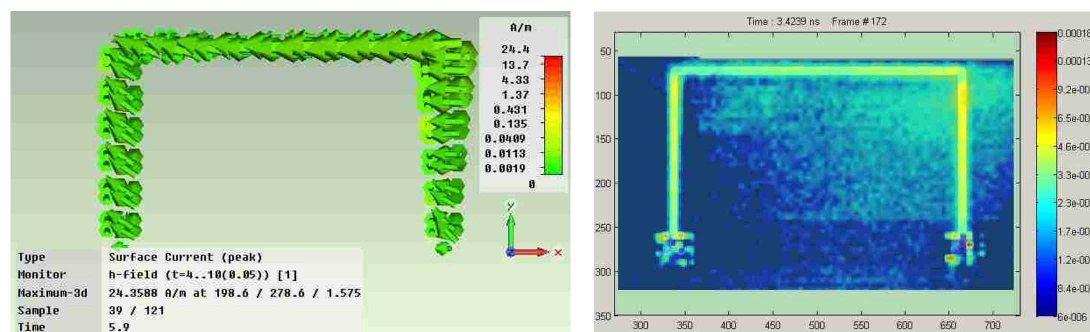

Frame 4 (after 0.3 ns)

Figure 5-35. Comparison of simulated and reconstructed trace current in spreading

(Note: the simulation result is scaled in A/m; the reconstructed current by scanning is scaled to A)

From the analysis, the conclusion is that the coupled trace current scanning with differential Hz probe can measure local trace current with the interference from local field changes, the coupled trace current cannot be precisely recovered as the injected surface current. However, the bottom line for such coupled trace current recovery method is that the scanning result still shows the correct time delay and is at the same order of magnitude as the coupled trace current. Therefore the reconstructed result is still very useful for coupled trace current analysis.

Figure 5-35 shows several frames comparing the coupled trace current spreading results between simulation and measurement. The timing of the current spreading between simulation and measurement matches very well.

The measurement result also contains the influence from ground plane current as the probe's surface current rejection is not perfect - some of local Hx and Hy component are forced into the probe loop and the edge current on the board top side also brings Hz components to influence the local differential Hz value.

The comparison of time domain signal between simulated trace port current and reconstructed trace current near the port is shown in Figure 5-36. From the comparison, the trace current from processed scanning data reflects the coupled trace current in the same order of magnitude.

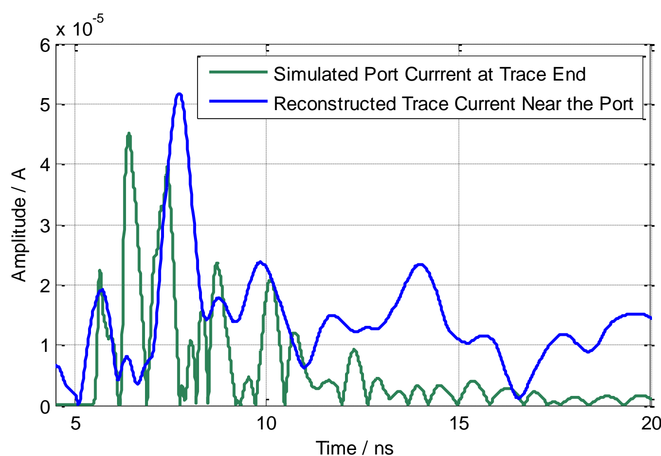

Figure 5-36. Comparison of simulated and reconstructed trace current

6. SYSTEM-LEVEL CURRENT RECONSTRUCTION SCANNING

The long term objective of the current reconstruction scanning by near-field scanning research is to correlate system-level analysis with local sensitivity results. Although many aspects of the scanning technology show room of improvements, such as the probe design, the data process and visualization algorithm, the methodology is tentatively applied in two directions here. One direction is to correlate the current reconstruction scanning results with the geometry of device for its local response and resonance analysis. Another direction is to connect the system-level ESD failures symptoms with device local ESD sensitivity.

6.1. LOCAL RESONANCE AND RESPONSE ANALYSIS

6.1.1. Background and Objective. When interference such as ESD or EFT is excited at the outside of a system, the signal will inject a broadband energy into the system. Depending on the system geometry inside, deferent objects such as wires, traces and bond wires will have different responses to the excitation and some of them with strong resonance (self or chassis resonance) to the excitation might get severe interference and cause system failures.

The advantage of applying the current reconstruction scanning on a device is that one can correlate the scanning results with the geometry of device to find out the what local interference signal is (view the response), how the interference spreads to local area (see the possible coupling paths), what kind of resonance the local response has (do a FFT for local response) and might also be able to see how a local resonance is created by looking the local current / field spreading and bouncing movie.

6.1.2. Experimental Setup. An experiment for analyzing the local response to an injection signal outside the system is conducted with a Macbook laptop. The experimental setup is shown in Figure 6-1, Figure 6-2, and Figure 6-3:

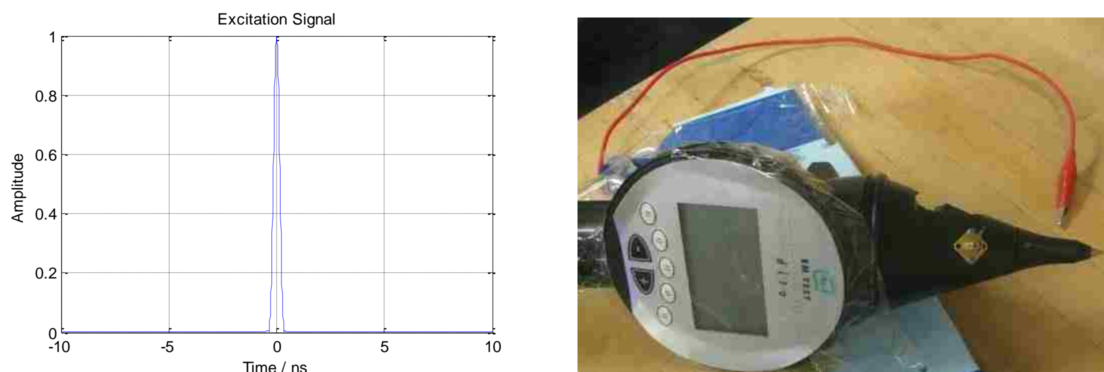

Figure 6-1. Excitation signal and modified frequency domain ESD gun

Figure 6-2 Injection location and ground strap connection at the Macbook

Figure 6-3. Shielded H_z field probe for near-field scanning

From the setup, the scanning result will show the detail of how the Hz components spread and interact with local objects.

6.1.3. Scanning Results Analysis. Several frames showing how the magnetic field spreads are followed from Figure 6-4 to Figure 6-8:

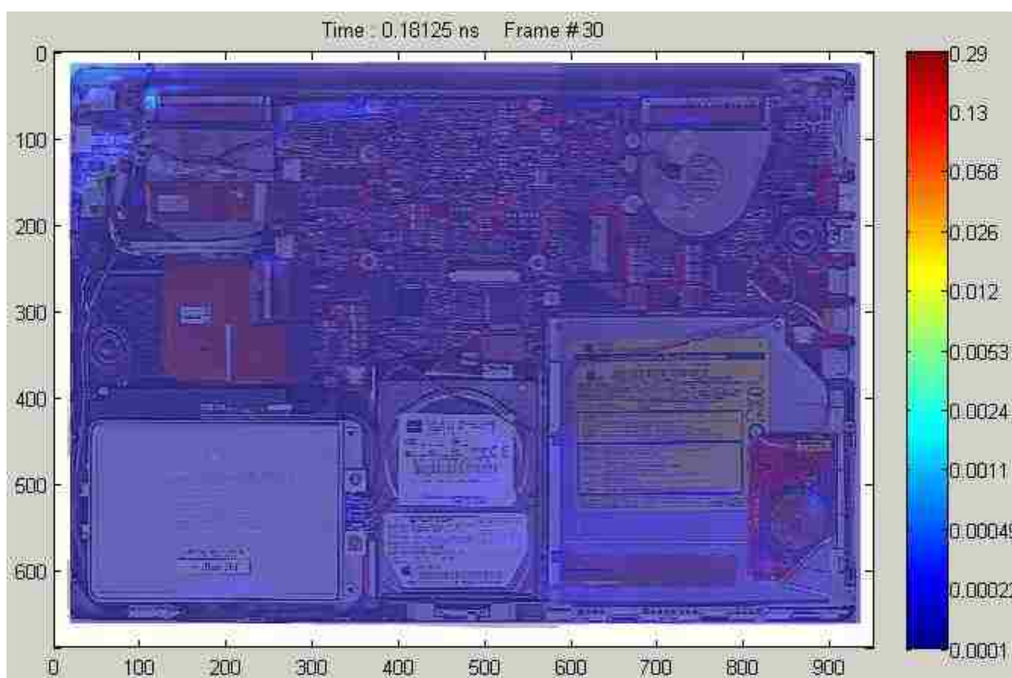

Figure 6-4. Measurement result showing injection is not started

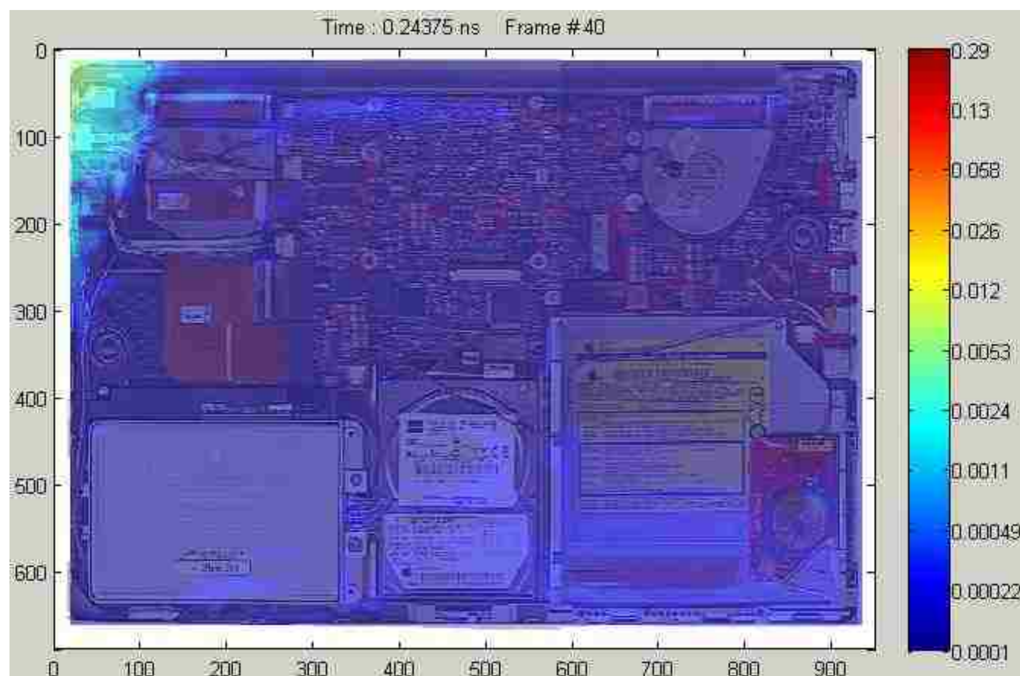

Figure 6-5. Measurement result shows injection current reaches USB port

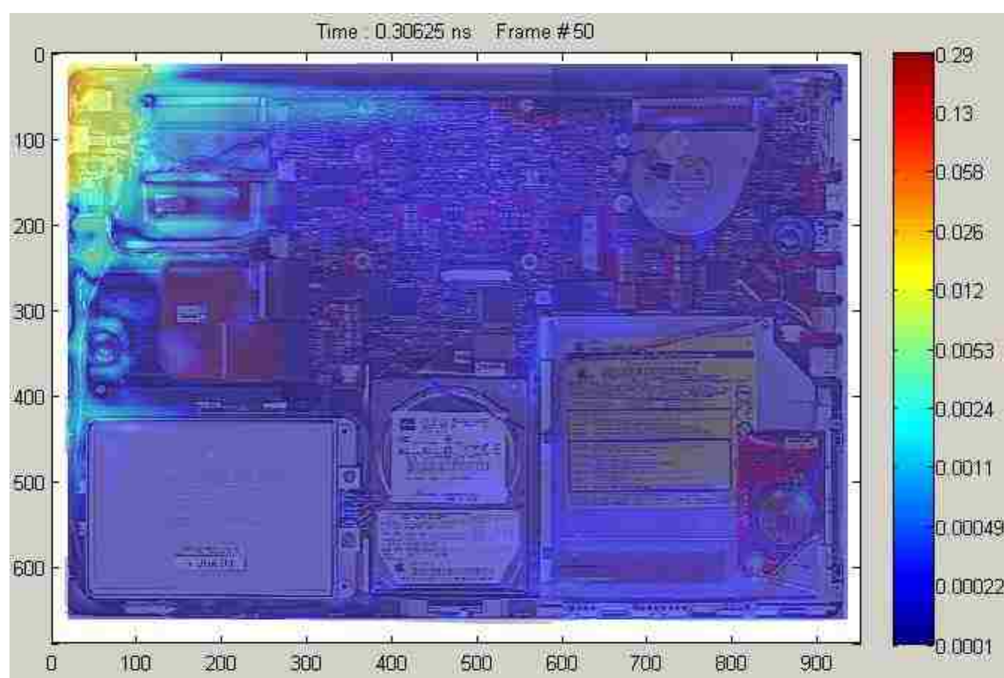

Figure 6-6. Measurement result shows current and H_z field spreading at 0.3ns

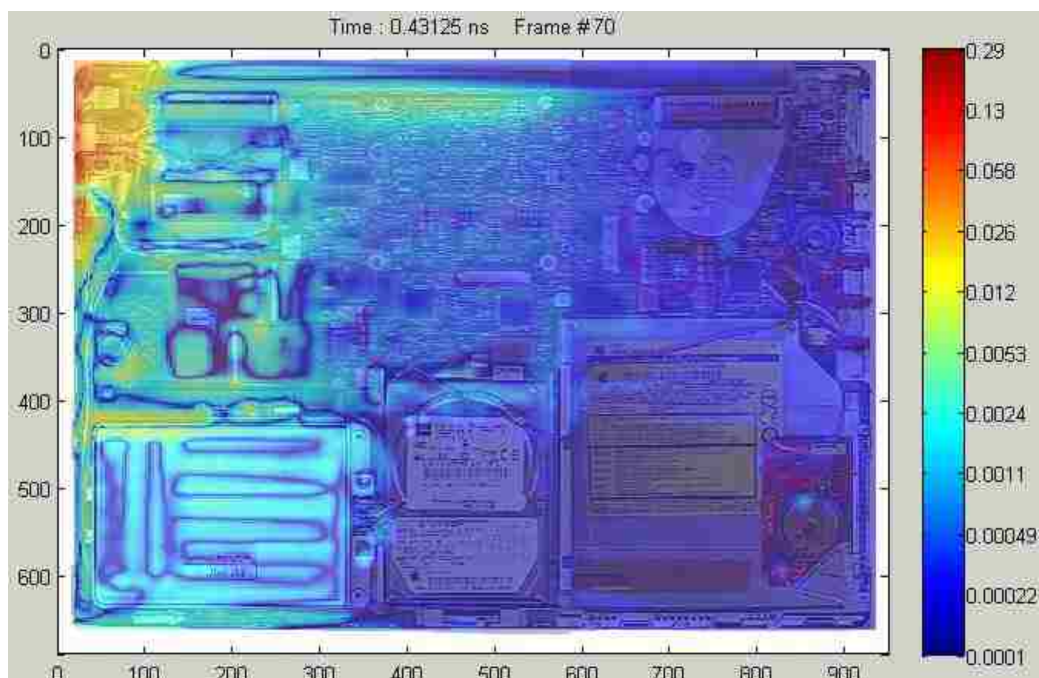

Figure 6-7. Measurement result shows current and H_z field spreading

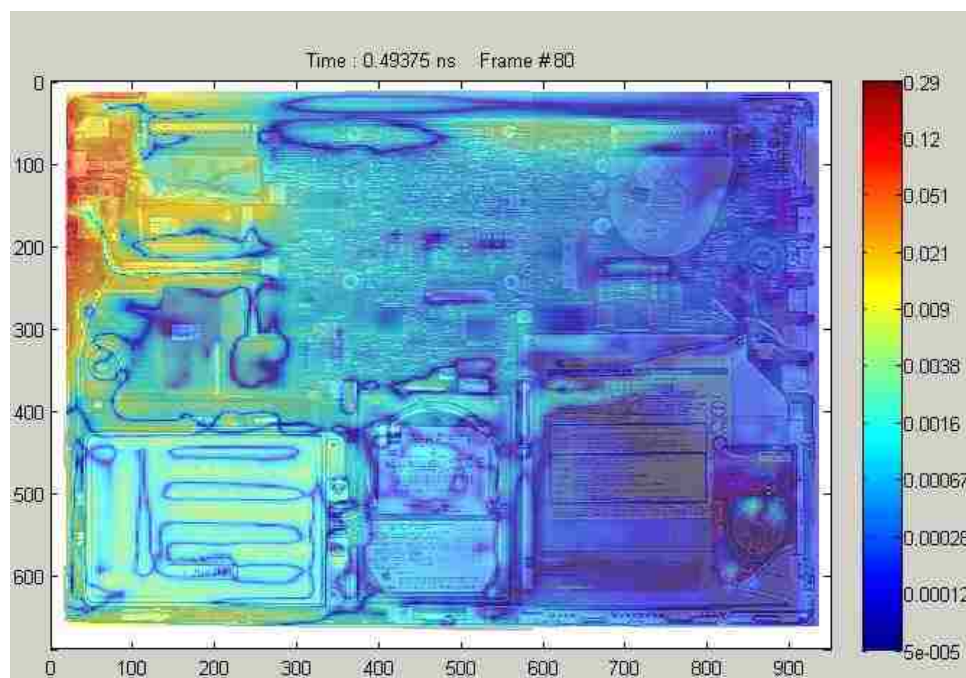

Figure 6-8. Measurement result shows current and H_z field spreading

From the results, the current spreading or field coupling paths are visualized from measurement data. Also the local response can be viewed from the current reconstruction viewer as Figure 6-9 shows.

A zoomed view as Figure 6-10 shows that there is header connected to USB port carry the maximum local resonance and the resonance frequency is roughly at 1.92 GHz. A FFT on the time domain signal would allow a better view of the resonance from USB port injection.

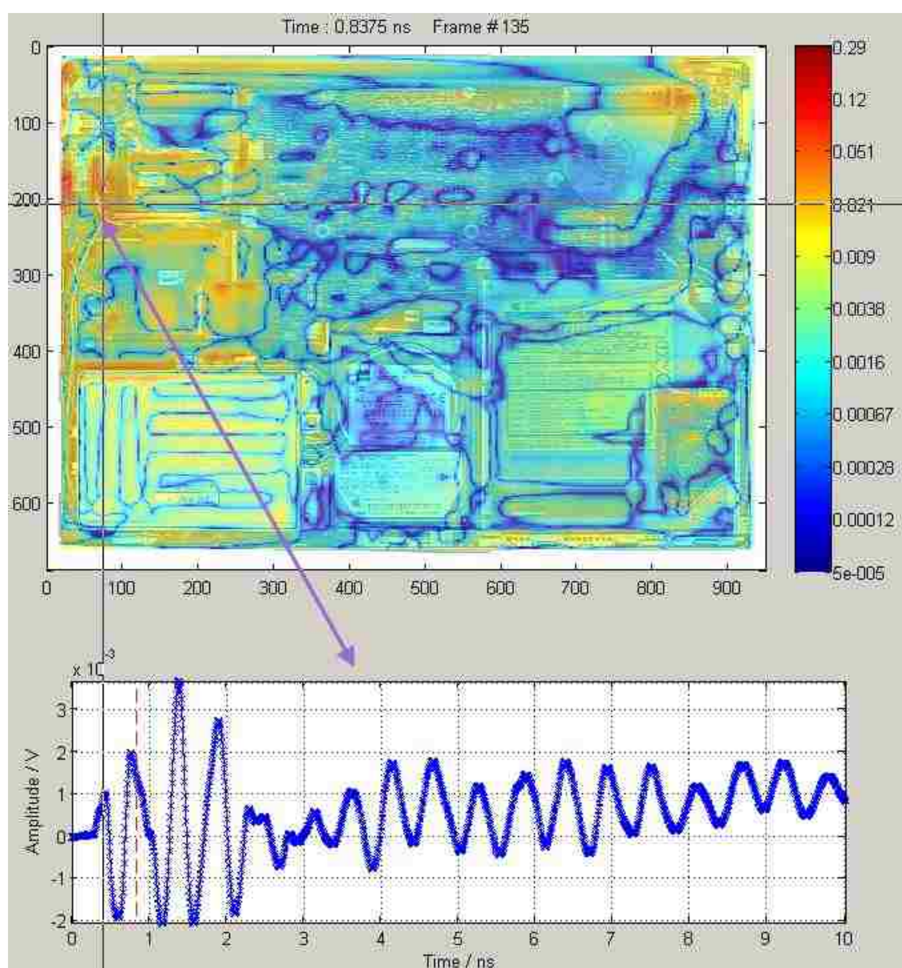

Figure 6-9. Locate local response in current reconstruction viewer

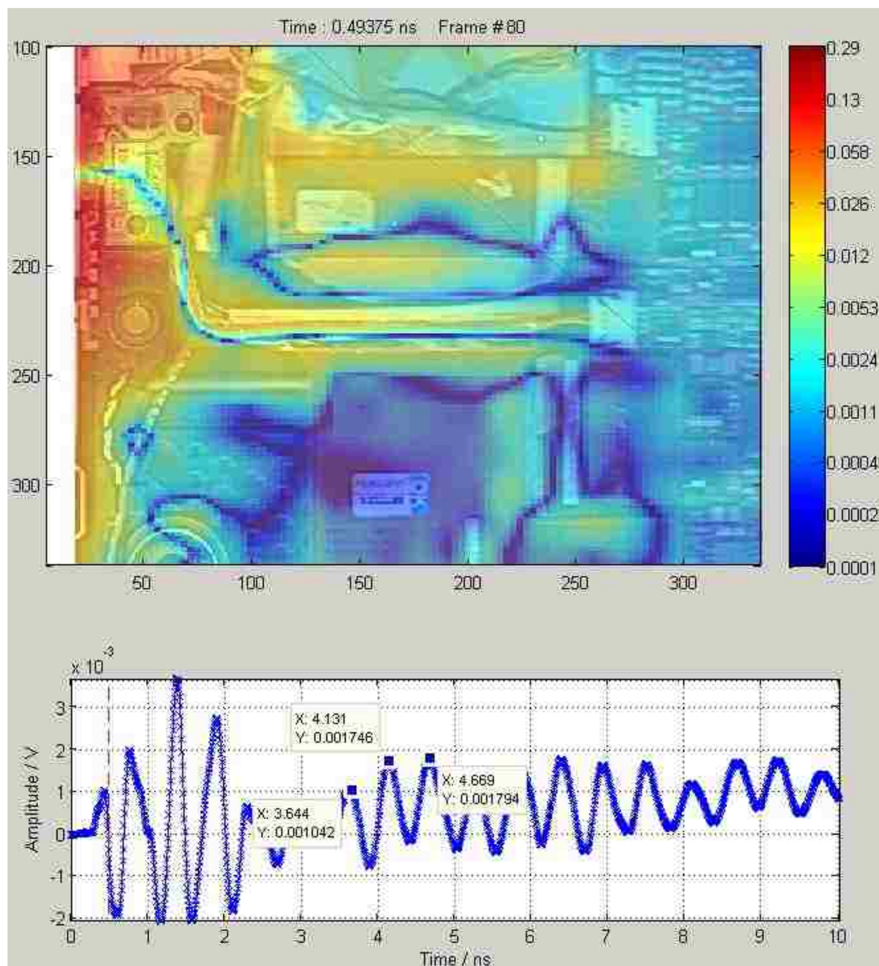

Figure 6-10. Zoomed in to find resonance object and frequency

Also some of the structure resonance can be seen from the current spreading and bouncing along an object. Figure 6-11 shows a long wire with interference current running on it. Its length brings the self-resonance is correlated with the resonance scanning result at around 620 MHz.

It obviously also carries higher resonance frequency but was not measured in resonance scanning. A frequency domain transform back would indicate the detailed frequency response or resonance.

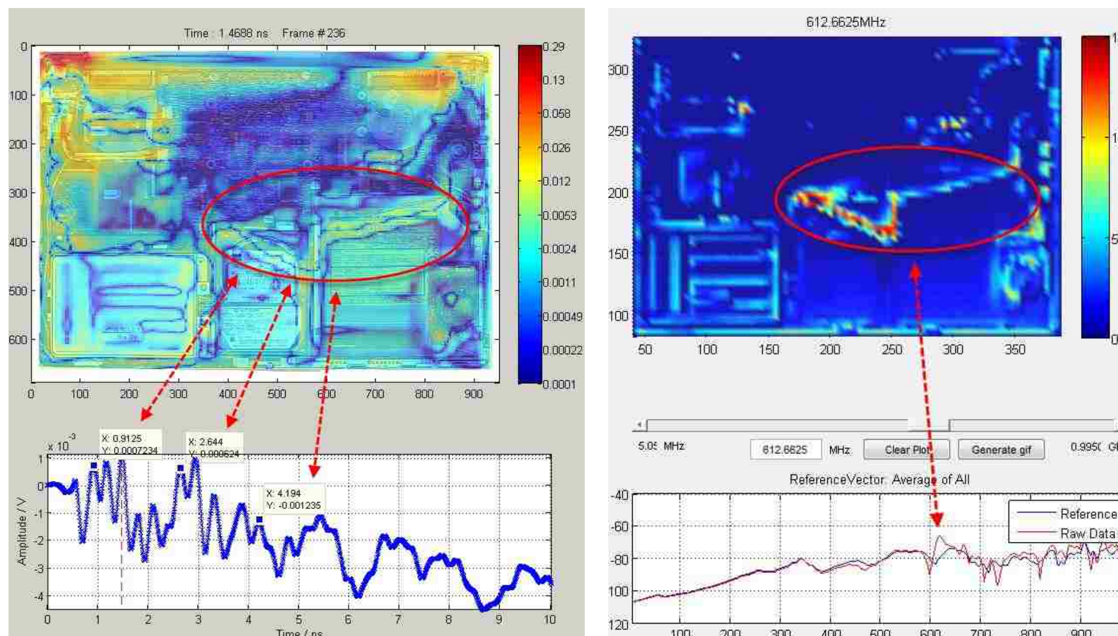

Figure 6-11. Correlated current reconstruction and resonance scanning results

6.2. SYSTEM-LEVEL ESD INTERFERENCE ANALYSIS

6.2.1. Background and Objective. When a system shows very repeatable ESD failure for a known excitation location and several possible events that can trigger the failure are concluded from either circuit analysis or local ESD sensitivity scanning results. It is likely that the injected interference spreads through the system, reaches the local sensitive area, induced strong enough signal to trigger the system ESD failure. However, the analysis of possible coupling paths or failure causes becomes harder and harder when the system complexity is increased.

Upon such assumption, the injected current reconstruction by near-field scanning method becomes a new approach to connect the excitation and response in time and spatial domain, supporting the analysis between system-level upset, local interference response and sensitivity, possible coupling paths and failure event triggers.

6.2.2. Experimental Setup. A very repeatable system failure is found on a printer server: Ethernet connection resets when USB shielding gets transmission line pulser (TLP) discharge at 1.5KV or higher level. The injection setup is shown in Figure 6-12 and Figure 6-13:

Figure 6-12. Injection location of printer server

Figure 6-13. Printer server prepared for double side scanning

The measurement is conducted with frequency domain scanning method; a step function is injected in the same way as TLP injection, the excitation signal is a step function as Figure 6-14 shows:

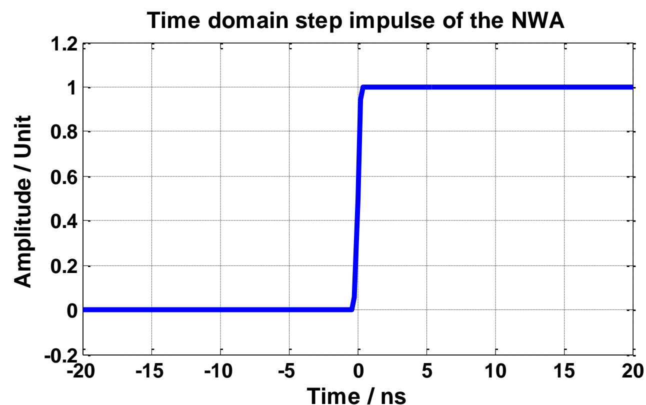

Figure 6-14. Network analyzer step function excitation

To find the local sensitivity of the system failure, a sensitivity scanning is conducted and the result is shown in Figure 6-15.

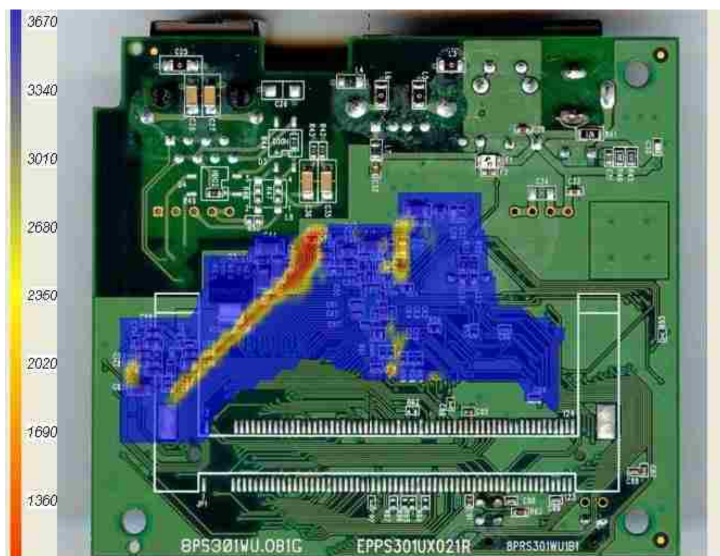

Figure 6-15. Board local sensitivity scanning result

The system layout is also present in Figure 6-16 for system-level failure analysis. Since the board local sensitivity scanning result indicates several regions with triggers for local ESD failure, a local in circuit measurement can precisely indicate the exact traces or pins triggering the failure events, and connect local interface with the system failures.

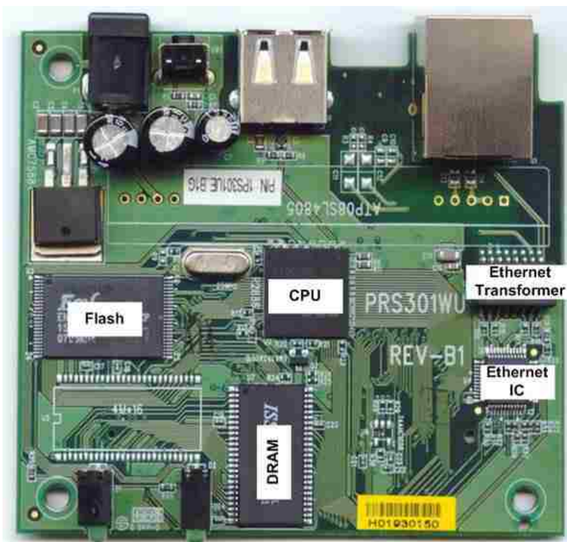

Figure 6-16. System function layout for failure analysis

6.2.3. Scanning Result Analysis. An overview of maximum injected current density (or its derivative – related to local induced loop voltage) shows a nice distribution of how strong the local interference was after an injection in Figure 6-17 and Figure 6-18.

Based on the distribution of injected maximum current density / H field strength or its derivative, analysis connecting local sensitivity with the system failure mechanism in the terms of current density influence is more promising.

Further develop of the connection between system-level failure and local sensitivity requires the calibration analysis of local trace or plane surface current injection from a probe. The method and tool development for such connection in current reconstruction analysis are ready and presented as the results show.

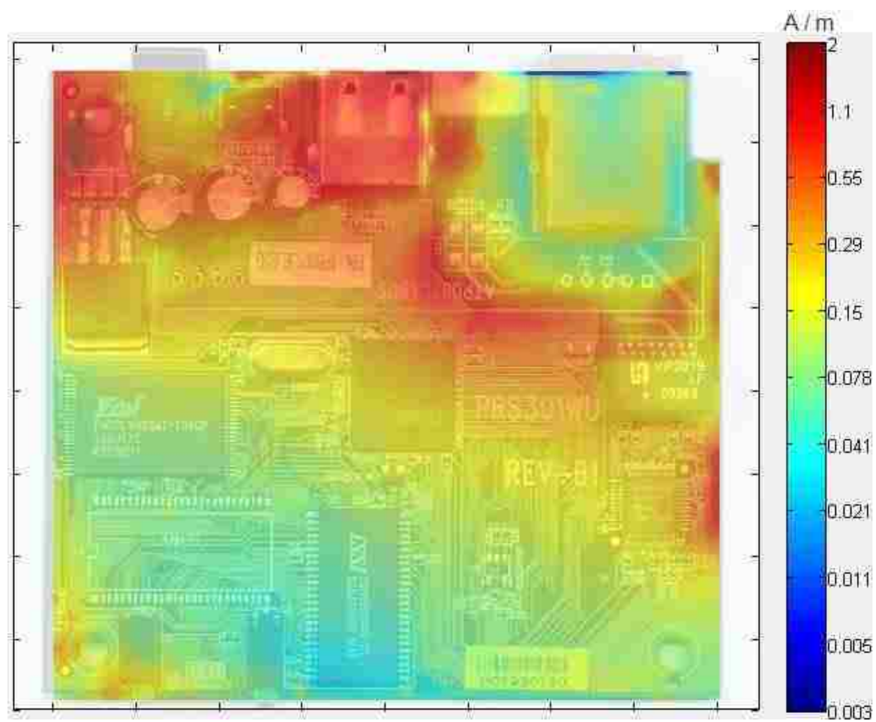

Figure 6-17. Max current density occurred during injection - top side

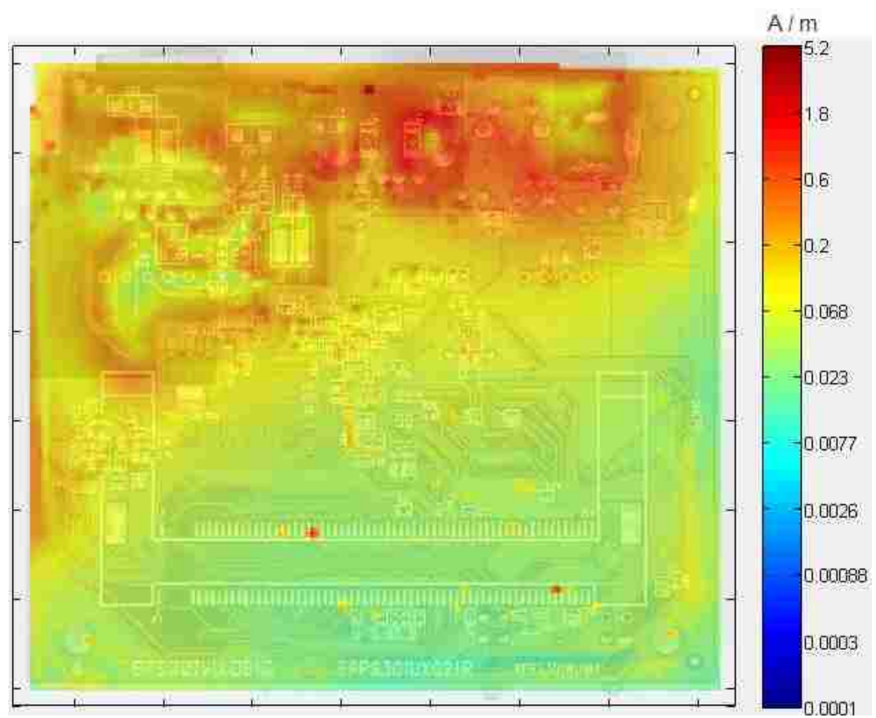

Figure 6-18. Max current density occurred during injection - bottom side

7. CONCLUSION AND FUTURE WORKS

7.1. CONCLUSION

The current reconstruction method by near-field magnetic scanning measurement was developed and analyzed in this thesis. The development covers test structure design and current spreading and field coupling analysis; current scanning probe design, characterization, modeling, and optimization; implementation and analysis of time domain and frequency domain scanning method; scanning raw data frequency and directional response compensation algorithm; current spreading visualization method and implementation; modeling of current injection structure and verification of current reconstruction results; two directions of system-level analysis with current reconstruction scanning method.

The noble current reconstruction scanning method and data process algorithm allows both precise recovery of injected surface current spreading or field coupling and acceptable recovery of coupled trace current. The recovered current or field results not only provide a direct visualization of current or field coupling from measurement results in time and spatial domain, but also bring a connection between system-level inference and failure to local response and sensitivity.

7.2. FUTURE WORKS

7.2.1. Predict of Local Response for Arbitrary Excitations. The basic idea is that when the s21 data of a linear system is known, the response can be calculated from known excitations and S21 data, as below shows.

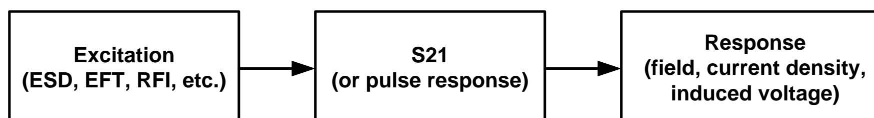

Figure 7-1. Predict of local response from excitation and scanning results

7.2.2. Analysis of a Probe's Influence on Local Field. To fully understand a probe's characteristic and compensate them to precisely recover field components from measurement, the analysis of probe's influence for local field is also important in additional to the probe's frequency and directional response, especially when a probe has complex and relatively large geometry or when the measurement object is sensitive to nearby structure change. This is the cause of the shortcoming for non-precise recovery of coupled trace current with present probe and reconstruction algorithm.

BIBLIOGRAPHY

[1] Cai Qing, Jayong Koo, Argha Nandy, and David Pommerenke, "Advanced Full-Wave ESD Generator Model for System-Level Coupling Simulation", *IEEE EMC Symposium, Aug 2008.*

[2] Chong Ding, David Pommerenke, "Laser Optical In-Circuit Measurement System for Immunity Applications", *IEEE EMC Symposium, Aug 2006.*

[3] David Pommerenke, Martin Aidam, Technical University Berlin, Einsteinufer, "To what extent do contact-mode and indirect ESD test methods reproduce reality?", *Electrical Overstress/Electrostatic Discharge Symposium Proceedings, 1995.*

[4] Kai Wang, Jayong Koo, Giorgi Muchaidze, Dr. David J. Pommerenke, "ESD Susceptibility Characterization of an EUT by Using 3D ESD Scanning System", *IEEE EMC Symposium, Aug 2005.*

[5] Kai Wang, Dr. Pommerenke, Jian Min,Zhang, Ramachandran Chundru, "The PCB level ESD immunity study by using 3 dimension ESD scan system", *IEEE EMC Symposium, Aug 2004.*

[6] Frederic Lafon, Francois De-Daran, Julien Dupois, "Near-field imunity cartography method to characterize an IC to fields radiated by an ESD," *Blaise Pascal University, Clermont Ferrand.*

[7] Tun Li, Kuifeng Hu, Shaohua Li, Qing Cai, Wenfeng Pan, Jayong Koo, Zhe Li, David Pommerenke, "Overview on electric field, magnetic field, current and voltage probes used in the EMC lab for EMI analysis and for injecting signals during immunity analysis", *UMR EMC Laboratory Technical Brief, Mar 2007.*

[8] David Pommerenke, Tun Li, Weifeng Pan, Thomas Van Doren, "Probe Selection Strategy", *UMR EMC Laboratory Technical Brief, Mar 2007.*

[9] Qing Cai, Jayong Koo, Tun Li, David Pommerenke, "Characterization of different types of PCB loop probes", *UMR EMC Laboratory Technical Brief, Mar 2007.*

[10] Agilent 8753ES Manual

VITA

Wei Huang was born in Hunan, China in 1986. He received B.E. Degree in Communications Engineering from Beijing University of Posts and Telecommunications, Beijing, China, in 2007. Right after that, he enrolled in Missouri University of Science and Technology (formerly University of Missouri-Rolla) for master degree program in Electrical Engineering and joined Electromagnetic Compatibility Laboratory for research mainly on EMC/ESD related research projects, and partially works on digital and (RF) analogue design projects.